DYNAMICS OF SEMICONDUCTOR LASER DIODES WITH DELAYED OPTICAL FEEDBACK AND THEIR APPLICATION FOR THE HIGH-BIT-RATE GENERATION OF RANDOM-NUMBER SEQUENCES

A Thesis
Presented to
The Academic Faculty

by

Byungchil Kim

In Partial Fulfillment
of the Requirements for the Degree
Doctor of Philosophy in the
School of Electrical and Computer Engineering

Georgia Institute of Technology
December 2016

DYNAMICS OF SEMICONDUCTOR LASER DIODES WITH DELAYED OPTICAL FEEDBACK AND THEIR APPLICATION FOR THE HIGH-BIT-RATE GENERATION OF RANDOM-NUMBER SEQUENCES

Approved by:

Dr. David Citrin, Advisor
School of Electrical and Computer Engineering
Georgia Institute of Technology

Dr. Alexandre Locquet
School of Electrical and Computer Engineering
Georgia Institute of Technology

Dr. Paul Voss
School of Electrical and Computer Engineering
Georgia Institute of Technology

Dr. Paul Yoder
School of Electrical and Computer Engineering
Georgia Institute of Technology

Dr. Benjamin Klein
School of Electrical and Computer Engineering
Georgia Institute of Technology

Dr. Michael Chapman
School of Physics
Georgia Institute of Technology

Date Approved: 26 August 2016

To my wife, Ji hye Kim

ACKNOWLEDGEMENTS

Semiconductor lasers are not only key components in modern technology; they are also highly nonlinear systems. Both features make them a fascinating and challenging topic of research. This thesis deals with the nonlinear dynamics of these devices when they are subjected to external delayed optical feedback. Most of the material presented here has been published in refereed scientific journals as rapid communications or letters and presented at international conferences. My publications are listed hereafter.

The present PhD research has been prepared in the framework of collaboration between the Georgia Institute of Technology (Georgia Tech, USA) and GT-Lorraine(France).

I wish to express my sincere gratitude to Professor David Citrin, promoter of this thesis, for his helpful comments, constructive discussions, continuous supervision, his warm hospitality and for his firm support during last five years. His kindness and trust were an integral part of my scientific achievements.

I also thank Professor Alexandre Locquet, my co-advisor, for his accessibility, his judicious comments on my research work. Despite the number of times I disturbed him, he always received me with his friendly smile. These two amazing advisors have taught me that the work of the scientist goes beyond research and discovery and helped me to improve my communication skills. I could not have imagined having a better supervisors for my Ph.D and even my life.

TABLE OF CONTENTS

LIST OF TABLES

LIST OF FIGURES

SUMMARY

This thesis focuses on the chaotic dynamics of an external cavity semiconductor laser (ECSL) and their application for the high-bit-rate generation of random-number sequences. On the one hand, we are interested in experimentally studying fundamental nonlinear dynamics phenomena by using semiconductor laser systems. Considerable and systematic information concerning the dynamical regimes and the bifurcations between them is conveyed by the bifurcation diagram (BD) obtained by fixing all but one parameter and then mapping out the extremal values of a conveniently measured dynamical variable as the parameter varies. BDs provide a global picture of the dynamical system and it enables systematic investigations of the rich variety of dynamical behavior observed in ECSLs, including laser diode (LD) stationary dynamics, multistability, intermittency between stable states, and various routes to chaos, in terms of transitions between these types of behavior. We focus on the measurement of intensity time series and the mathematical and numerical analysis of generated (and simulated) time series, extracted random-number sequences, the information-theoretic estimation of bounds on the rate of random-number generation, and the information-theoretic analysis of post-processing techniques

With regard to fundamental properties, we show the statistical nature of chaotic intensity time series from ECSLs and their use for random-number generation. Also, we report the experimental investigation of two different approaches to random bit generation based on the chaotic dynamics of a semiconductor laser with optical feedback. The first approach is based on computing high-order finite differences of the chaotic laser intensity time series. The second approach is based on pragmatic considerations and could lead to rates of 2.2 Tb/s by extracting 55 bits per sample.

CHAPTER I

GENERAL INTRODUCTION

The study of nonlinear dynamics, which was prompted by the discovery of *deterministic chaos* by Lorenz in 1963 in a simplified model of the earth's atmosphere [112], has become one of the most active fields in modern science. With this finding, solutions of deterministic models can exhibit extreme sensitivity against small changes of the initial conditions resulting in exponentially diverging nearby trajectories. His pioneering work on deterministic chaos marked a breakthrough in the understanding of nonlinear systems and eventually initiated this rapidly growing scientific field of nonlinear dynamics and chaos. At the beginning, the study of nonlinear dynamics and chaos was considered as a mathematical curiosity, or as a nuisance. In the following fifty years, due to the spread of high-speed computers and refined experimental techniques, deterministic chaos has been found in multiple systems as diverse as forced pendulums, chemical reactions, stimulated heart cells, biological models for population dynamics, fluids near the onset of turbulence, classical many-body systems, lasers and nonlinear optical devices [188]. Especially, from the early years on, the development of nonlinear dynamics has been substantially supported by many experiments in optics because laser systems possess inherent instabilities which were experimentally verified for gas lasers [94] and solid state lasers [91] as well. The observation of instabilities and chaos in widely used semiconductor lasers, also referred to as laser diodes (LD), has attracted attention and it has accelerated research on nonlinear dynamics and chaos in nonlinear optics, for example, in laser systems.

The study of nonlinear dynamics in laser was initiated by Haken in 1975 [53] when he established the mathematical isomorphism between the Maxwell-Bloch equations,

which describe the dynamics of the electric field, the mean polarization of the atoms and the population inversion, and the Lorenz equations for atmospheric convective flow [112]. Since the work of Haken, much attention has been devoted to the nonlinear dynamics of lasers in general, and semiconductor LDs in particular. Semiconductor lasers are considered the most suitable and efficient source of coherent light in many modern technological applications. Their advantages include small size, integrability, low cost and high efficiency. As reliable devices, they offer a stable single-mode operation. Therefore, extensive study of chaos and instabilities in these lasers has gained a great deal of attention to develop a highly stable source of light. Surprisingly, dynamical instabilities and chaos in semiconductor lasers have become recently a focus point due to the many promising applications including random-number generations and cryptographical communications.

Among the ways of studying chaos and instability in a semiconductor laser is that of an external cavity laser. A mirror is added at the output of the semiconductor laser. It forms an external cavity, where the emitted light propagates, and is partially reinjected into the laser cavity. The roundtrip introduces a time delay to the lasers dynamics and adds an infinite number of degrees of freedom to the dynamical equations. External cavity semiconductor lasers (ECSL) can also lead to a variety of nonlinear dynamics and chaotic behaviour, which have great practical and theoretical significance.

It can be shown that at least three degrees of freedom are necessary but not sufficient for a dynamical system to be chaotic [189]. Semiconductor lasers are generally characterized by optical power, phase, and the carrier number. Since the optical phase is a slaved dynamical variable, semiconductor lasers are required to have at least one more degree of freedom to create the occurrence of chaos; optical injection from another laser [213], modulated current [106], or time-delayed optical feedback [63]. Among them, semiconductor lasers with time-delayed feedback, also

referred to as ECSLs, are well-suited model-systems for studying high-dimensional nonlinear dynamics phenomena. The dynamics of ECSLs are known to be complex and difficult to control, however in view of the rich dynamical behavior as well as the technological importance of these devices, the laser dynamics have been widely investigated [21, 115, 123, 132, 204].

This thesis focuses on the chaotic dynamics of an ECSL and their application for the high-bit-rate generation of random-number sequences [78, 158, 201]. On the one hand, we are interested in experimentally studying fundamental nonlinear dynamics phenomena by using semiconductor laser systems. Our chaotic ECSLs are built with standard distributed feedback lasers; they are subjected to optical time-delayed feedback via an external mirror (hence ECSL). Such chaotic semiconductor lasers are both of intrinsic and extrinsic interest. In the first instance, the dynamics of such systems are extremely rich, involving various qualitative regimes and the bifurcations leading from one to another. In addition to the intrinsic interest in such chaotic systems, LDs with time-delayed feedback may enable novel applications such as secure communications, light detection and ranging (LIDAR), random-number generation (RNG), and reservoir computing. Among these applications, we will focus on extracting random-number sequences from the time-dependent output intensity. Such random-numbers can be extracted with the bitrate well in excess of 10 Gb/s and are of intense interest, for example, for secure cryptography, quantum key distribution, and Monte Carlo simulations.

This chapter provides a general introduction to the ECSLs topics including historical background. The scope of the study with the outline is also presented at the end of this chapter.

1.1 Historical Background

This section provides an overview of the previous work by scanning the literature of nonlinear dynamics, ECSL and their application such as the random-number generation and chaos communication. This review is meant to give the reader general background of the investigated topics where we briefly review the most important and relevant contributions rather than covering the whole literature.

More than a century ago, when Poincaré worked on the three body problem [151], he figured out the existence of extremely complex trajectories and he gave a first indication for complex dynamical behavior, called chaos and complexity. After more than 60 years, based on Poincaré's contribution, Lorenz's work [112] on the earth's atmosphere showed numerically that solutions of deterministic models can exhibit extreme sensitivity against small change of the initial conditions and this deterministic chaos marked a breakthrough in the understanding of nonlinear systems and eventually initiated this rapidly growing scientific field of nonlinear dynamics and chaos. In the following thirty years, much attention has been paid to the emergence of chaotic behavior and four universal routes to chaos have been identified in low-dimensional systems, namely, the quasi-periodic route [169], the period-doubling cascade [40], intermittency [43], and crisis [48]. Contemporaneously, experiments on various systems in diverse areas of science, such as biology, chemistry, and physics, have shown the existence of chaotic dynamics, e.g. in population dynamics, blood-cell production, neurons, macroeconomic,sea clutter, and many different laser systems [30]. Also, the effect of delayed feedback on dynamical systems has been studied in many different areas. These systems, which are commonly encountered in nature, often show a complex behavior and they challenge many intuitive and theoretical descriptions. Worth noting here, the technological impact of optical feedback on SL applications is exemplified by the considerable literature developed on this subject in the last three decades [12, 203, 212].

1.1.1 Dynamics of External-cavity Semiconductor Lasers

Shortly after Haken initiated the study of nonlinear dynamics in lasers in 1975 [53], effects of time-delayed feedback on LDs were reported [160] and the research on such system was actually spanned by Lang and Kobayashi [91] who developed a model for semiconductor lasers dynamics when subjected to external optical feedback. Figure 1 shows a schematic representation of an ECSL. Semiconductor lasers are frequently affected by reflections from distant system components which can easily destabilize the laser and result in unstable emission dynamics. Therefore, until a few years ago, this chaotic behavior of semiconductor-based systems was viewed as an unwanted irritation to be engineered away. Nowadays, rather than simply being avoided, such dynamical instabilities are of intense interest for applications, such as secure communications [164, 193, 222], light detection and ranging (LIDAR) [105], RNG [132, 184, 201], and reservoir computing [11, 139].

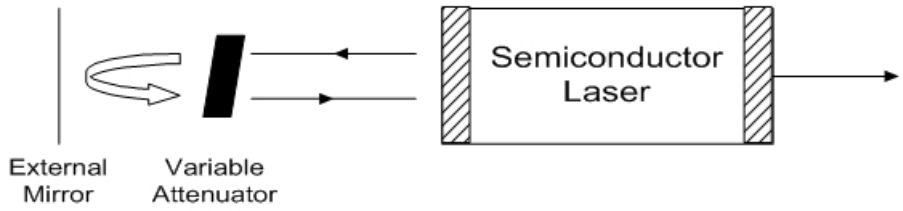

Figure 1: Schematic representation of an external cavity semiconductor laser (ECSL)

A laser configuration with feedback is an infinite dimensional dynamical system. Various types of chaotic transitions of ECSLs have been identified experimentally under specific conditions of cavity length L, injection current I, and feedback strength. A common transition is the quasi-periodic route to chaos [124], in which a stable mode (ECM) is replaced by an attracting periodic orbit at a frequency close to the relaxation-oscillation frequency, f_{RO} of the solitary laser and this periodic attractor turns into a torus as the feedback strength increases. In addition, a period-doubling route to chaos has been reported [220]. In this case, a cascade of period-doubling

bifurcations, creating oscillations at frequencies close to sub-multiples of f_{RO}, occurs. Sub-harmonic bifurcations have also been reported for a system with tilting of the external mirror giving rise to sub-harmonics of the round-trip frequency [125]. Moreover, when the operating conditions are such that several ECMs are destabilized simultaneously, generalized multistability occurs as several attractors or attractor ruins coexist in phase space [115] and numerous phenomena related to attractor switching can be expected to be observed in a BD. Examples include the switching between a low-frequency-fluctuation (LFF) state and a state of stable emission [60] and the hopping between different relaxation oscillations in [123].

Despite these experimental observations, there was no theoretical model that could accurately describe the origins of the dynamical operation of semiconductor lasers with time delayed feedback. In 1980, Lang and Kobayashi presented a work showing that the dynamical changes in the carrier density of the SL due to optical feedback lead to a modifcation of the refractive index, which in turn alters the resonant frequency of the laser [91]. They also demonstrated that this information could be used to describe some of the dynamical behaviour of the laser's output power with optical feedback. Most of the theoretical models presented in the literature are based on the LK equations [115, 124, 164].

1.1.2 Chaos and Bifurcation

The word chaos was first used by two mathematicians, Li and Yorke [194]. This word scientifically means "non-periodic oscillatory state, which stems from the nonlinear nature of the deterministic physical systems [10]. Therefore, a chaotic system can simply be defined as a dynamical system that is neither static nor periodic. Chaos is found in a wide variety of systems including lasers, chemical reactions, fluid dynamics, weather and earthquakes [10].

Shortly after the invention of lasers, scientists noticed that a continuously pumped

ruby laser exhibited unstable behaviour (output of a series of spikes with random amplitude and occurrence) even with a fixed excitation [128]. However, the lack of computational tools as well as mathematical concepts at that time made it impossible for such behaviour to be explained. In time, scientists realized that the invention (lasers) that they considered the most stable oscillators could show a huge variety of chaotic and unstable dynamics under certain conditions.

Haken [53] recognized in 1975 that single-mode lasers could exhibit large-amplitude chaotic oscillations under certain conditions. Chaos was then reported in a loss-modulated CO_2 laser [12], multimode He-Ne laser [210], diode lasers [131], lasers with saturable absorbers [2], and semiconductor laser subject to optical feedback from an external mirror [91]. Although chaos and instabilities were seen for a few decades as unwanted effects that should be eliminated in semiconductor lasers, chaotic dynamics in semiconductor lasers has become a hot topic due to their extraordinary advantages from a practical and fundamental nonlinear physics point of view. In the following section we discuss the suitability of lasers and particularly semiconductor lasers for dynamical investigation.

In semiconductor lasers, chaos suggests a physical-layer encryption technique known as chaotic communication. The use of chaos in secure communications was first demonstrated by Pecora and Carol [141]. The idea is to carry (encode) the transmitted message on a chaotic waveform and decode it on the receiver if the latter is synchronized to the transmitter.

The external optical feedback in semiconductor lasers leads, in addition to chaos, to a rich diversity of nonlinear dynamics through the bifurcation of the system. Bifurcation is a Latin word that means, "forking into two and in the context of nonlinear dynamics means the point where a sudden qualitative change in the behaviour of a system occurs. This change is usually due to smooth variation of a control parameter [87]. There are several forms of bifurcations that are categorized according to

how stability is lost [87, 215].

Considerable and systematic information concerning the dynamical regimes and the bifurcations between them is conveyed by the BD obtained by fixing all but one parameter and then mapping out the extremal values of a conveniently measured dynamical variable as the parameter varies. Investigation of BDs therefore provides new vantage point from which to view ECSLs. In particular, BDs provide clear and systematic experimental evidence of the way in which instabilities of various nature develop in an ECSL.

There are two important motivations to the further investigation of ECSL BDs that reveal links between various types of dynamical behavior. The first is that it provides a global picture of the dynamical system. Second, and more important, it enables systematic investigations of the rich variety of dynamical behavior observed in ECSLs, including LD stationary dynamics, multistability, intermittency between stable states, and various routes to chaos, in terms of transitions between these types of behavior. A typical experimental BD, obtained by taking local extrema (maxima and minima) of the intensity time series from a high-speed oscilloscope as a function of increasing feedback strength, is shown in Fig. 2.

Several theoretical and numerical works have studied in detail the BDs of ECSLs as a function of the feedback strength such as a single-mode SL [212], vertical cavity surface-emitting lasers [49], and ring lasers [34]. Also, some experimental BDs for Er-doped fiber lasers [157], optically injected solid-state lasers [203], and gas lasers [12] have been mapped out. However, there is an almost total lack of experimental BDs available for ECSLs because there are several experimental hurdles. Even though there are numerous studies of the dynamics of ECSLs in restricted regimes, yet a comprehensive picture—and on that reconciled experiment and theory across a range of operating parameters—remained, surprisingly, until now unavailable. A global understanding of the dynamical regimes, however, is essential to gain a fundamental

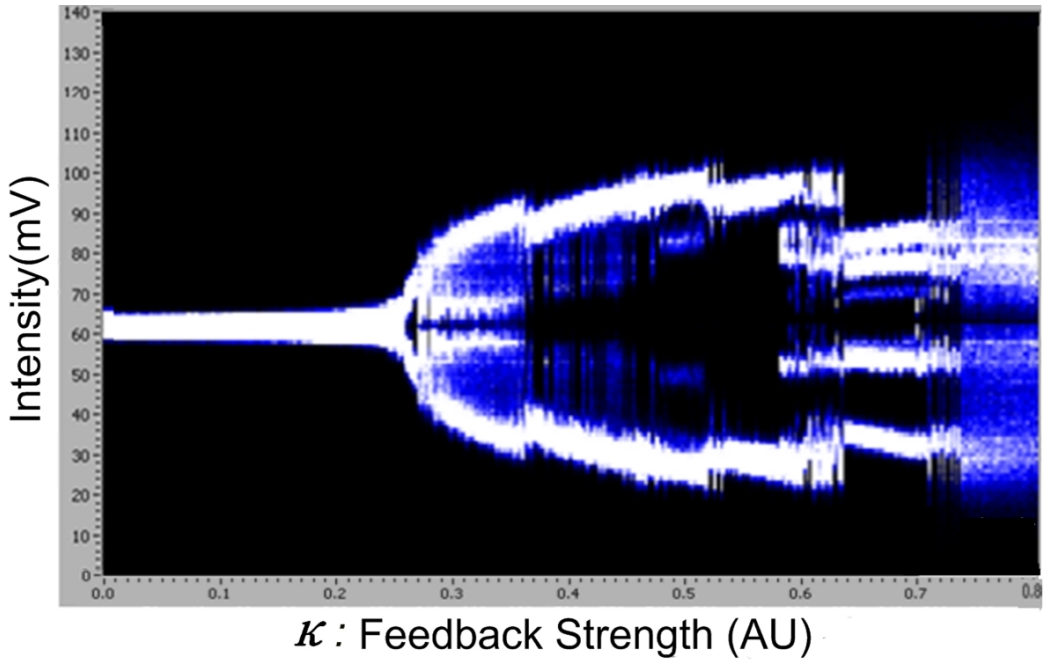

Figure 2: Typical experimental BD for an ECSL as a function of feedback strength obtained from the intensity time series (the injection current I=21.24 mA and the externalcavity length L=30 cm). Light-color areas show intensity of local maxima and minima. Bifurcations associated with qualitative changes in the dynamics can be easily seen.

understanding of the study of semiconductor lasers nonlinear dynamics.

1.1.3 Random Number Generation

Random numbers play important roles both in cryptography and Monte Carlo simulation methods [29]. Techniques for RNG are either based on pseudo-RNG (PRNG) [85] or physical RNG (PhyRNG) [31, 52, 103, 155, 186, 216]. PRNG uses certain deterministic logical operations to generate pseudo-random sequences based on a short bit sequence called a seed. Numerous realizations of this type of system exist; algorithms are either run on a UCT-driven board or are implemented on programmable gate arrays (e.g., FPGA-based systems) or with ASIC integrated circuits. A number of these algorithms have already been standardized in the International Standards Organization document ISO 28640:2010. Although sequences generated by such algorithms pass standard randomness tests, such as the NIST [171] and Diehard [114] tests, their

perfectly deterministic nature makes them ill-suited in applications requiring large amounts of random-numbers, or high speed generation, as in some cryptographic setting or Monte-Carlo simulations. Furthermore, it is sometimes even possible to infer the seed by observing part of a generated pseudo-random sequence (e.g. [76]).

In contrast, physical-based systems produce random sequences by sampling and quantizing the realizations of a random process that governs the behavior of a physical experiment. A first approach consists in relying on certain quantum properties for RNG. In this case, the randomness stems directly from the quantum nature of the systems used [149]. However, the generation rate of such quantum-based systems is typically not larger than a couple of tens of Mb/s, because of constraints on the rate and power of the mechanisms for extracting noncorrelated bits [25, 33].

An alternative solution consists in exploiting the nonlinear dynamics of a physical system for RNG. The advent of chaos theory has separated the notions of determinism and predictability. The nonlinear dynamics of a physical system that displays a chaotic steady-state behavior is purely deterministic, but its long-term behavior cannot usually be predicted due to sensitivity to initial conditions. This property of chaos implies that two states, initially very close, become very different with time. Since it is impossible to know the state with arbitrarily high precision, it also implies that it may be in practice impossible to perform long-term prediction of the evolution of a chaotic system. Specifically, LD based systems are well suited for high-speed RNG because of the subnanosecond decorrelation of the dynamical variables (typically the optical intensity), which allows for multi-Gb/s random rates [158, 201]. Therefore, there has been recent interest in systems that use the chaotic dynamics of a deterministic system to mimic the properties of a truly random system [14, 59, 130, 135]. In addition, with some post-processing of the pseudo-random signal, bit rates of the order of hundreds of Gb/s have been reported [5, 78]. A few research groups have

already experimentally demonstrated that the digitized chaotic dynamics of the optical intensity of a semiconductor laser could be used to generate binary sequences passing the NIST [171] randomness test at rates of tens of Gb/s [57, 100]. It was also recently shown that further post-processing of the chaotic time series could lead to random bit rates well over hundreds of Gb/s [78]. However, in all of the existing works, randomness is mainly tested against standard tests but is not analyzed based on information-theoretic principles, and in most existing works the essential post-processing is not implemented in real time.

1.1.4 Chaos Synchronization

Chaotic communication systems have many unique features when compared to conventional communication systems. Such advantages include sufficient use of channel bandwidth, utilization of the intrinsic nonlinearities in communication devices, large signal modulation, reduced number of components and secure communications [28, 119, 168].

The first full optical scheme for secure communication based on chaotic synchronization was reported in 1996 by Annovazzi-Lodi et al [9]. Using two chaotic systems each made by two coupled semiconductor lasers, they proposed two approaches for secure communication, namely chaotic masking and chaotic shift keying (CSK). In CSK, also known as chaotic switching, the transmitter is switched between two different chaotic orbits by means of current modulation of the injecting laser. The message is then decoded by subtracting the output of the receiver from the transmitted signal. This scheme offers more efficiency and security but it is complicated and difficult to implement. On the other hand, chaotic masking is much easier to implement but with less efficiency and security. In this scheme the signal is not encoded on, but just summed up to chaos to prevent any detection by observing the time or frequency domain.

Since then, several approaches to achieve chaotic synchronization have been experimentally and numerically produced [23]. J. Liu et al [107] proposed a novel chaotic optical communication system in 2001. They experimentally implemented a message encoding and decoding scheme for optically injected chaotic communication system. The system has broadband chaos on the order of many gigahertz to hundred gigahertz with high speed lasers. A year later, the same group [119] demonstrated chaotic optical communication system at a bit rate of 2.5 Gb/s and numerically studied the system performance at 10 Gb/s. They also concluded that for high-bit-rate chaotic optical communications, noise from all sources should be eliminated to minimize noise-induced desynchronization bursts and synchronization deviation.

A recent study [108] has experimentally demonstrated for the first time the existence of two types of synchronization in coupled optically injected semiconductor lasers. The first type is found for small frequency detuning when the injection strength matches the feedback strength of the ML. The semiconductor laser then dynamically follows the ML. In contrast, the second type is found over a wide range of detuning when the injection strength is much stronger that the feedback strength. In this synchronization state, the semiconductor laser is directly driven by the injected signal. Phase locking in chaotic synchronization has also been reported in 2003 [126]. This locking was found to make synchronization in phase dominant over intensity synchronization within a parameter range. Although, the phase synchronization is very accurate, it can easily be destroyed once the phase locking becomes unstable due to exited resonance oscillation.

The first realization of chaotic secure communications used an analog-circuit implementation of the Lorenz [27] system. Since then, a host of other electronic cryptosystems has been demonstrated. Shortly after these electronic realizations, the optics community sought to realize cryptosystems based on chaotic lasers. The focus

was to combine the security provided by chaotic communications with well-known advantages of laser optical communications, e.g., very high bit rates and low loss. The first experimental evidence of laser chaos synchronization is when [167] demonstrated the synchronization of two mutually coupled solid-state Nd:YAG lasers and [190] observed synchronization of two CO_2 lasers. The main drive was to exploit synchronization for secure communication. [26] was the first to prove numerically optical encryption and decryption of a message. The first experimental realization of optical chaotic secure communication is [206] which demonstrated the transmission of a 126 Mb/s pseudorandom binary message using chaotic Er-doped fiber-ring lasers.

After this early work, LDs drew more attention since they are the preferred light source in telecommunications and are an ideal testbed for various fundamental issues in nonlinear dynamics [109]. The first transmission of a message using LDs with external nonlinearities is [46] in which Goedgebuer *et al.* demonstrated encryption/decryption of a 2 kHz sinusoidal message using two synchronized wavelength-chaos generators. The first experiment exploiting internal nonlinearities of LDs was [182] where a 2.5 kHz square wave was successfully hidden in the chaotic fluctuations of a LD subjected to external optical feedback, i.e., an ECSL.

Since these early results, digital transmission at a few Gb/s has been demonstrated for various LD-based systems. For cryptosystems exploiting the chaotic dynamics of ECSLs, several papers have shown transmission, encoding schemes, and synchronization regimes [110, 111]. [32] reported transmission over 120 km of a commercial fiber-optic network of a 1 Gb/s NRZ pseudo-random binary sequence with a bit error rate (BER) of 10^{-7} and of a 2.4 Gb/s sequence with a BER of $\sim 5 \times 10^{-2}$, using a dispersion-compensation module. Recent experiments have shown photonic integrated circuits with time-delayed feedback could also be used to generate chaos and convey information at 2.5 Gb/s over 100 km of optical fiber and with a BER of 10^{-12} [13, 16]. This work on integrated circuits prove that these kinds of chaotic

systems can be built in a compact, robust, and repeatable way.

1.2 Scope of the Study and Thesis Outline

This thesis aims to investigate the nonlinear dynamics of ECSL subject to delayed feedback. The thesis will consist of two closely coupled components: fundamental properties and applications. As such, it will bridge topics of applied mathematics, electrical engineering, and physics as well as information theory and computer science. We will ground our discussion in extensive theoretical studies based on the Lang-Kobayashi (LK) equations thus providing a means to attain physical insight into the observed dynamics. Also, with regard to fundamental properties, we have observed the BD tracking the intensity time series of the output light as the feedback strength is varied from essentially zero to large values. We track at the dynamical regimes of an ECSL as key parameters are varied in order to determine conditions most propitious to high-rate RNG. Our aim is to ground such an optimization in a thorough understanding of the dynamical behavior of the ECSL, rather than in a trial-and-error approach.

The layout of the thesis is as follows. In Chapter 1, we provide a general review of the related literature including the early work on ECSL and their applications. Our work is put in context and our contributions are highlighted.

In Chapter 2, we describe the theoretical approach to the study of the equilibrium and stability of LDs subject or not to optical feedback from an external cavity. After recalling the underlying principles of LDs, the equations appropriate to single mode without feedback. Also, we extensively study the emission properties of semiconductor lasers which are subject to delayed optical feedback. In particular, we focus on investigation and characterization of high-dimensional broadband chaotic emission dynamics, in which we are interested in terms of fundamental nonlinear dynamics and with regard to novel functionalities. The derivation of the LK equations for single mode operation with coherent optical feedback is inspired from the book of Ohtsubo [132]. The LK equations allow to explain the main features of the regime

and the LFF regime.

Chapters from 3 to 6 are presented to discuss the dynamics of the distributed feedback laser with delayed optical feedback. Despite the numerous studies of ECSLs, we have seen that the detailed dynamics for ECSLs remain an open question. Our work examines several aspects of fundamental importance for dynamics of an ECSL using tools from bifurcation theory. This offers perspectives for an ECSL to understand the effect of the various operating parameters, such as the feedback strength, the injection current I, and the external cavity length L (creating a delay τ).

- Chapter 3 reports experimental BDs of an ECSL that focused on the case of an ECSL biased just above threshold and subjected to feedback from a distant reflector [long-cavity (LC) case] and observed a cascade of bifurcations.

- Chapter 4 reports experimental BDs of a semiconductor laser, biased well-above threshold, subjected to external optical feedback.

- Chapter 5 presents experimentally in a high-dimensional dynamical system experiencing generalized multistability, the sensitivity of the route to chaos on the initial state relying on a novel initial-state selection method. As the feedback level determined by the effective mirror reflectivity is increased, chaos develops from a different mode of the external-cavity depending on the initial mode experimentally specified.

- Chapter 6 shows that the bifurcations between dynamical states originating in the nonlinear dynamics of an ECSL at constant current can be detected by its terminal voltage. Also, we show that the LD terminal voltage is directly related to the signal on an optical feedback such as a reflection. The intensity level of the external feedback is shown to affect the carrier density in the conduction band in direct band-gap of a compound semiconductor active region of the LDs. Therefore, we show that measuring the laser terminal voltage is the simple alternative way of measuring the feedback strength in an ECSL.

We start with a full description of the basic rate-equation model used in our

simulation. It also discusses the agreement between theory and experiment. More importantly, these chapter presents the universal picture of nonlinear dynamics by mean of novel BDs. We reiterate: the results map out detailed BDs of ECSLs as function of a feedback strength for various L and I, thus covering a significant portion of parameter space. We have grounded our discussion in the extensive theoretical studies based on the LK equations and observed a cascade of BDs in accordance with our experimental results. Also, with regard to fundamental properties, we plan to track to dynamical regimes of an ECSL as key parameters are varied. The latter is thoroughly investigated with the accompanied phenomena. Thus far, we have presented the main known results related to the chaotic dynamics of an ECSL.

The generation of random sequences plays a crucial role in numerous applications, including the simulation of complex systems with Monte Carlo methods, high-speed encryption, and quantum cryptography. Deterministic algorithms based on algebraic techniques and generating pseudo-random sequences, for example with linear feedback shift registers, have long been studied but are ill-suited for high-speed generation because of periodicities in the generated sequences. New systems are thus needed to respond to the demand for high-speed random-number generation. In particular, an alternative to pseudo-random-number generation consists in extracting random-numbers from physical processes that have a random-like character (noise, chaos, etc.), using appropriate post-processing. However, despite recent advances, for instance using optical chaotic systems and quantum systems, there is presently little fundamental understanding of the operation of such systems. In the following, we adopt a holistic approach to the problem by addressing the following two challenges:

Task I: The realization of a physical system based on ECSL, modeling and analysis of its random properties, and the determination of the theoretical limit of the RNG rate.

Task II: The design of algorithms leading to high-speed RNG with provable quality.

We plan to track dynamical regimes of an ECSL as key parameters are varied in order to determine conditions most propitious to high-rate RNG. Our aim is to ground such an optimization in a thorough understanding of the dynamical behavior of the ECSL, rather than in a trial-and-error approach. For example, our work, discussed in chapters 3 and 4, has observed the BD tracking the intensity time series of the output light as the feedback strength is varied from essentially zero to large values. The nonlinear dynamics of an ECSL can be well described by an established numerical model known as the LK equations thus providing a means to attain physical insight into the observed dynamics. The LK equations can thus be used to track the phase-space trajectory of the LD model (electric-field amplitude and phase, inversion) to understand features in the time series and how they correlate with the dynamics involving system variables that are difficult to observe (e.g., the inversion and the electric field as opposed to the easily observed intensity). More specifically, we aim to use intensity time series obtained from ECSLs to generate random number sequences at very high bit-rate.

Chapters 7 and 8 focus on the generation of random sequences. In these chapter, we presents on the measurement of intensity time series and the mathematical and numerical analysis of generated (and simulated) time series, extracted random-number sequences, the information-theoretic estimation of bounds on the rate of random-number generation.

- Chapter 7 briefly reviews the state of the art knowledge on the links between dynamics of ECSL and RNG and we study experimentally and theoretically based on the LK model first- and second-order statistical measures of the optical intensity of a chaotic ECSL in fully-developed coherence-collapse. The second-order statistic is characterized by the autocorrelation function, for which we achieve consistent experimental and theoretical results over the entire parameter range considered.

- Chapter 8 focuses on extracting random-number sequences from the time-dependent

output intensity. We report the experimental investigation of two different approaches to random bit generation based on the chaotic dynamics of a semiconductor laser with optical feedback. The first approach is based on computing high-order finite differences of the chaotic laser intensity time series. The second approach is based on pragmatic considerations and could lead to rates of 2.2 Tb/s by extracting 55 bits per sample. The randomness of the bit sequences obtained from the two approaches is tested against three standard randomness tests (ENT, Diehard, and NIST tests), as well as by calculating the statistical bias and the serial correlation coefficients on longer sequences of random bits than those used in the standard tests. Such random-numbers are of intense interest, for example, for secure cryptography, quantum key distribution, and Monte Carlo simulations. As such, it will bridge topics of electrical engineering and physics as well as information theory, applied mathematics, and computer science.

Finally, in Chapter 9, we summarize the main results of the thesis and presents some perspectives and possible directions to investigate.

CHAPTER II

THEORETICAL DESCRIPTION OF LASER DIODES WITH AND WITHOUT OPTICAL FEEDBACK

2.1 Semiconductor Lasers

In this section, we describe the theoretical approach to the study of the equilibrium and stability of LDs subject or not to optical feedback from an external cavity. After recalling the underlying principles of LDs (Section 2.1.1), the equations appropriate to single mode (Section 2.1.2) without feedback are obtained following the procedure outlined in Petermann [145]. In the following Section 2.2, we extensively study the emission properties of semiconductor lasers which are subject to delayed optical feedback. In particular, we focus on investigation and characterization of high-dimensional broadband chaotic emission dynamics, in which we are interested in terms of fundamental nonlinear dynamics and with regard to novel functionalities. The derivation of the LK equations for single mode operation with coherent optical feedback is inspired from the book of J. Ohtsubo [132]. The LK equations allow to explain the main features of the regime and the low-frequency fluctuation regime.

2.1.1 General Description of Semiconductor Lasers

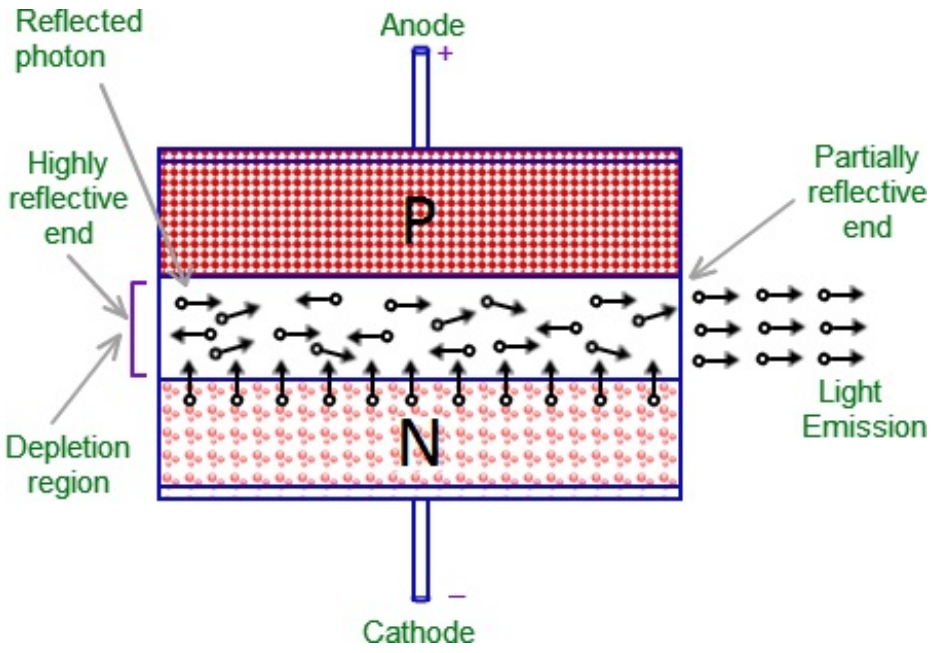

Figure 3: Schematic representation of a typical edge-emitting semiconductor laser

A laser is a physical system that generates light by amplification of stimulated emission of radiation (LASER) [32]. Semiconductor lasers are based on the p-n junction of semiconductor materials where the lasing is achieved by the emission of light due to carrier recombination between the conduction and valence bands. Its principle of operation can be phenomenologically described by a two-level atomic system in a resonant unidirectional (ring) cavity. A laser is an optical oscillator that comprises an externally pumped active medium and a resonant cavity. The resonant cavity provides an adequate feedback mechanism. The role of the active medium is twofold. On the one hand, it provides a spontaneous emission noise input that may initiate an oscillation process. On the other hand, it can amplify the light propagating within the cavity. For the type of lasers under study, the active medium consists of a semiconductor material that can be pumped optically or electrically. The feedback mechanism regenerates part of the light to increase the amplification and select the modes of the electromagnetic field to be amplified.

In the following, we focus on a Fabry-Perot type LD. Figure 3 sketches a typical edge-emitting semiconductor laser with a double heterostructure. The resonator is a Fabry-Perot cavity where the light travels parallel to the surface of the wafer on which the laser is built and is partially reflected on laser facets. The length of the cavity is typically 250 μm. A thin layer (thickness of about 0.1 μm) of a direct-band-gap semiconductor material is embedded between two p-type and n- type cladding layers with larger band-gaps. Under forward bias, electrons and holes move freely to this region but cannot cross over to the other side because of the potential barrier resulting from the band-gap difference. This allows for a large concentration of electrons and holes in this region, usually referred to as active region. The double heterostructure also allows optical confinement because the cladding layers have a smaller refractive index than the active layer. The resulting waveguide confines the light and therefore reduces the internal loss. In the active region, electrons and holes can recombine through radiative or nonradiative mechanisms. Nonradiative recombinations, such as Auger recombination, trap and surface recombinations are not helpful for laser operation. Radiative recombinations can be either spontaneous or stimulated [Fig. 4 (a) and (b)]. In the case of spontaneous emission, photons are emitted in random directions and without phase relation; thus the emitted light is incoherent. By contrast, when electron-hole recombination is stimulated by an already existing photon, the emitted photon has the same wavelength, phase and direction as the incoming photon. This results in coherent amplification of the incident light.

Since a photon in the active region may be absorbed to generate an electron-hole pair [Fig. 4 (c)], stimulated emission must compete with absorption. At low values of the injection current, the number of electron-hole pairs supplied by the injection current is small; absorption dominates amplification and the net rate of stimulated emission, namely the difference between the stimulated photon rate and the absorption rate, is negative. The net rate of stimulated emission increases with the injection

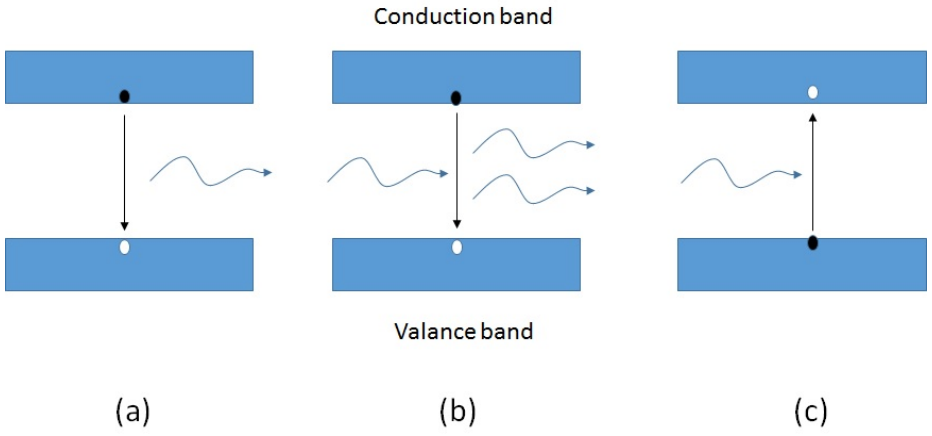

Figure 4: Schematic illustration of (a) spontaneous emission, (b) stimulated-emission and (c) absorption processes.

current. The semiconductor is said to be optically transparent when the rates of stimulated emission and photon absorption are equal. Beyond transparency, the condition known as population inversion is achieved when the net rate of stimulated emission is positive. However, depending of the value of the injection current, the net rate of stimulated emission can be positive but not sufficient to overcome the transmission losses at the laser facets, the internal losses due to photon absorption inside the cavity without generation of carrier and the loss due to light scattering. The diode starts lasing when the injection current exceeds a critical value called threshold current at which the net gain overcomes all losses. Above threshold, the number of electron-hole pairs remains almost clamped to its threshold value. The laser output increases almost linearly with the injection current as most of the electron-hole pairs that are injected in excess recombine through stimulated emission within the selected cavity modes. In the same time, the spectral width of the laser narrows considerably because of the coherent nature of the stimulated emission.

We have so far considered Fabry-Perot type LDs in which the light is partially reflected on laser facets. The feedback mechanism can however be achieved by other ways; distributed feedback laser and distributed bragg reflector (DBR) laser. In

distributed feedback laser, single-mode operation in semiconductor lasers is usually achieved by incorporating a periodic thickness variation in one of the cladding layers to form part of the heterostructure. The feedback is not localized at the cavity facets but is distributed throughout the cavity length. This is achieved by using a periodic index perturbation integrated along the laser structure. Such structure is the so-called distributed feedback laser, which is the only type of semiconductor laser investigated in this thesis. The laser usually oscillates at or near the maximum of the gain profile, which is, i.e. the peak gain, typically described as a linear function of carrier density. The oscillating (resonance) frequency is also dependent on the carrier density, which plays a vital role in semiconductor lasers. In DBR lasers, gratings are etched outside the active medium. In these last two types of lasers, gratings are used to select a single longitudinal mode of oscillation. Due to this spectral feature, those lasers are of particular interest for optical fiber communications.

The fact that the carriers cannot follow the photon decay rate leads to the well-known relaxation oscillation. Any disturbance, a step input in the current for example, leads to the oscillation of the population inversion or the output power, which consequently causes oscillation for the other quantity. The two quantities periodically exchange the energy contained inside the laser cavity before damping and returning to the steady state. Semiconductor lasers exhibit strongly damped relaxation oscillation with rather high relaxation oscillation frequencies (ROF). Therefore, semiconductor lasers cannot produce sustained oscillations by themselves. However, ROF can easily be excited by a step change of the injection current or external perturbation such as external feedback or injection. Thus, it is believed that the relaxation oscillation of the solitary laser plays a crucial role in the induction of instabilities in semiconductor lasers especially when subject to delayed optical feedback.

2.1.2 Single-mode Solitary Laser Diode

2.1.2.1 The Maxwell-Bloch Equations and Laser Categories

In this section, we address the question whether the presented model of lasers, which is based on Maxwell's equations and self-consistent solutions, can be simplified to a practical mathematical model. In order to achieve this goal, several physical assumptions and mathematical approximations can be made for simplification [205]. In the following, we outline the particular simplifications that can be made for reduction of the model leading to the well-known Maxwell-Bloch laser equations. Based on the simplifications and approximations of [205], we are able to derive a model that describes the emission properties of homogeneously broadened, single-mode, two level unidirectional ring lasers in the plane wave approximation. We obtain three differential euqations for the dynamical variables, which are the electrical field $E(t)$, the polarization $P(t)$, and population inversion $N(t)$; all of them are mutually coupled via the optical gain g. These equations are referred to as the semi-classical Maxwell-Bloch equations [211].

$$\dot{E}(t) = -(iw_E + \gamma_E)E(t) - i_g P(t), \tag{1}$$

$$\dot{P}(t) = -(iw_P + \gamma_P)P(t) + gE(t)N(t), \tag{2}$$

$$\dot{N}(t) = J - \gamma_N N(t) - i_g[E(t)^* P(t) - E(t)P(t)^*], \tag{3}$$

The resulting Eqs. (1)$\sim$(3) comprise relevant laser device characteristic frequencies: the resonance frequency of the laser resonator w_E, and the frequency of the optical transition w_P. Furthermore, the following laser specific decay rates, originating from the properties of the light-matter interaction in the laser cavity, are of particular importnace from the dynamics point of view: the decay rate of the optical

field in the laser resonator γ_E, often referred to as cavity decay rate; the decay rate of the macroscopic polarization γ_P; and the decay rate of the inversion γ_N. Finally, the bias current of the semiconductor laser is considered in the pumping coefficient which represented by J.

These parameters are of great importance for the dynamical properties of the laser, since they result from the characteristics of the light-matter interaction in the laser cavity. The relevant time scales related to the three decay rates, γ_E, γ_P, and γ_N, which are given by the material properties of the laser, can be considered for further reduction of the Maxwell-Bloch equation, Eqs. (1)$\sim$(3). These considerations allow for classification into three different laser categories, for which the appropriate model equations exhibit different nonlinear dynamics properties. Reduction of the model can be achieved, if one of the decay rates is sufficiently faster than the others. In this case, it is possible to adiabatically eliminate the corresponding variable form the system of equations reduction the number of equations by one. Based on this consideration, it is possible to classify lasers into three categories with different nonlinear dynamics properties. Depending on the category of laser, either one, two, and three equations are required for appropriate description of the dynamics; or in other words, lasers which can be described by the Maxwell-Bloch equations are categorized according to their number of degrees of freedom. Form the dynamics point of view, this result is very relevant, since it is well-known from the Poincare-Bendixon-Theorem [7, 188] that systems with two or fewer degrees of freedom cannot exhibit chaotic behavior. For such laser systems the number of degrees of freedom needs to be increased to allow for chaotic dynamics. This can occur, e.g., via application of external perturbations.

1. *Class-A* lasers

   For class A laser the decay rates of the polarization γ_P and the inversion γ_N are sufficiently larger than the decay rate of the electrical field γ_E. Hence, the corresponding variables can be adiabatically eliminated and the dynamics is

descrived by a single rate-equaton for the electric field $E(\mathrm{t})$. Therefore, Class-A lasers belong to the class of one-dementional systems for which only time independent solutions exist. Examples of class-A lasers are He-Ne lasers

2. *Class-B* lasers

   For Class-B lasers only the decay rate of the polarization γ_P is distinctly larger than the decay rates of the inversion γ_N and the electric field γ_E, respectively. Therefore, the dynamics of Class B lasers is captured by two rate-euations for $E(\mathrm{t})$, and $N(\mathrm{t})$. Accordingly, Class B laser represent two-dimensional systems for which periodic solutions are possible. These periodic oscillations are called "carrier" relaxation oscillations of lasers, because the laser energy oscillates between inversion and optical field. Examples of class-B lasers are Nd-YAG, CO_2 and semiconductor lasers.

3. *Class-C* lasers

   For Class-C lasers the three decay rates are of similar order of manitude. In this case, description of the dynamics requires the full set of the Maxwell-Bloch equations. Therefore, Class-C lasers belong to the class of three-dimensional systems which can exhibit chaotic dynamics. Examples of class-C lasers are the NH_3 and He-Ne lasers.

Since we are interested in high-dimensional nonlinear emission dynamics of semiconductors, the Class B laser rate-equations represent the starting point for derivation of the model equations which we require for complementary analysis to our experiments. Furthermore, additional degrees of freedom are needed to be introduced into the dynamically two dimensional semiconductor laser system to allow for chaotic behavior. In semiconductor lasers, high-demensinal chaotic dynamics can be easily generated by modulation of the pump current (changing the inversion) [88, 106, 174];

by optical injection [174, 180]; or by application of time-delayed feedback to the relevant variables [80, 123, 174]. In particular, semiconductor lasers which are subject to time-delayed optical feedback are very promising candidates for experimentally studying high-dimensional chaos and it is the type of nonlinear dynamics of semiconductor laser investigated in this thesis. Before we study the influence of delayed optical feedback on the emission dynamics of semiconductor lasers, we highlight characteristic features of the emission properties of solitary semiconductor lasers. As starting point and as mathematical/numerical foundation, we derive semiconductor laser rate-equations which describe fundamental features of the emission properties of solitary semiconductor lasers.

2.1.2.2 Semiconductor Laser Rate-Equations

In this section, we discuss characteristic properties of semiconductor lasers which are relevant for their dynamical behavior. Initially, we consider their characteristic time scale to derive a simple rate-equation model for unperturbed solitary semiconductor lasers. On the one hand, the semiconductor lasers rate-equations will serve as basic equations for modeling feedback induced instabilities in semiconductor lasers.

So far, we have seen that for certain physical conditions the Maxwell-Bloch rate-equation can be reduced to a one, or two-dimensional equation system by adiabatic elimination of one, or two, of the three variables; γ_P, γ_N, and γ_E. This allowed for classification into three laser classes, depending on the specific time scales of the three decay rates of the lasers. In order to derive an appropriate model for the emission properties of semiconductor lasers, it is necessary to consider the fact that electron-electron scattering destroys coherence of the coupling between the states of the conduction-band and state of the valence-band, quickly damping polarization oscillations in the semiconductor material. For simplicity, we assume that the laser structure is designed to support a single lateral and transverse mode. Considerable

simplification occurs if we assume that the material response is instantaneous so that the polarization can be adiabatically eliminated from the model. This approximation is justified since the material response, which is governed by the intraband scattering processes, is relatively fast (∼0.1 ps) compared to the photon lifetime (∼1 ps) and the carrier recombination time (∼1 ns) [4]. As a result, we obtain two coupled rate-equations for the electric field and the inversion of the semiconductor laser which take the following form for specific transformation of the variables:

$$\dot{E}(t) = \{iw(N(t)) + \frac{G(N(t))}{2} - \frac{\Gamma}{2}\}E(t), \tag{4}$$

$$\dot{N}(t) = J - \gamma_N N(t) + G(N(t))|E(t)|^2, \tag{5}$$

In these equations, the following parameters, describing device-specific properties and operation conditions, are relevant for appropriate modeling of the dynamical properties of specific semiconductor lasers: the resonator losses Γ; the carrier decay rate γ_N; and the pumping coefficient, J, which is related to the experimental pump parameter,

$$p = \frac{I_{DC}}{I_{th}}, \tag{6}$$

$$J = \frac{pI_{th}}{e}, \tag{7}$$

where I_{DC} denotes the injection current, I_{th} the laser threshold current, and e the electron charge. Furthermore, description of the characteristic behavior of the optical gain, *G(N(t))*, and the laser frequency, $\omega(N(t))$, of the specfic semiconductor laser is requried, both being nonlinear functins of the carrier density *N(t)*. However, for conventional operation conditions, linearizion of *G(N(t))* and $\omega(N(t))$ around the laser threshold is justified:

$$G(N) = G(N_{th}) + \xi(N - N_{th}) = \Gamma + \xi\Delta N, \tag{8}$$

$$\omega(N) = \omega_o + \omega_N(N - N_{th}) = \omega_o + \frac{\alpha}{2}\xi\Delta N, \tag{9}$$

Here, ξ denotes the differential gain; while ω_o, stands for the laser frequecny at threshold; and $\alpha = \frac{2\omega_N}{\xi}$ represents the so-called linewidth enhancement factor of the semiconductor laser. Sustituion of the linearized expressions for the optical gain, Eq. 8, and the oscillation frequency of the laser, Eq. 9, into Eqs. 6 and 7 leads to the well-known semiconductor rate equations. these equations descrive the nonlinear relation between slowly varying amplitude of the complex electrical field, $E(t) = |E(t)|e^{i\phi(t)}$, and the carrier density, $N(t)$:

$$\dot{E}(t) = \frac{1}{2}(1 + i\alpha)\xi\Delta N(t)E(t), \tag{10}$$

$$\dot{N}(t) = J - \gamma_N N - (\Gamma + \xi\Delta N(t))|E(t)|^2, \tag{11}$$

Thus two-dimensional equation can be solved analytically, while the solutions can be given in a closed manner. Since the semiconductor laser rate-equation represent a two-dimensional system, the equations only allow for periodic solutions, and not for chaotic behavior. Dimensionality of dynamical systems can be increase by introduction additional degrees of freedom to the systems. If the dimension of the modified systems is three of higher, the systems distinguish themselves from the previous systems in the their dynamics can exhibit extreme sensitivity against small changes of the initial conditions. In other words, such modified systems allow for deterministic chaos.

2.2 Semiconductor Lasers as Dynamical Systems

In the late 1970s, it was reported that the emission properties of semiconductor lasers considerably change if the semiconductor laser is subject to external optical feedback (FB) from a distant reflector. Since then, semiconductor lasers with FB have been intensively studied and motivated by two major reasons. On the one hand, the high sensitivity of semiconductor lasers to FB is very important for technical applications of semiconductor lasers. In many applications. Semiconductor lasers are unintentionally subject to reflections from distant system components which can easilv destabilize the laser and result in complex emission dynamics. This effect can impair functionality of various devices which are based on semiconductor technology, e.g, in CD/DVD data storage/readout systems or in optical fiber based high-speed telecommunication devices.

Semiconductor lasers allows for application of nonlinear dynamics for controlled suppression of feedback induced instabilities. Within the last four decades, sophisticated solutions have been developed utilizing delayed feedback for stabilization of the output of semiconductor lasers and for narrowing the linewidth of the emitted light [3, 62, 138]. In contrast to the commonly desired stabilization of the emission dynamics of semiconductor lasers, modern technology even aims for utilization of feedback induced instabilities. Recently, the intriguing properties of high-dimensional chaotic dynamics have attracted much attention since they offer potential for realization of novel applications which are based on utilization of chaotic signals. In particular, semiconductor lasers with FB offer auspicious dynamical properties which can be harnessed for realization of innovative optical technology, e.g., for encrypted communication devices [163, 193], for optical data readout systems and frequency tuning [173], or for high-resolution chaotic LIDAR systems [105].

From the nonlinear dynamics point of view, semiconductor lasers with FB are well-controllable nonlinear systems. Therefore, in recent years, the emission dynamics of

such semiconductor laser systems has been intensively studied and various nonlinear dynamical phenomena, comprising high-dimensional chaotic intensity dynamics, has been identified [175, 198]. The appearance of different dynamical regimes in these semiconductor laser delay systems essentially depends on the pump parameter and on the main feedback parameters; the strength of the optical feedback; i.e., the amount of light that reenters the active region of the semiconductor laser, the length of the external cavity and the feedback phase [195]. In general the degrees of freedom in lasers are confined in a few experimentally controllable ones. That along with their fast timescale, which allows clear distinction of dynamical states rather than transients, makes lasers ideal candidates for dynamical investigation among many other dynamical systems. Many of the results obtained so far have given an insight into key questions of the field of nonlinear dynamics highlighting the high value of these practical experimental systems.

So far, the dynamics of lasers can be described by a set of equations known as Maxwell-Bloch equations for the electric field, polarization and population inversion. According to the decay rates of these three quantities, lasers can be categorized into three classes. In class A lasers, the polarization and population inversion decay on much shorter timescale than the electric field and the two quantities become adiabatically followers of the electric field. Consequently, Maxwell-Bloch equations can safely be reduced to one equation describing the electric field amplitude. Therefore, class A lasers are the most stable lasers with a high Q-factor among other lasers. Nevertheless, this class of lasers can exhibit chaotic behaviour by external perturbation of two or more extra degrees of freedom. In class C lasers, the three decay rates are comparable and the system has to be described by the full set of Maxwell-Bloch equations.

In class B lasers as in the case of semiconductor lasers, the polarization time constant is small enough compared to that of the other quantities, i.e. electric field

and population inversion, and the polarization equation is adiabatically eliminated. In other words, semiconductor lasers are intrinsically stable lasers that can be fully described by two quantities: the electric field and the population inversion. The interplay between these two quantities produces the light-carrier density oscillation or the so-called ROF. In contrast to other lasers, the population inversion is simply replaced by electron concentration and the electric field is employed with its complex amplitude, i.e. the amplitude and the phase of the field. Therefore semiconductor lasers are usually described by three rate equations, the two equations for the electric field and electron concentration and a third equation for the phase.

Although semiconductor lasers are intrinsically stable lasers, it is possible to produce instabilities and chaos in a single-mode semiconductor laser by adding at least one additional degree of freedom. For accomplishing such task, there are several approaches that can be implemented :

1. Modulation of the injected current:

   This method represents the easiest way to produce chaos in semiconductor lasers. As the modulation frequency of the injection current exceeds the relaxation oscillation frequency, period-doubling bifurcation appears. Transition to chaos is achieved by further increasing the modulation frequency.

2. External optical feedback:

   In this method, the laser is perturbed through the injection of its output by means of a distant feedback reflector. This scheme is advantageous in producing high dimensional chaos due to the delay-induced dynamics and in achieving high bandwidth. Moreover, it is very simple to be implemented and analysed and it has been used in chaotic synchronization [31]. However, the fact that semiconductor lasers are circuit elements with inherent capacitance, conductance, and resistance may limit a perfect use of these two approaches.

3. External optical injection:

   This perturbation mechanism seems to be the most efficient approach to produce controlled and accessible instabilities. Its main attractive feature is that the laser is perturbed with an independent optical field, which provides direct information about the laser cavity and gain medium. This method has been successfully implemented to achieve a number of applications including injection locking, frequency stability, and noise reduction. Among them, the generated chaos and injection locking are the most interesting and promising advantage of external optical injection and hence are briefly discussed in the following section.

From the nonlinear dynamics point of view, semiconductor lasers with feedback are well-controllable nonlinear systems. Therefore, in recent year, the emission dynamics of such semiconductor laser systems has been intensively studied and various nonlinear dynamical phenomena, comprising high -dimensional chaotic intensity dynamics, has been identified. During the last years it has been shown that *External Cavity* configurations are very practical and versatile configuration for studying feedback induced dynamics in semiconductor lasers.

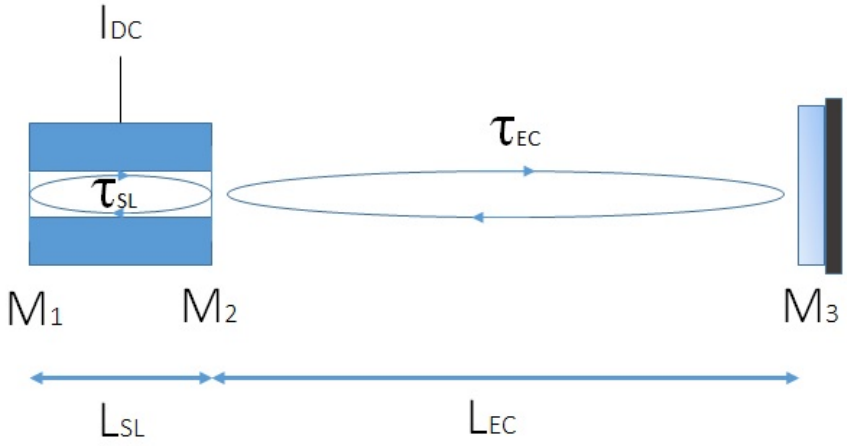

Figure 5: Scheme of a semiconductor laser subject to delayed optical feedback.

Figure 5 schematically illustrates an ECSL. In this configuration a solitary semiconductor laser with facet reflectivities M_1 and M_2 is pumped by a constant injection current I_{DC}, while the light emitted by the semiconductor laser propagates towards a distant mirror, with reflectivity M_3, from which it is reflected back into the semiconductor laser after a time delay τ_{EC}. Hence, the semiconductor laser is subject to time-delayed optical feedback. In the figure L_{SL} and L_{EC} denote the length of the semiconductor laser cavity and the external cavity (EC), respectively. Here the external cavity is defined by the front facet of the semiconductor laser and the external mirror. Corresponding to both lengths, one additional relevant time scale is present in the ECSL system, in addition to the time scales of the light-matter interactions in the semiconductor laser which we have discussed in Section 1.1. For this reason, ECSLs exhibit a large hierarchy of time scales which enter the dynamical properties. The time corresponding to one round trip of the light inside the semiconductor laser cavity: For conventional semiconductor laser with a cavity length of $L_{SL} \sim 300$ μm the round trip.

2.2.1 Modeling Feedback-Induced Dynamics of Semiconductor Lasers

ECSLs dynamical properties are very interesting from the fundamental nonlinear dynamics point of view. Detailed experimental analysis of ECSLs which can give insight into the fundamental properties of the dynamics is possible, but it requires sophisticated measurement technology. Experimentally we only can gain insight into properties of dynamics utilizing accessible parameters and variables. In real-world experiments, however, usually some of the relevant system variables and parameters are difficult to measure or are even inaccessible. In particular, in ECSLs this applies to gain properties and phase of the complex electric field. In this context appropriate modeling can provide further insight into fundamental processes underlying the dynamics. This is due to the inherent property of models that the included parameters

and variables are principally, mathematically accessible. Of course, the major difficulty of modeling consists in developing an appropriate model that accurately mimics the experiment.

As the expression "model" already implies, mathematical modeling refers to a theoretical construct which is devised to mimic processes of real-world systems. Therefore, mathematical models necessarily represent subjective and therefore simplified representations of real world systems. From the physical point of view, modeling serves as a means to enhance the scientists insight into the real-world system by uncovering experimentally hidden processes. In that sense, a model can be treated as a good model if it not only reproduces observed phenomena, but even more so if it provides new insight into inaccessible processes and if it allows for predictions of new physical phenomena. Predictions, in turn, are obliged to be categorically verifiable. Conversely, a mathematical model needs to be abandoned or refined if its predictions are in contradiction to experimental observations.

In the next subsection, we will follow these considerations and present a simple mathematical model for description of the emission properties of ECSLs. We will demonstrate that although the model is based on several, to some extent even severe, assumptions its results and predictions are in excellent agreement with experimentally observed phenomena of conventional ECSLs. The model provides insight into fundamental processes leading to the dynamical instabilities of ECSLs and their characteristic emission properties.

2.2.2 LK Semiconductor laser Rate-Equations

The LK model provides a single-longitudinal-mode description of a semiconductor laser in terms of rate equations. It must be born in mind that this approach integrates out spatial degrees of freedom; nonetheless, while obtaining perfect agreement between theory and experiment is not expected, the LK equations reliably predict

some dynamical trends as a function of various parameters [132].

We model the LD as a Fabry-Perot resonator consisting of a dielectric medium confined between two mirrors. The light traveling both in the forward and in the backward directions is amplified due to stimulated emission; it is furthermore partially reflected and partially transmitted at each mirror [Fig. 3].

In the previous section, we have discussed the semiconductor laser rate-equation model Eqs. 10 and 11 which have become an established model for description of the emission properties of solitary semiconductor lasers. The semiconductor laser rate-equations can serve as basis for modeling ECSLs. To describe the dynamics of ECSLs, one has to account for delayed optical feedback in the model. In 1980, Lang and Kobayashi proposed an extended version of the semiconductor laser rate-equations [91]. In their model, they introduced an additional feedback expression ($\kappa e^{-i(\Phi(t)+\Phi_o)}E(t-\tau_{EC})$) to the equation of the complex electric field, Eg. 10, incorporating delayed optical feedback. The resulting equations are commonly referred to as LK equations (LK):

$$\dot{E}(t) = \frac{1}{2}(1+i\alpha)\xi\Delta N(t)E(t) + \kappa e^{-i(\Phi(t)+\Phi_o)}E(t-\tau_{EC}), \tag{12}$$

$$\dot{n}(t) = (p-1)\frac{I_{th}}{e} - \frac{n(t)}{T_N} - (\Gamma + \xi n(t))|E(t)|^2, \tag{13}$$

The first term on the right-hand side of the field equation Eq. 12 attributes to the solitary emission. The second term accounts for the external optical feedback, including the external cavity round trip time τ_{EC}, and the feedback rate κ, respectively. Multiple trips of the light in the external cavity are neglected. The phase simulated by the electric field within one round trip in the external cavity is $\Phi_o = \omega_o\tau_{EC}/mod(2\pi)$, where ω_o represents the optical frequency of the solitary laser. In the equations the variables are expressed with respect to the threshold conditions of the solitary laser. Therefore, $n(t)$ represents the excess carrier number (density) with respect to the

solitary laser threshold level: $n(t) = N(t) - N_{th}$, The other parameters are the α-parameter, α; the differential gain, ξ; the solitary laser threshold current, I_{th}; the pump parameter, $p = \frac{I_{DC}}{I_{th}}$; the electron charge, e; the carrier lifetime, $T_N = \frac{1}{\gamma_N}$; and the cavity decay rate, Γ .

The LK rate-equations, Eqs. 12 and 13, represent a dissipative, deterministic model for ECSL. However, in the LK-equations the implementation of delayed optical feedback is based on several assumptions. The major ones comprise neglect of multiple reflections of the light, in the EC and restriction to coherent feedback fields. Furthermore, this base model does not consider noise effects which, under certain conditions, might become important because of the high sensitivity of semiconductor lasers even to small perturbations. Additionally, nonlinear gain saturation effects are not taken into account which potentially can influence the dynamics for moderately strong feedback and high injection currents. Both effects, noise and nonlinear gain saturation, can be included in the model. if required. In this case it is convenient to describe the dynamics of the ECSL in terms of the physically relevant absolute values of the output variables, which allows for direct comparison of experimentally obtained from modeling. On the other hand, the corresponding notation better reveals the influence of gain saturation effects. Accordingly, the rate-equations governing the electric field and the carrier number read:

$$\dot{E}(t) = \frac{1}{2}(1 + i\alpha)\xi\Delta N(t)E(t) + \kappa e^{-i(\Phi(t)+\Phi_o)}E(t - \tau_{EC}) + F_E, \tag{14}$$

$$F_E = \sqrt{2\beta N}\zeta, \tag{15}$$

$$\dot{N}(t) = \frac{pI_{th}}{e} - \frac{N(t)}{T_N} - \mathcal{G}|E(t)|^2, \tag{16}$$

$$\mathcal{G} = \frac{\xi(N(t) - N_o)}{1 + \varepsilon|E(t)|^2}, \tag{17}$$

In the model, complex Gaussian random terms $\zeta(t)$ are added in the field equations to model spontaneous emission processes. These numbers have zero mean $\langle\zeta(t)\rangle = 0$ and auto-covariance function $C_x(t-t') = \langle\zeta(t)\zeta(t')\rangle = 2\zeta(t-t')$. β is a spontaneous-emission noise factor. The gain function in Eq. 17 is approximated to depend linearly on the instantaneous carrier number and accounts for gain-suppression effects. Meaning of the remaining parameters can be found in Table 1. Other parameters will be specified in the context. In order to give an impression of reasonable values for numerical modeling. We also present device-typical values for the Mitsubishi distributed feedback Laser diode (ML725B11F). figure 8 shows

Table 1: Physical and device parameters for modeling

Symbol	Meaning	Value
$\mathcal{G}$	optical gain	8.1×10^{-13} m^{3}s^{-1}
α	linewidth enhancement factor	3
Γ	cavity decay rate	200 ns^{-1}
T_N	carrier life time	1 ns
N_o	transparent carrier number	1.1×10^{24} m^{-3}
ε	gain suppression coefficient	5×10^{-7} ns^{-1}
β	spontaneous emission factor	$0 \sim 1000$
I_{th}	solitary threshold current	$\approx 10mA$

Depending on the particular experiment, we utilize both versions of the LK-equations for complementary analysis of the experiments. On the one hand, analytical treatment of the LK-equations can give insight into local and global structures of the phase space in which the dynamics evolves. However, analytical treatment is challenging because the LK-equations are differential delay equations which are mathematically infinite dimensional. Additional difficulties arise from the broad range of time scales involved in the dynamics. Therefore, analytical insight into the dynamical properties of ECSLs is challenging. Nevertheless, such analytical treatment of the

LK-equations is far from being simple so that most of the insight into the dynamical properties of the LK-equations is currently restricted to basic solutions, such as determination of fixed points and periodic solutions with its corresponding stability analysis. On the other hand, numerical modeling allows for application of methods of time series analysis. Once the model parameters are experimentally determined and the model agrees with the experiment, the equations can be numerically integrated with appropriate step size. Then, numerically obtained time series allow for quantitative estimation of information-theory based measures, such as Lyapunov Exponents, Information Dimension, Kolmogorov-Sinai entropy. This is very useful, since these measures are experimentally not accessible because of existing limits in detection bandwidth and resolution.

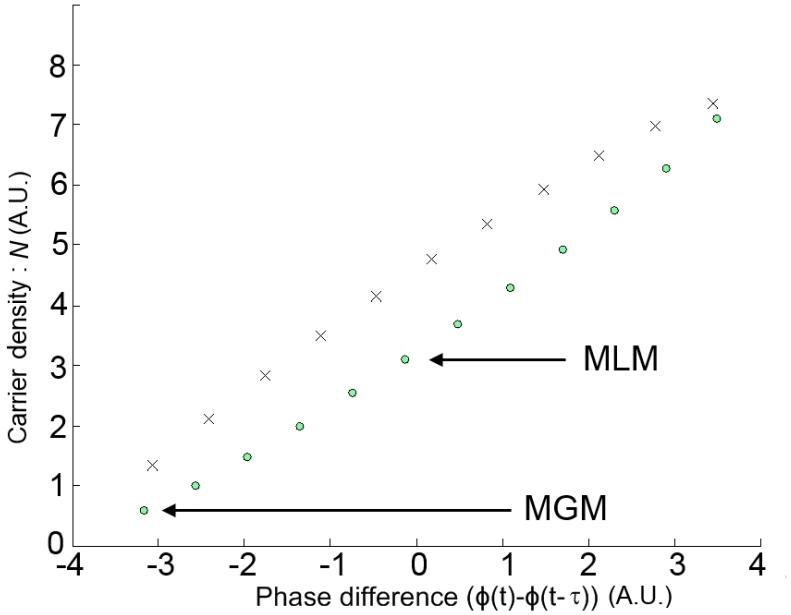

Figure 6: Ellipse structure of fixed points in the phase-difference-vs.-N plane for κ = 0.007 and τ_{EC}= 1 ns. Circles represent ECMs; crosses represent antimodes.

To attain fundamental information about the dynamical properties of the LK-model, it is straightforward to analyze the fixed point structure of the deterministic model equations, Eqs. 14 and 16. The fixed point solutions can be obtained by substituting the $E(t) = Ae^{i\omega t}$, $n(t) = n = constant$ into Eqs. 14 and 16 leading to a

set of equations, Eqs. 18 and 19:

$$\Delta\omega\tau_{TC} = \kappa\tau_{EC}\sqrt{1+\alpha^2}sin[(\omega_o + \Delta\omega)\tau_{EC} + \arctan\alpha], \tag{18}$$

$$(\kappa\tau_{EC})^2 = (\Delta\omega\tau_{EC} - \frac{\alpha}{2}n\xi\tau_{EC})^2 + (\frac{n\xi\tau_{EC}}{2})^2, \tag{19}$$

The solutions to this problem reveal a fixed point structure located on an ellipse around the solitary laser mode in the phase space spanned by the inversion, n, and the frequency ω. In this space, each of the fixed points is defined by a constant optical frequency $\omega = \omega_o + \Delta\omega$ and a constant carrier number n, where ω_o denotes the frequency of the solitary laser mode. The fixed points on the ellipse occur pairwise while the two fixed points of each pair have different stability properties. These two solutions are referred to as Mode and Anti-Mode. The first is the possibly stable ECMs, while the second are the unstable antimodes that correspond to saddle points [115]. These solutions, when plotted in the $N(t)$ versus phase-difference $\Delta\Phi(t) = \Phi(t) - \Phi(t-\tau)$ plane, lie on an ellipse [66] as shown in Fig. 6, where the ECMs are indicated by circles while antimodes are represented by crosses. The solitary laser mode is located in the center of the ellipse appointing it name as the *Minimum Linewidth Mode* (MLM). The MLM is the ECM most proximate in frequency to the solitary laser mode. For increasing the feedback rate κ, the modes and anti-modes consecutively are created in pairs at the low frequency end of ellipse. This occurs in a *Saddle-Node* bifurcation from which the modes follow the stable branch, while the anti-modes follow the unstable branch. Subsequent to the saddle-node bifurcation, each newly created mode may destabilize to a *Hopf* bifurcation for increasing feedback rate. However, at least one mode at the low inversion edge of the ellipse is always stable. Since for this mode inversion is lowest, it exhibits highest gain, appointing its name as the *Maximum Gain Mode* (MGM).

Physically, the modes represent solutions corresponding to constructive interference condition between the feedback field and the field in the semiconductor laser, while the anti-modes to the destructive interference condition. For this reason, the fixed point solutions are also referred to as *External Cavity Modes*. The ellipticity, the orientation and the extension of the ellipse in the $N(t)$ versus phase-difference $\Delta\Phi(t) = \Phi(t) - \Phi(t-\tau)$ plane, additionally, the number of cavity modes influence the dynamical properties. In the general time-dependent case, a trajectory in the space shown in Fig. 6 is traced out parametrically in time, indicating the detailed evolution of all dynamical variables of the system. The time-dependent intensity can be extracted from the phase-space trajectory and used to construct a theoretical BD which in turn can be compared with the experimental BD. Thus the connection between dynamical regime as manifested in the BD and the detailed dynamics can be made.

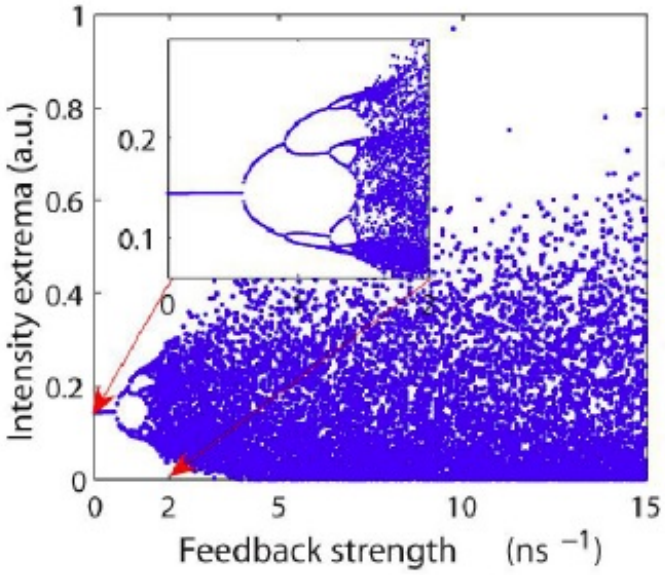

Figure 7: The BD of route to chaos by an ECSL when $p = 1.08$ and $\tau_{EC} = 1$ ns.

We have depicted in fig. 7 the BD of a route to chaos undergone by an ECSL with Lang and Kobayashi semiconductor rate-equation, when the feedback strength

κ is taken as the bifurcation parameter. In fig. 8, we also show chaotic intensity time series $I(t) = |E(t)|^2$ and the associated RF spectrum and phase diagram. Detailed studies on the destabilization of ECM and existence of various routes to chaos have been reported, for instance, in [198, 220].

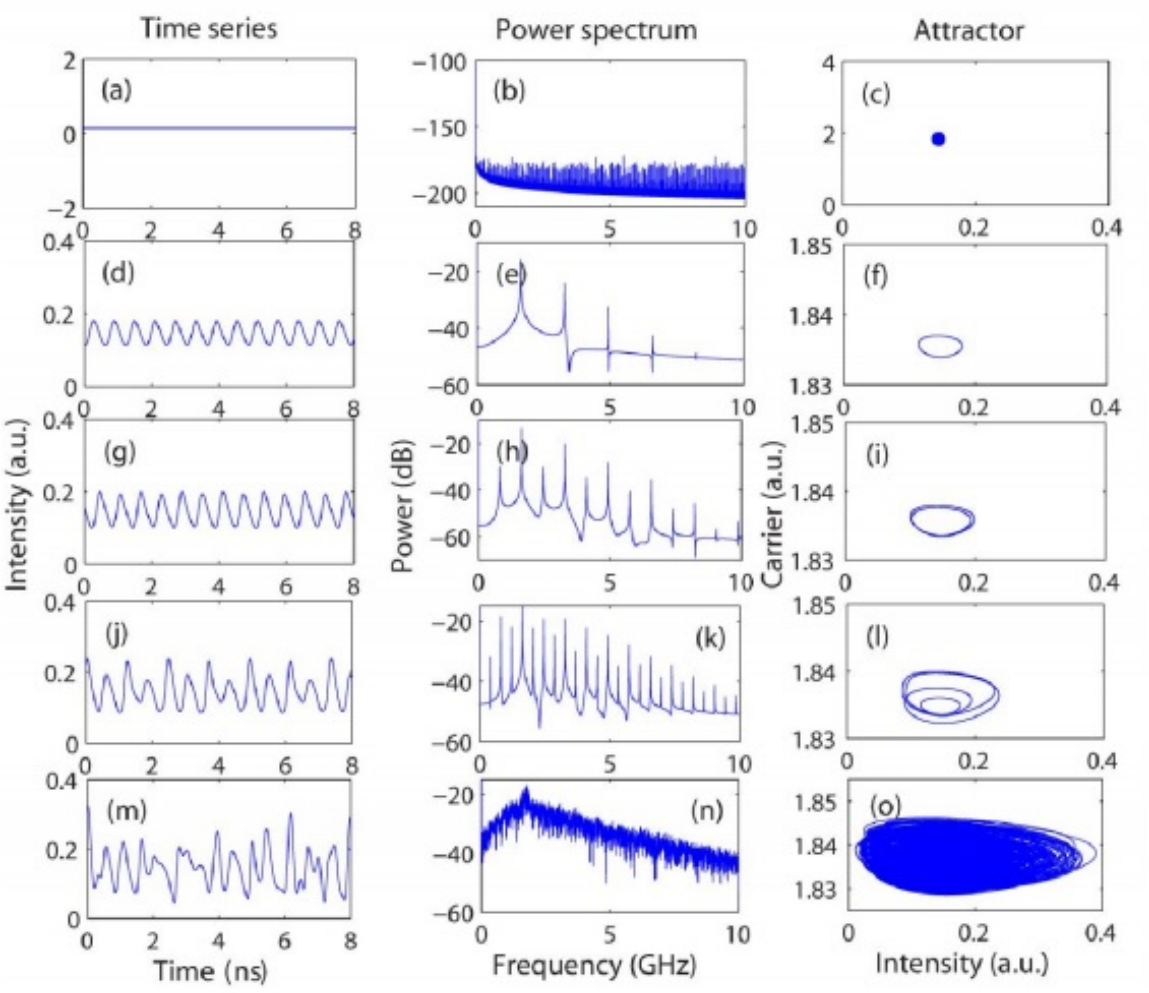

Figure 8: (a)-(c): $\kappa = 0.2$ ns^{-1}, (d)-(f): $\kappa = 0.7$ ns^{-1}, (g)-(i): $\kappa = 0.9$ ns^{-1} (j)-(l), $\kappa = 1.3$ ns^{-1}, and (m)-(o): $\kappa = 3$ns^{-1}

The great advantage of the LK-model originates from its balance between complexity and simplicity. The model is complex enough to capture numerous nonlinear dynamics phenomena, but, it is just simple enough to allow for some elementary analytic investigations and to facilitate physical interpretation of the results. However, some peculiar ECSLs or conventional ECSLs under extreme operation conditions

exhibit dynamical phenomena are beyond capability of the LK-model. To prevent inappropriate application of the LK-model, its restrictions need to be considered with respect to the particular experimental conditions.

During the last decade, analysis of the dynamics of ECSLs has mainly focused on ECSLs operating in the long cavity regime (LCR) in which the external cavity round trip frequecy $f_{EC} = 1/\tau_{EC}$ is sufficiently smaller than the relaxation oscillation frequency f_{RO} of the semiconductor laser. This is motivated by two reasons. On the one hand, experiments in the LCR are very robust and the essential system parameters are well-controllable. On the other hand, the dynamics in this regime reveals interesting nonlinear phenomena comprising also dynamics which exhibits conspicuous features on comparatively slow time scales that are experimentally well-accessible, e.g random switching between stable emission and dynamics, and irregular intensity dropouts in LFF dynamics. For these reasons, ECSLs operating in the LCR are excellently suited for studying the on-set of chaotic dynamics in high-dimensional delay systems, especially when limitations in resolution and bandwidth of the detection devices are inevitable. Therefore, our experimental work has mainly focused on investigation of the emergence of ECSLs in the LCR.

CHAPTER III

BIFURCATION DIAGRAM OF AN EXTERNAL-CAVITY SEMICONDUCTOR LASER IN LOW INJECTION CURRENT CASE

We report detailed experimental BDs of an ECSL. We have focused on the case of a distributed feedback laser biased up to 1.6 times the threshold current and subjected to feedback from a distant reflector. We observe bifurcation cascades resulting from the destabilization of external-cavity modes that appear successively when the feedback is increased, and explain, in light of the LK model, how the cascading is influenced by various laser operating parameters (current, delay, feedback phase) and experimental conditions. The qualitative agreement between experiments and simulations validates over a large range of operating parameters, the LK model as a tool for reproducing the salient aspects of the dynamics of a distributed feedback laser subjected to external optical feedback.

This chapter is based on the following publications:

1. Byungchil Kim, Locquet, A., Nianqiang Li, Daeyoung Choi, Citrin, D.S., "Bifurcation Cascade Diagrams of an External-Cavity Semiconductor Laser: Experiment and Theory," in Quantum Electronics, IEEE Journal of , vol.50, no.12, pp.965-972, (2014).

2. B. Kim, N. Li, A. Locquet, and D.S. Citrin, "Experimental bifurcation-cascade diagram of an external-cavity semiconductor laser," Opt. Express 22, 23482357 (2014).

3. B. C. Kim, N. Li, A. Locquet, and D.S. Citrin, "Bifurcation diagram of an

external-cavity semiconductor laser: experiment and theory," SPIEs Photonics Europe 2014, Proceedings of SPIE paper 9134-77, Brussels, Belgium.

3.1 Introduction

An ECSL, which utilizes the external cavity to provide time-delayed optical feedback into the gain region of the LD, displays various dynamical behaviors depending on the operating and design parameters. In particular, delayed feedback induces an infinite-dimentional phase space and allows for chaotic behavior in ESCLs [77, 132]. More broadly, the dynamics of ECSLs has been extensively studied [21,69,115,123,184,204] and they are expected to be employed for numerous applications such as secure communication [16, 17, 164, 200], light detection and ranging (LIDAR) [105], random-number generation [78,200,201], and reservoir computing [11]. Despite years of interest in these systems, experimental investigations on ECSLs have suffered from a lack of detailed knowledge of the various dynamical regimes that can be accessed as a function of the various operating parameters, such as the feedback strength, the injection current I, and the external cavity length L (creating a delay τ), for example. Valuable information concerning the detailed dynamical regimes, and transitions between them, can be conveniently summarized in easily visualized BDs. Several theoretical and numerical works have studied in detail the BDs of ECSLs as a function of the feedback strength [34, 49, 212]. Though experimentalists have investigated changes in intensity time series or in the optical/RF spectra for a discrete set of operating parameters but before our recent work [81], no BD based on a continuous tuning of a parameter had been obtained. In this chapter, we seek to further elucidate the dynamics of ECSLs by means of BDs.

The chaotic transitions in long-cavity ECSLs for given L, I, and feedback strength fall under a rich range of types, and various routes to chaos have been observed. A common one is the quasi-periodic route [124], in which a stable ECM is replaced by a periodic oscillation at a frequency close to the relaxation-oscillation frequency f_{RO} of the solitary LD, then quasi-periodicity, involving a second frequency close to $1/\tau$, and chaos are observed. A period-doubling route to chaos has also been observed [220],

in which a cascade of period-doubling bifurcations creates oscillations at frequencies close to sub-multiples of f_{RO}. Other possibilities also exist. When the conditions are such that several ECMs are destabilized simultaneously, generalized multistability ensues as several attractors or attractor ruins coexist in phase space [115, 150]. In this case, numerous phenomena related to attractor switching may be expected in a BD. One remarkable example is the switching between a LFF state and a state of stable emission as was observed in [60].

Considerable and systematic information concerning the dynamical regimes and the bifurcations between them is conveyed by the BD obtained by fixing all but one parameter and then mapping out the extremal values of a conveniently measured dynamical variable as the parameter varies. Investigation of BDs therefore provides a new vantage point from which to view ECSLs. In particular, BDs provide clear and systematic experimental evidence of the way in which instabilities of various nature develop in an ECSL. There are two important motivations to the further investigation of ECSL BDs that reveal links between various types of dynamical behavior. The first is that it provides a global picture of the dynamical system. Second, and more important, it enables systematic investigations of the rich variety of dynamical behavior observed in ECSLs, including LD stationary dynamics, multistability, intermittency between stable states, and various routes to chaos, in terms of transitions between these types of behavior.

By way of providing context for our work, a number of theoretical studies of ECSL BDs as a function of the feedback strength have been presented [77, 132]. Experimental BDs have been obtained for other kinds of lasers such as erbium-doped fiber lasers subjected to pump modulation [157], optically injected solid-state lasers [203], Q-switched gas lasers [12,117], and bifurcations transitions have been identified in LDs subjected to optical injection [181,214]. In our recent paper [81], we overcame the experimental difficulties, prevented the existence of BDs for ECSLs, which η is

controlled in small steps by means of a motorized rotation stage in high-stability conditions which allows for very good horizontal resolution of the BDs.

In this Chapter, we present a more systematic investigation, in light of experimental BDs, of the influence of operational parameters (current, length, feedback level, feedback phase) and conditions (forward and reverse BDs, influence of noise) on ECSL dynamics. Furthermore, to elucidate the underlying dynamics observed experimentally, we provide extensive theoretical studies based on the LK model. It is worth noting here that in the simulation we have identified the dynamical regimes and the instabilities involved in the cascade of bifurcations, as well as the influence of I and L on the cascade thus illustrating the dynamical regimes and their bifurcations over a wide range of parameters. More importantly, our numerical results show good qualitative agreement with the experimental results, validating the effectiveness of the BDs obtained experimentally. Our work thus connects the measured experimental BDs with theoretical phase-space trajectories, i.e., the multidimensional dynamics of the system. The agreement between experiment and simulation validates, within the boundary of the parameters range considered and of the examined phenomena, but over a large range of continuously tuned parameters, the LK model as a tool for reproducing the salient aspects of the dynamics of a distributed feedback laser subjected to coherent optical feedback.

3.2 Theoretical Framework

The LK model provides a single-longitudinal-mode description of a semiconductor laser in terms of rate equations. It must be born in mind that this approach integrates out spatial degrees of freedom; nonetheless, while obtaining perfect agreement between theory and experiment is not expected, the LK equations reliably predict some dynamical trends as a function of various parameters [77, 132]. They are thus widely used. In the LK model, the external cavity is described by three parameters:

theoretical feedback strength κ (proportional to experimental feedback strength η), delay time τ (proportional to L), and the feedback phase $\omega_o\tau$, with the solitary laser angular frequency ω_o. The (complex) electric-field amplitude $E(t)$ and the carrier density $N(t)$ are the solutions of

$$\frac{dE}{dt} = \frac{1+i\alpha}{2}\left(\mathcal{G} - \frac{1}{\tau_p}\right)E(t) + \frac{\kappa}{\tau_{\text{in}}}E(t-\tau)e^{-i\omega_o\tau} + F_E, \tag{20}$$

$$\frac{dN}{dt} = pJ_{\text{th}} - \frac{N(t)}{\tau_s} - \mathcal{G}|E|^2. \tag{21}$$

with $\mathcal{G} = G[N(t) - N_o]$ being the optical gain where G is the gain coefficient and N_o is the carrier density at transparency. In addition, τ_p is the photon lifetime, τ_s the carrier lifetime, τ_{in} the optical round-trip time within the laser cavity, α the linewidth-enhancement factor, p the pumping factor, and J_{th} the threshold current. The spontaneous-emission noise is modeled by a term $F_E = \sqrt{2\beta N}\xi$, where β is a spontaneous-emission noise factor and ξ is a complex Gaussian white noise of zero and auto-covariance function $C_x(t-t') = \langle\xi(t)\xi(t')\rangle = 2\xi(t-t')$. We numerically integrated Eqs. 20 and 21 with the following parameters: $G = 8.1\times10^{-13}$ m^{3}s^{-1}, $N_o = 1.1\times10^{24}$ m^{-3}, $\tau_p = 1$ ps, $\tau_s = 1$ ns, $\tau_{\text{in}} = 8$ ps, $\alpha = 3$, and $\omega_o\tau = 0$. Other parameters will be specified in the context.

The time-dependent intensity can be extracted from the phase-space trajectory and used to construct a theoretical BD which in turn can be compared with the experimental BD. Thus the connection between dynamical regime as manifested in the BD and the detailed dynamics can be made.

3.3 Experimental Setup

The experimental setup is shown in Fig. 9. Light from the LD is split into two free-space optical paths using a beam splitter (BS). One optical path is used for feedback into the LD and the other is for coupling and/or observing the dynamics

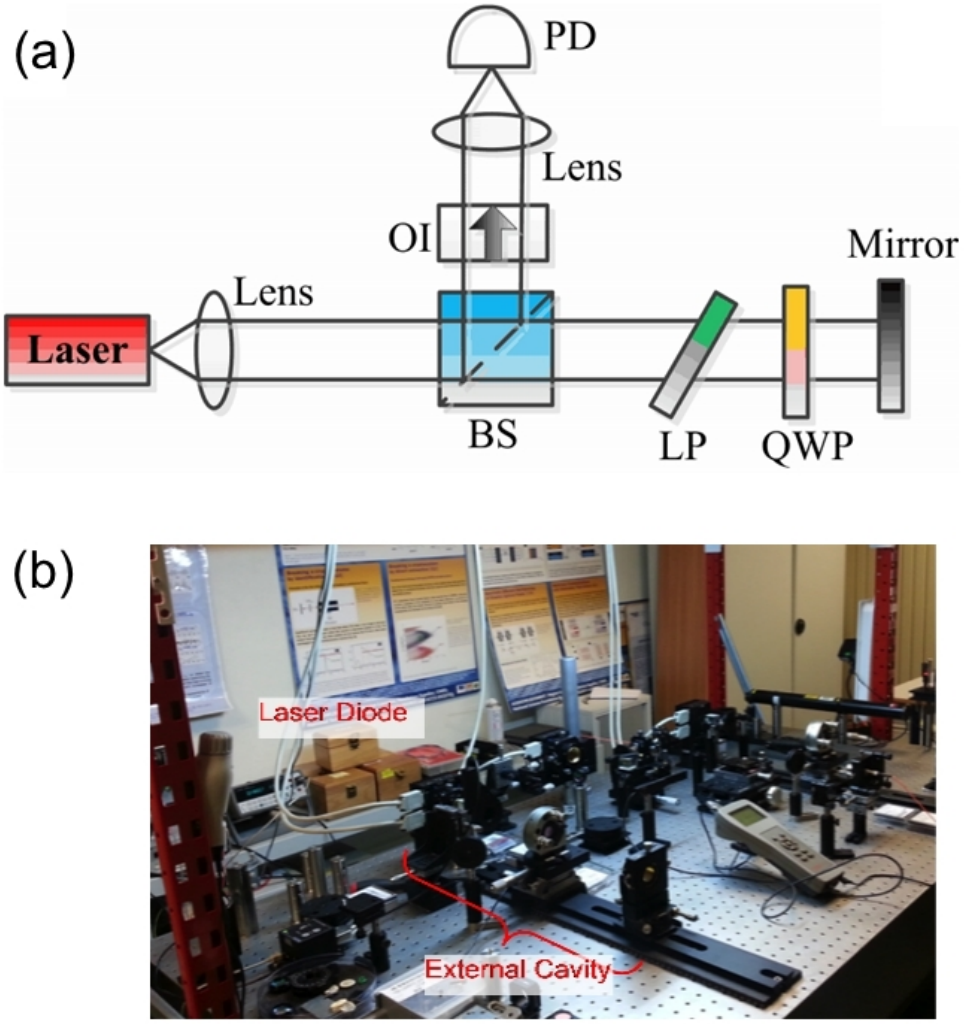

Figure 9: (a) Experimental setup. PD: photodiode, BS: beam splitter, LP: linear polarizer, QWP: quarter-wave plate, OI: optical isolator. (b) A setup showing an ECSL in the lab at GTL

of the intensity detected at the photodiode. The semiconductor laser used in our experiments is an intrinsically single-longitudinal mode InGaAsP distributed feedback laser that oscillates at wavelength 1550 nm with maximum power of 15 mW. The free-running threshold current ($I_{\rm th}$) is 9.27 mA. A real-time oscilloscope with 12 GHz bandwidth is employed to capture the time series of the optical-intensity time series. In addition, we measure the RF spectrum of the optical intensity with a spectrum analyzer with a 23 GHz bandwidth. The optical spectrum is measured with a scanning Fabry-Perot interferometer of 10 GHz free spectral range and finesse equal to 150. L

is variously chosen to be 15, 30, or 65 cm which corresponds to external-cavity round time $\tau = 1$, 2, or 4.3 ns, respectively.

It is essential to have highly stabilized temperature (temperature stability / 24 hours $< 0.002\,^\circ$ C) and current I (drift / 24 hours $< 100\ \mu$A) to ensure reproducibility. In addition, η is controlled in small steps by slowly changing the angle of the quarter-wave plate (QWP) in the external cavity by means of a motorized rotation stage. This allows for very good horizontal resolution of the BDs; indeed, the rotation velocity is 0.01 degree/minute and the resolution of the angle of QWP is 1/100 degree, leading to a 4500 possible different values of the feedback in a BD. The maximum feedback attainable in our experiment, corresponding to $\eta = 0.8$, is reached when the QWP is such that the polarization is not subjected to any rotation. Then, approximately 20% of the optical power is fed back onto the collimating lens.

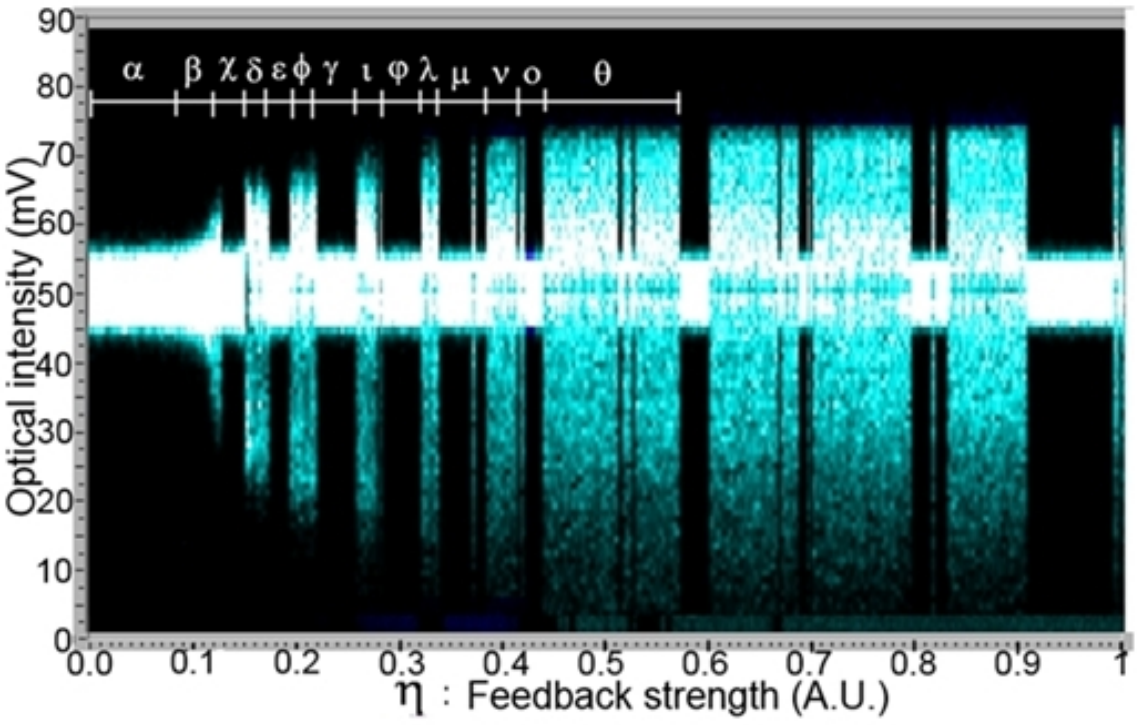

Figure 10: Experimental BD of I=11.24 mA and L=30 cm.

3.4 Experimental Bifurcation Diagram

Figure 10 shows the experimentally observed BD for injection current $I = 11.24$ mA. Here $L = 30$ cm, resulting in a frequency spacing between ECMs of ∼500 MHz. The experimental BD is obtained by taking the local extrema of the intensity time series from the high-speed oscilloscope used in the experiment as a function of feedback strength η. Density is high in white (blue in the color figure) but low in black regions. A bifurcation cascade between apparently stable and unstable regions is observed. Maximum feedback, corresponding to η=1.0, is reached when the QWP angle is such that the polarization is not subjected to any rotation. In that case, ∼20% of the optical power is fed back onto the collimating lens.

Because of the low current chosen, the photodetected optical intensity is weak and does not always stand out of system noise. Consequently, the thinner regions in the optical intensity, that we call stable, do not necessarily correspond to stable CW behavior but also contain regimes in which instabilities around a single ECM have developed. The wider regions in the optical intensity, referred to as unstable regions, typically correspond to regimes in which trajectories wander around several ECMs and thus clearly stand out of noise.

To further explore the correspondence between experiment and modeling, we show the optical spectrum in Fig. 11, for $I = 11.24$ mA, corresponding to relaxation-oscillation frequency f_{RO} ∼3.2 GHz, as η is increased. It illustrates how the sequence of bifurcations and of ECMs involved corresponds to the numerical predictions. For η ∼0, corresponding to region α of Fig. 12, the optical spectrum of Fig. 11(a) shows that the laser-output power remains in ECM 0, which is close in frequency to the longitudinal mode of the solitary laser (0 GHz). With increasing η, the optical spectrum of Fig. 11(b) shows that 2 neighboring ECMs, called ECMs 1 and -1, at ±0.5 GHz, become active, and f_{RO} becomes undamped and is manifested as sidebands, that appear at around ±3.2 GHz from the ECMs [Figs. 12(β) and 11(b)]. For a further

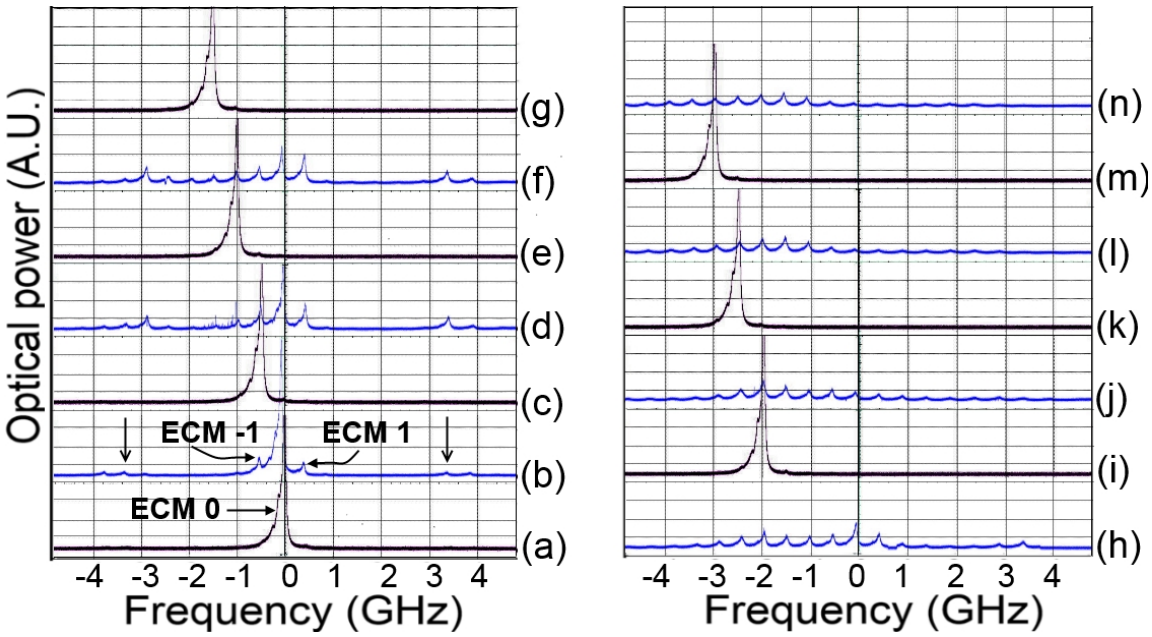

Figure 11: Experimental optical spectrum with FP interferometer for (a) η= 0.0, (b) 0.10, (c) 0.13, (d) 0.16, (e) 0.18, (f) 0.2, (g) 0.24, (h) 0.26, (i) 0.3, (j) 0.33, (k) 0.35, (l) 0.4, (m) 0.42, and (n) 0.48. $I = 11.24$ mA and $L = 30$ cm. The arrows indicate the relaxation sidebands.

increase in η, the spectral peaks at $\pm$0.5 GHz (ECMs 1, -1) become stronger and we observe in the time series of the optical intensity the dropout events typically associated with LFF. As we further increase η, at $\eta = 0.12$, instability stops and stable emission occurs on ECM 1, as can be seen in Figs. 12(χ) and 11(c). We then observe that the same sequence of events, *i.e.* the stable ECMs become destabilized and itinerancy between several neighboring ECMs results until the laser stabilizes again on an ECM shifted in frequency by -0.5 GHz. This occurs experimentally for a total of 10 ECMs, over the entire range of experimentally accessible η.

Moreover, in the unstable regions, we systematically identify LFF, and in particular the typical random power dropouts [Fig. 12(β), 12(δ), 12(ϕ), and 12(ι)], until $\eta \sim$0.26 is reached. In contrast, for higher η, we do not observe LFF but rather a regime of fully developed coherence-collapse. The two regimes can be easily discriminated experimentally by analyzing the optical spectrum; when the dominant modes are around the MLM in unstable regimes [Fig. 11(b), 11(d), 11(f), and 11(h)], LFF

is typically observed; in contrast, when the dominant modes are near the MGM [Fig. 11(j), 11(l), and 11(n)], fully developed coherence collapse is the observed chaotic behavior. It is important to determine the region of validity of the bifurcation casacade between ECMs as the mechanism leading to fully developed coherence collapse. We have observed consistently the presence alternating "stable" and "unstable" regions for all values of the current between $I_{\rm th}$ and 1.5 $I_{\rm th}$. In addition, LFFs are still observed until 1.2 $I_{\rm th}$ when the ECMs lose stability, but the average time between the LFF dropouts typically becomes shorter, as reported in [64].

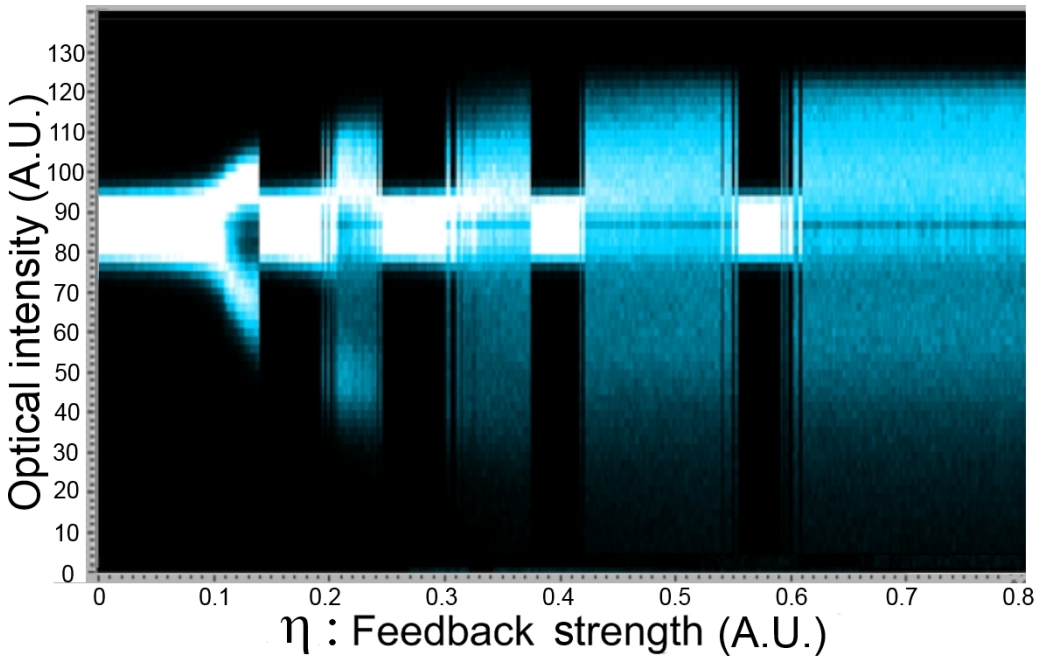

Figure 12: Experimental BD for I=10.54 mA and L=15 cm.

An example of an experimental BD is shown in Fig. 12 for I = 10.54 mA with L = 15 cm, corresponding to a frequency spacing between ECMs of ∼1 GHz. The BD is obtained by taking the local extrema of the intensity time series from the high-bandwidth oscilloscope used in the experiment as a function of η. A probability density function of the extrema of the intensity time series is obtained and plotted with a color map, in which density is high in white (blue in the color figure) but low in black regions. A bifurcation cascade between apparently stable and unstable

regions is observed.

Because of the low current chosen, the photodetected optical intensity is weak and does not always stand out of system noise. Consequently, the thinner regions in the optical intensity, that we call *stable* regions, do not necessarily correspond to stable CW behavior but also contain regimes in which instabilities around a single ECM have developed. The wider regions in the optical intensity, referred to as *unstable* regions, typically correspond to regimes in which trajectories wander around several ECMs as a result of chaotic itinerancy and thus clearly stand out of noise. The first experimental report of a cascade of bifurcations is due to Hohl and Gavrielides [69]. This observation was mainly based on an analysis of the optical spectrum. A detailed study of the optical spectrum can also be found in our previous work [81].

3.5 Varying the Current

In order to analyze the effect of I, we compare the experimentally observed bifurcation cascades for $I = 11.84$ mA, 12.70 mA, 14.67 mA, and 16.01 mA [Fig. 13]. We observe three marked phenomena with increasing I.

For another example, we compare the experimentally observed bifurcation cascades for $I = 11.24$ mA [Fig. 10] and 14.69 mA [Fig. 15(a)]. We observe three marked phenomena with increasing I. The first is that alternating stable and unstable regions are observed, but no longer a systematic cascade involving the successive MGMs. The second is that as I is increased, the BD tends to exhibit large regions of uninterrupted chaotic behavior. Indeed, we have observed consistently the presence of alternating *stable* and *unstable* regions for all values of the current between $I_{\rm th}$ and $\sim 1.6 I_{\rm th}$. However, when $I > \sim 1.6 I_{\rm th}$, we cannot observe any stable region in the entire BD; we conclude that in this case, our laser never lies on or in the vicinity of a single ECM and therefore its dynamics necessarily involves attractor ruins of several ECMs. The third is that for larger I, the stable regions, though limited in number,

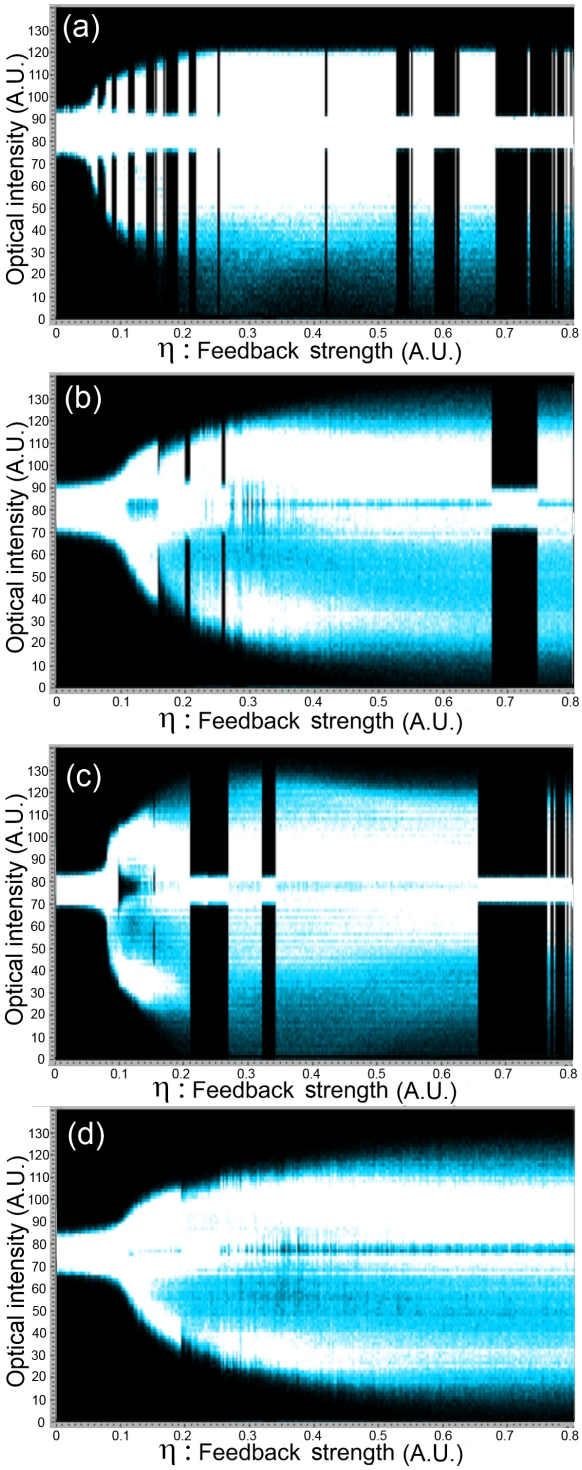

Figure 13: Experimental BDs for $L = 30$ cm with (a) $I = 11.84$ mA, (b) 12.70 mA, (c) 14.67 mA, and (d) 16.01 mA.

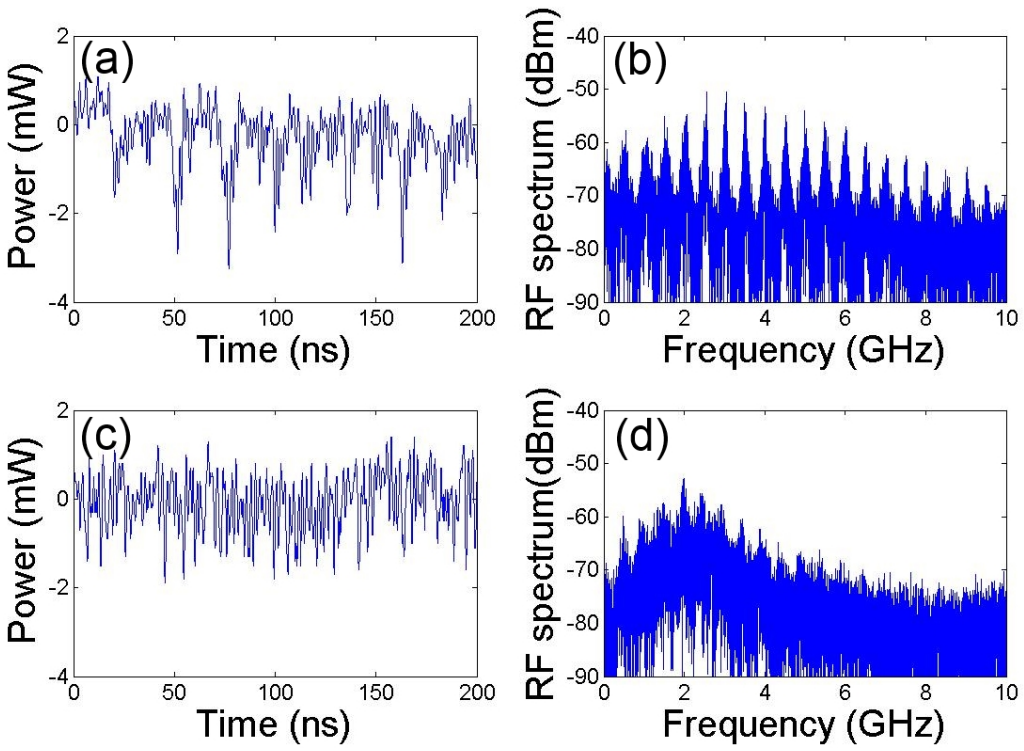

Figure 14: Experimental intensity time series after applying a 350 MHz low-pass filter (first column) and RF spectrum (second column) for $I = 11.84$ mA; (a)(b) $\eta = 0.11$ and (c)(d) $\eta = 0.35$.

persist for a larger range of feedback levels than is the case for low I.

The first is that alternating stable and unstable regions are observed, but no longer a systematically cascade involving the successive MGMs that appear when η increased. The second is that as I is increased, the BD tends to exhibit large regions of uninterrupted chaotic behavior. The third is that for larger I, the stable regions, though limited in number, persist for a larger range of feedback levels than is the case for low I.

The first observation shows the relative experimental robustness of the bifurcation cascade. Indeed, we have observed consistently the presence of alternating *stable* and *unstable* regions for all values of the current between $I_{\rm th}$ and $\sim 1.6 I_{\rm th}$. However, when $I > \sim 1.6 I_{\rm th}$, we cannot observe any stable region in the entire BD; we conclude that in this case, our laser never lies on or in the vicinity of a single ECM and therefore its

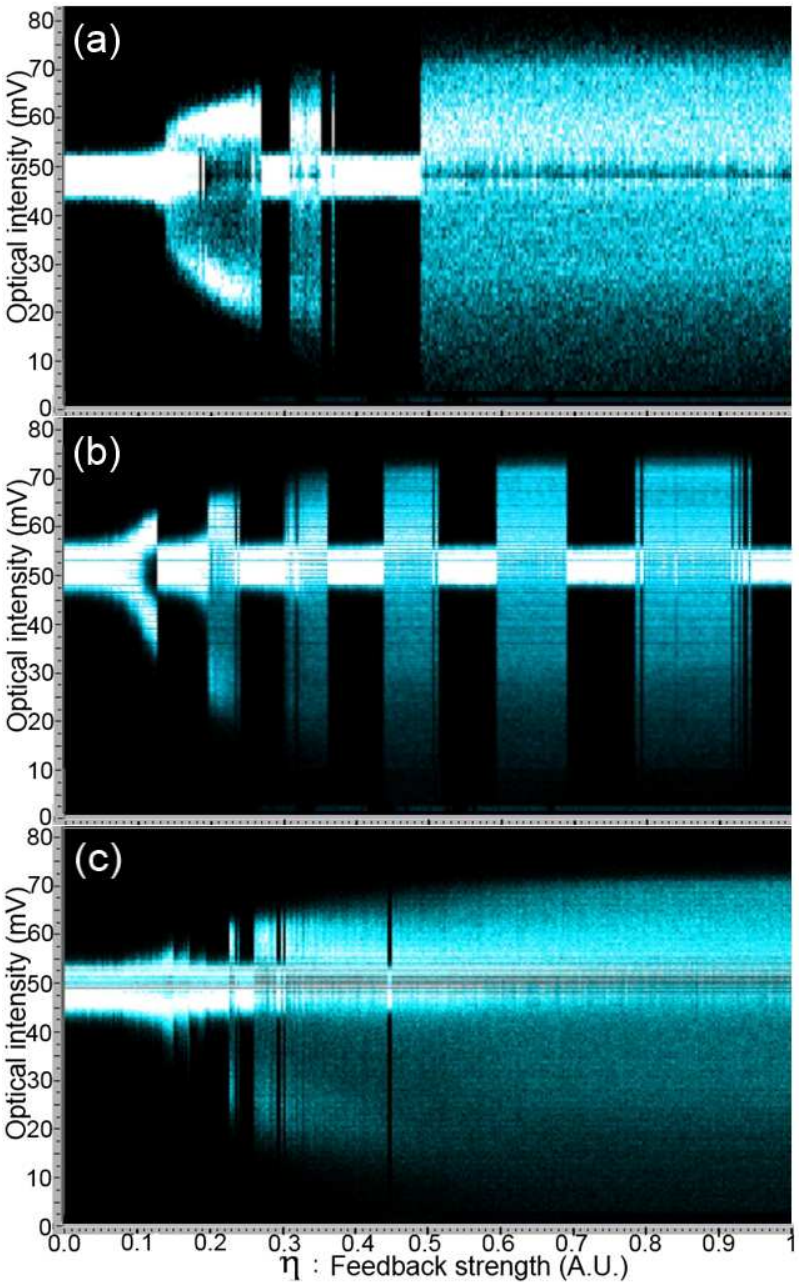

Figure 15: Experimental BDs for (a) $I = 14.69$ mA with $L = 30$ cm, $I = 11.24$ mA with $L =$ (b) 15 cm and (c) 65 cm.

dynamics necessarily involves attractor ruins of several ECMs. The analysis of the time series, RF, and optical spectra [81] also reveals that the dynamical behavior in the first few unstable regions of the cascade is typically LFF for currents up to $1.2I_{\rm th}$, while larger feedback and current levels lead to fully-developed coherence collapse.

To help us interpret different parts of the experimental BDs, the intensity time series and the corresponding RF spectra both in LFF and coherence collapse regimes are shown in Fig. 14, which includes the results for $\eta = 0.11$ and 0.35 at $I = 11.84$ mA corresponding to the BD of Fig. 13(a). In order to clearly characterize the power dropouts during LFF, a low pass filter with a bandwidth of 350 MHz was used to filter out the high-frequency components of the time series. As discussed in previous work [81], in the unstable regions for low η, we systematically identify LFF [Figs. 14(a) and (b)], and in particular its typical random power dropouts. In contrast, for higher η, we do not observe LFF but a regime of fully developed coherence collapse [Figs. 14(c) and (d)]. We systematically identify LFF until $\eta \sim 0.18$ is reached in Fig. 13(a) while for larger I, we do not observe LFF. A detailed study of the optical spectrum related to LFF and coherence collapse is presented in [81].

3.6 Varying the External Cavity Length

The dependence of the BD on L is explored in Fig. 16. The experiment is executed for four different cavity lengths $L = 10$, 30, 50, and 65 cm, at $I = 11$ mA. For a short cavity with small L, we again observe a cascade of bifurcations, but with significantly longer stable regions during which the laser-output power dwells on a single ECM before moving into the subsequent unstable regime, itself followed by the next ECM [Fig. 16(a)]. Moreover, we also observe a well-resolved experimental Hopf bifurcation of the first ECM that appears in the cascade, thanks to the increased stability of short cavities. In Fig. 16(d), when $L = 65$ cm, we barely observe a cascade of bifurcations for small η ($0.05 \leq \eta \leq 0.08$). The laser-output power remains briefly on a single ECM,

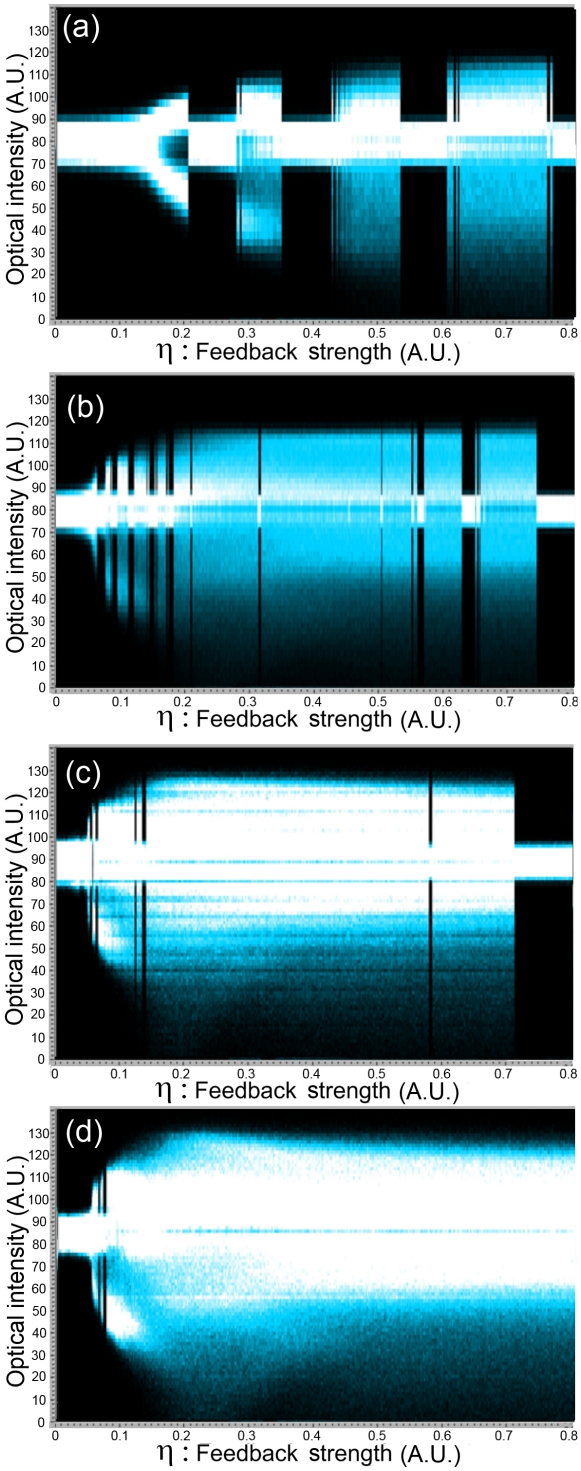

Figure 16: Experimental BDs for $I = 11$ mA with (a) $L = 10$ cm, (b) 30 cm, (c) 50 cm, and (d) 65 cm.

then moves into an unstable regime followed by the next stable ECM over a small range of η and we cannot observe any cascading behavior by further increasing η. The absence of a cascade in such case is consistent with the numerical results, as will be shown in section 3.9.

3.7 Effect of the Feedback Phase

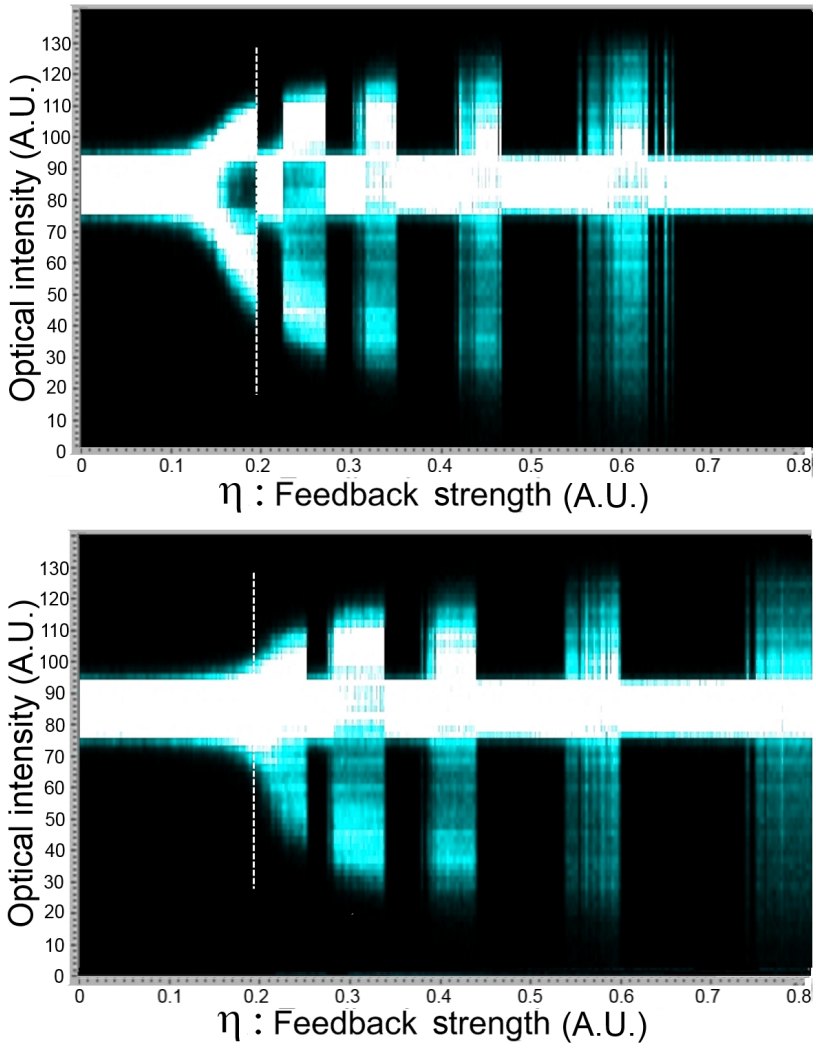

Figure 17: Experimental BD for $I = 10.88$ mA and $L = 13$ cm. The values of the feedback phase in (a) and (b) differ by 1.22 rads. The vertical dotted line corresponds to identical feedback strengths.

The feedback phase $\omega_o\tau$ can be varied by changing the cavity length on the sub-wavlength scale. The change is so small that, in terms of its dynamical effects, the

delay itself can be considered to be constant. We experimentally control the optical feedback phase of the reflected light by a piezoactuated translation stage. Figure 17 shows the BDs for $I = 10.88$ mA and $L = 13$ cm, when the feedback phases differ by 1.22 rad. We observe that the essential features of the BD, namely the presence of a cascade between stable and unstable states and the number of elements in the cascade, are preserved when $\omega_o\tau$ is changed. Feedback-phase effect merit further study and are currently being explored in the group.

3.8 Forward and Reverse Bifurcation diagrams

We compared both forward (increasing η) and reverse (decreasing η) BDs. The corresponding results are shown in Fig. 18 for (a) increasing η and (b) decreasing η. Although we can observe the cascade behavior in both cases, the transitions between stable and unstable regions typically occur at smaller η in the reverse cascade. These differences are an illustration of the generalized multistabilty of the system: as several attracting steady-states coexist for a given set of parameters, the initial state will influence the observed steady-state. In the forward BDs, the state of the ECM, as η increased, results from lower feedback, while in reverse BDs, the state results from higher-feedback attractors. It is thus normal to observe a shift to the left of the switching points between stable and unstable regimes, in the reverse BDs.

3.9 Numerical Bifurcation Diagram

Figure 19(a) presents a simulated BD of the optical intensity as a function of the theoretical feedback strength κ having first subtracted off the time-averaged intensity, as is done by the photodetector in the experiments. To further reflect our experiments where η is gradually ramped up, the initial state, for a given κ, is taken to be equal to the final state of the simulation corresponding to the previous, smaller value of κ. It is evident from the plot that alternating stable and unstable regions occur. Such numerical simulations facilitate the interpretation of the influence of L and I on the

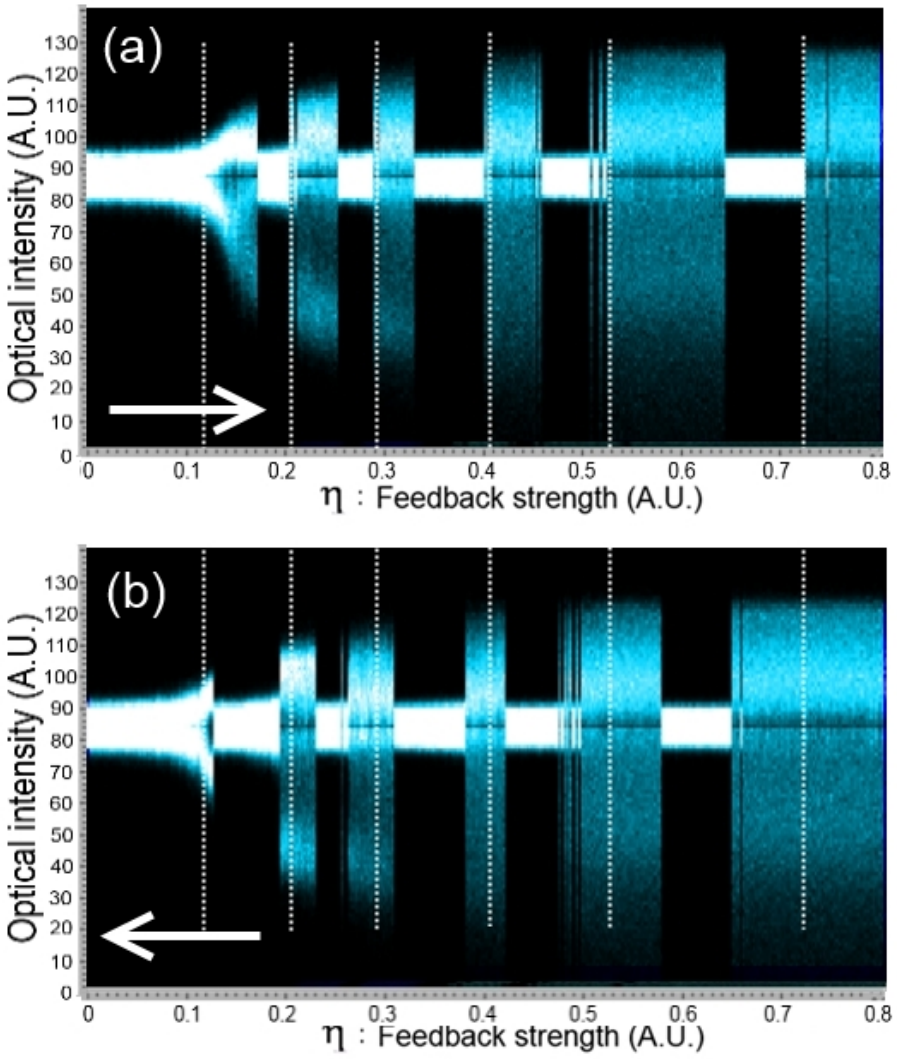

Figure 18: Experimental BD of (a) increasing the feedback strength(Forward BD) and (b) decreasing the feedback strength (Reverse BD) for $I = 11.03$ mA and $L = 15$ cm. The vertical dotted lines correspond to identical feedback strengths.

BD.

3.10 Varying the Operating Parameters: External Cavity Length, Current, and Feedback Phase.

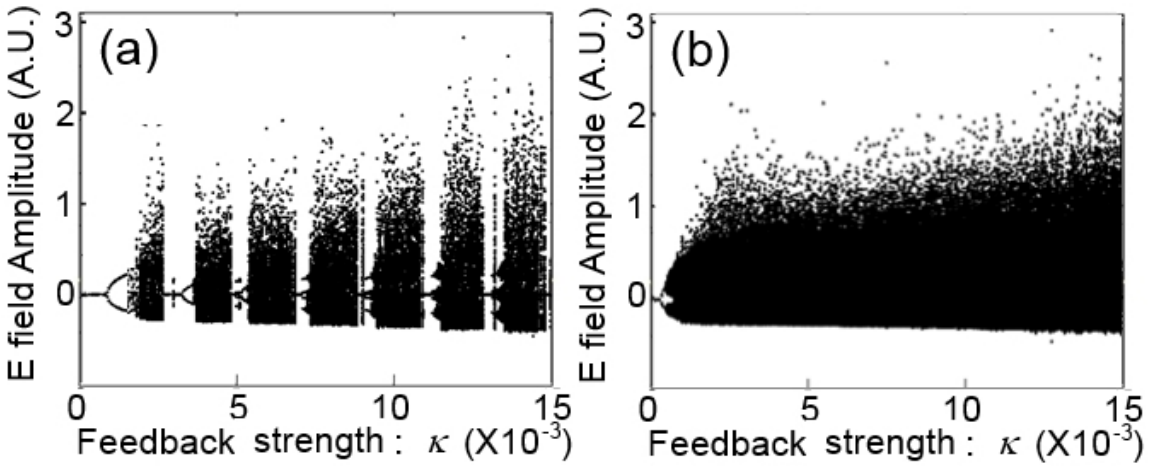

Figure 19: Numerical BD for (a) $L = 15$ cm and (b) $L = 65$ cm at $p = 1.03$.

Figures 19(a) and (b) show the simulated BDs for different external cavity lengths ($L = 15$ cm and 65 cm). With short L, we observe a cascade of bifurcations, but with significantly longer stable regions during which the laser-output power dwells on a single ECM before moving into the subsequent unstable regime, itself followed by the next ECM. As explained in [115], we observe that the chaotic behavior initially develops around a single ECM and then extends to several ECMs as the ruins of neighboring attractors merge through an attractor-merging crisis (region φ of Fig. 20) [137]. This crisis leads to an abrupt change in the optical intensity range. We interpret the *unstable regions* we observe in the experiments as corresponding to the onset of these crises that make the amplitude jump above the noise level.

When L is large, the spectral separation between ECMs is reduced (e.g., 1 GHz→15 cm, 500 MHz→30 cm, 233 MHz→65 cm) in the optical spectrum. Therefore, each participating mode being close in phase space, large-amplitude itinerancy between several modes is easily observed. In the limit of a very long L, Ruiz-Oliveras and

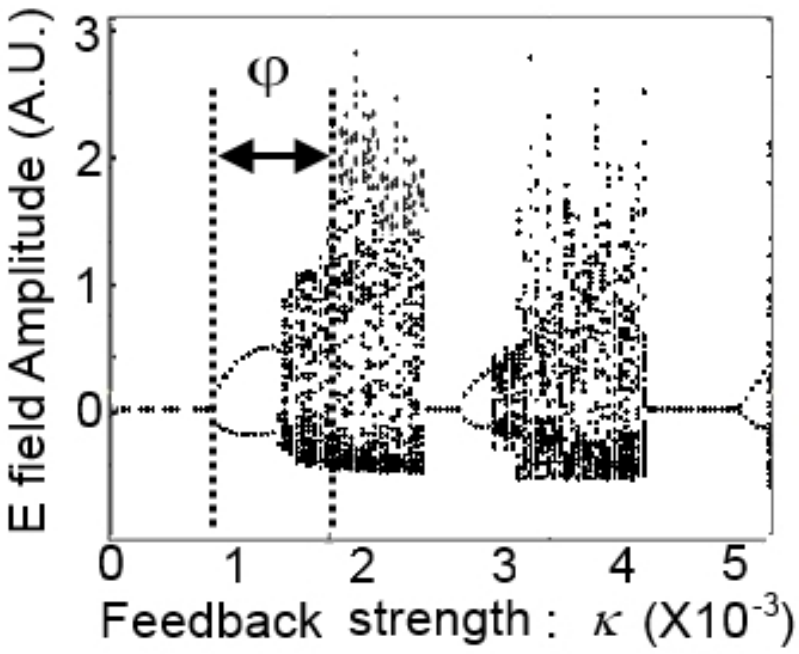

Figure 20: Numerical BD for $p = 1.03$ and $L = 15$ cm ($0 \leq \kappa \leq 5.5\times10^{-3}$).

Pisarchik have observed numerically that the laser is always unstable [170]. Indeed, numerical observation of the trajectories on the ellipse shows that the proximity to the ECMs impedes the development of independent stable attractors and thus prevents the existence of a cascade of stable and unstable regions, as confirmed by our experimental observations. Conversely, increased distance between the ECMs for shorter L means that larger η is needed before attractor merging occurs, thus explaining the longer stable regions as observed in the experimental BDs of Fig. 16.

Small variations of L lead to changes in the feedback phase. It is known that this in turn changes the stability conditions of the ECMs [199], thus affecting the duration and location of the stable regions. The global picture of the successive appearance of MGMs and their destabilization is though not affected by the value of the feedback phase, as is observed experimentally in Fig. 17.

Figures 21(a) and (b) show simulated BDs for different normalized pumping currents ($p = 1.02$ and 1.04) and Fig. 22 presents the trajectory in phase space for identical parameters except for the current level p.

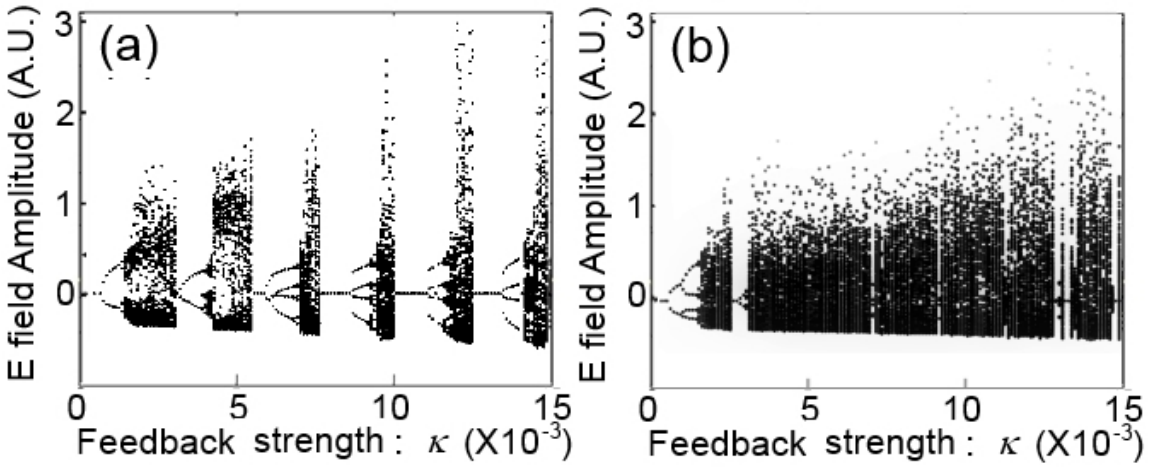

Figure 21: Numerical BD for (a) $p = 1.02$ and (b) $p = 1.04$ at $L = 15$ cm.

These help us interpret the influence of I on the BD. Larger I leads to larger changes in the optical intensity and thus to trajectories that explore a larger region of phase space. Also, at low I, the unstable regions typically correspond to the LFF regime, within which a drift toward the MGM is observed. At larger I, the unstable regions typically correspond to fully-developed coherence collapse in which chaotic itinerancy between ruins of ECMs is observed, with no drift toward the MGM. This behavior explains the increased difficulty in reaching the MGM as I is increased. In particular, it explains why we observe numerically that at larger I, either larger κ is needed to get out of an unstable region and reach the MGM, or the MGM is not reached at all. This in turn explains the perturbed aspect of the bifurcation cascades observed experimentally for larger I, in which some stable regions do not appear in the BD because the trajectory never settles on the MGM, and in which long uninterrupted regions of chaotic itinerancy are observed. We also observe numerically that above a certain feedback level, the dynamic regimes only correspond to chaotic itinerancy among ECMs that are far away from the MGM, with no drift toward the MGM, making the MGM inaccessible [77, 132]. This explains the experimental observation of the total absence of stable regions when the I is larger than $1.6I_{\text{th}}$.

Finally, we interpret the experimental observation that long stable regions can be

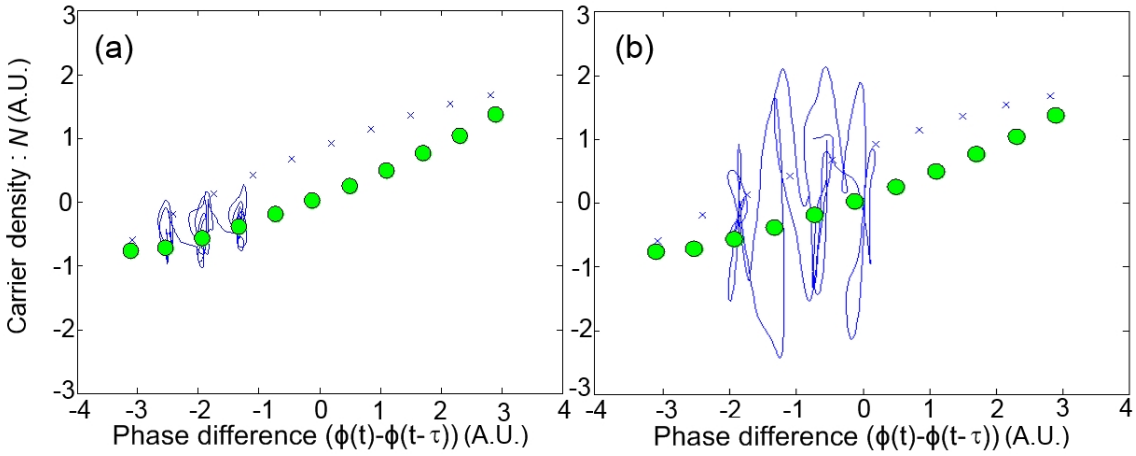

Figure 22: Trajectory in phase space with pumping currents (a) $p = 1.03$ and (b) $p = 1.05$ at $\tau = 2$ ns and $\kappa = 0.0025$.

observed at larger I as being linked to the fact that larger κ is needed to destabilize the MGM when I is increased. This interpretation has a good agreement with the Eq. 21 in [124] giving an approximated value for κ at which Hopf instability sets in. Thus, when the trajectory reaches the MGM, which happens rarely for large I, larger κ is needed to destabilize it, a phenomenon which is consistent with the longer stable regions observed for relatively large currents (but smaller than 1.6 I_{th}). We have also observed that another phenomenon can contribute to explain the long stable regions. Indeed, we have determined experimentally that what appears to be a single stable region can sometimes correspond, especially for large values of I, to two or more successive stable regions linked to different, successively appearing, ECMs. Thus long stable regions can be due to the slipping of the dynamics from one ECM to the next, without ever going through a phase of itinerancy around several ECMs.

3.11 Effect of Noise

We observe that the inclusion of noise in the LK model, through the addition of a Langevin noise source, tends to blur the low amplitude signal variations appearing when the laser bifurcates out of a CW state, making the simulated BDs closer-looking to the experimental ones.

The effect of noise is illustrated by the comparison of Fig. 23, in which a spontaneous noise level $\beta = 100$ is used, with Fig. 19(a), which does not include noise. Qualitative features such as the feedback level at which the laser jumps to the MGM does not seem to change significantly when noise is included. This observation, combined with the resemblance of the noisy simulated BDs with the experimental ones, corroborates the fact that noise does not seem to induce the qualitative features of the cascade. Therefore, this observation is in favor of a deterministic origin of bifurcation cascades in ECSLs.

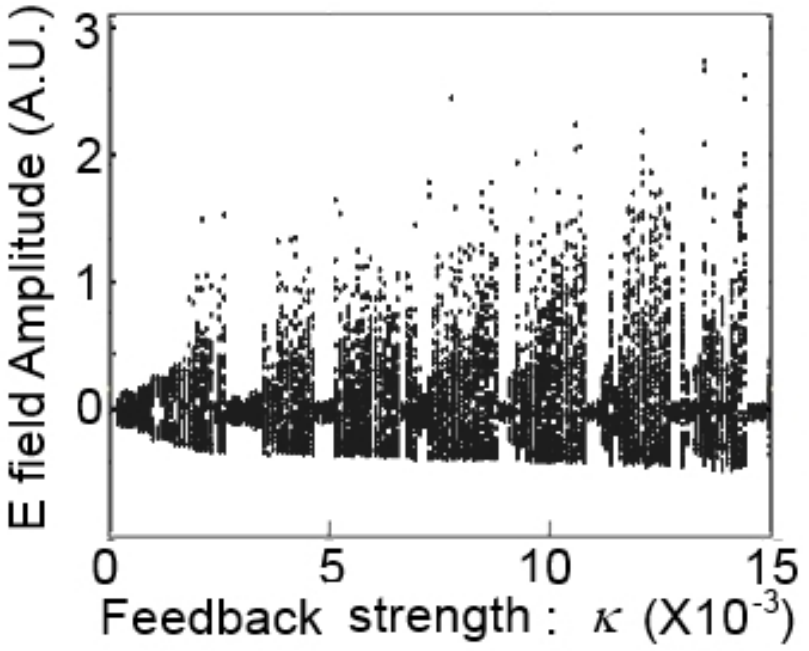

Figure 23: Numerical BD of $p = 1.03$ and $L = 15$ cm with $\beta = 100$.

3.12 Conclusion

We report detailed experimental BDs of an ECSL. We have focused on the case of a distributed feedback laser biased up to 1.6 times the threshold current [low injection current case] and subjected to feedback from a distant reflector. We observe bifurcation cascades resulting from the destabilization of external-cavity modes that appear successively when the feedback is increased, and explain, in light of the LK model,

how the cascading is influenced by various laser operating parameters (current, delay, feedback phase) and experimental conditions. The qualitative agreement between experiments and simulations validates over a large range of operating parameters, the LK model as a tool for reproducing the salient aspects of the dynamics of a distributed feedback laser subjected to external optical feedback.

A global experimental-based understanding of the various dynamical regimes is essential to gain a fundamental apprehension the dynamics of an ECSL. In this regard, we have examined several aspects of fundamental importance for the dynamics of ECSLs using BDs based on experimental time series of the optical intensity of a distributed feedback laser subjected to coherent optical feedback.

In order to validate our interpretation of the experimental results, we have carried out theoretical calculations based on the well known LK model. Despite its simplifications, this model can successfully reproduce the bifurcation cascade that is observed experimentally. Moreover, the experimental observation of a reduction in the number of stable regions with increasing I is consistent with the LK model. Indeed, LK predict that, at low I, the unstable regions correspond to the LFF regime, involving a drift toward the MGM, while at larger I, fully-developed coherence collapse occurs, with no drift toward the MGM. The observation of a gradual disappearance of the cascade with increasing L is also consistent with the model which shows an increase in attractor merging as a result of the increased proximity of ECMs in phase space. Our study thus connects the observed experimental BDs, based on the observation of the optical intensity only, with the behavior in the full phase space of the LK model. Additionally, the observation of differences between the forward and reverse diagrams is a clear illustration of the multistability of the ECSL. Finally, the good reproducibility of the experimental results, combined with their good match with a deterministic model, within a large range of continuously varied parameters, supplies global evidence for the deterministic origin of the salient aspects of ECSL dynamics.

CHAPTER IV

BIFURCATION DIAGRAM OF AN EXTERNAL-CAVITY SEMICONDUCTOR LASER IN HIGH INJECTION CURRENT CASE

4.1 Summary

We report experimental BDs of a semiconductor laser, biased well-above threshold, subjected to external optical feedback. As feedback is increased, we see a quasi-periodic route to chaos interrupted by several windows of periodicity corresponding to limit cycles, differing in frequency by multiples of the external-cavity free-spectral range that have developed around ECMs whose frequency is slightly larger than that of the solitary laser. Successive windows correspond to the transition between two limit cycles either on the same or neighboring ECMs. For larger feedback, the laser operates in a chaotic regime around numerous negatively shifted external-cavity modes. These are the first experimental observations, to our knowledge, detailing the bifurcations leading to fully developed chaos in this system, and further provide unprecedentedly detailed insight on the standard theoretical framework applied to these lasers.

This chapter is based on the following publication:

1. Byungchil Kim, Locquet, A., Daeyoung Choi, Citrin, D.S., "Experimental route to chaos of an external-cavity semiconductor laser," in Phys. Rev. A, vol.91, pp.061802, (2015).

4.2 Introduction

In an ECSL, the light produced by a LD is reinjected into its active layer upon reflection by an external mirror. The external-cavity time of flight τ creates an optical delay that leads to a high-dimensional dynamical system in which a variety of regimes have been observed, and in particular chaos of various complexities [184,204]. The tunability of the behaviors, depending on operating and design parameters, as well as their high-speed dynamics, have given to ECSLs, especially in the long-cavity case, a prominent role for fundamental studies of nonlinear dynamics [132] as well as for applications such as tunable laser sources [143], physical-layer security [17], light detecting and ranging (LIDAR) [105], high-speed random-number generation [201], and reservoir computing [22].

Understanding the sensitivity of LDs to optical feedback is of fundamental importance to achieve an adequate understanding of the route to chaos in ECSLs as well as more generally for control of ECSL dynamics for applications. Consequently, ECSL dynamics have been widely investigated [21,37,115,123,132,184,204], typically analyzed with the LK model [91]. On its basis, numerous authors have plotted BDs (BD) [69, 97, 124, 132, 198] as a BD is of utmost importance in the dynamical-system analysis. These theoretical BDs show a complex sequence of bifurcations, characteristic of high-dimensional systems, in which the route to fully-developed chaos is typically interrupted by windows of periodic or quasi-periodic behaviors and/or to a switch to a different attractor or set of attractors. Surprisingly, experimental support of those theoretical results is sparse. Contrary to the LK model, some experiments have reported simpler routes to chaos: quasi-periodic [124], period-doubling [220], and subharmonic cascaded bifurcation [125], that are typical of low-dimensional systems [19]. These claims are based on the observation, usually relying on a spectral analysis, of a succession of dynamical regimes for a few discrete parameter values rather than for a continuously tuned parameter. Thus a complete, experimentally

verified understanding of the dynamical regimes of an ECSL, and of the bifurcations between them, has not yet been attained.

Based on Section 2.1, we reported for the first time an experimental,partly resolved BDs [80, 81]. Injection current I just above threshold $I_{\rm th}$ was used, for which spontaneous-emission noise obscures the details of the bifurcations, and thus reliable identifications were not easily made.

In this Chapter, we consider the high-I case where spontaneous-emission noise plays a smaller role. We show fully resolved BDs of an ECSL biased well above $I_{\rm th}$ and unambiguously identify the bifurcation cascade leading to chaos. Thus, we report a conclusive experimental demonstration of a full route to chaos in a distributed feedback ECSL initiating with a Hopf bifurcation. The LD is biased at $I \sim$2-3I_{th} with external-cavity length L chosen so that the external-cavity free-spectral range (FSR) $f_\tau = c/(2L)$ is lower than, and is not a sub-multiple of, the relaxation-oscillation frequency of the solitary LD $f_{\rm RO}$. We observe a quasi-periodic route to chaos interrupted by windows of periodicity or quasi-periodicity and emphasize that the first two bifurcations seen are Hopf bifurcations as correctly predicted by the LK model in the common case in which $f_{\rm RO}$ is not an integer multiple of $f_\tau = \tau^{-1}$ [97, 124]. Also, in the periodic windows, we observe coexistence of several limit cycles on the same ECM for successive increasing feedback strengths, and on neighboring ECMs, separated in frequency by small multiples of f_τ.

4.3 Experimental Setup and Theoretical Framework

The experiment is shown in Fig. 24(a) [81]; $I_{\rm th} = 9.27$ mA. Temperature and I are stabilized. An oscilloscope (12 GHz bandwidth) captures the optical intensity $\mathcal{I}(t)$ emitted by the laser. We also measure the RF spectrum with a spectrum analyzer (23 GHz bandwidth) and the optical spectrum with a high-resolution optical spectrum analyzer (APEX AP2440) (10 MHz optical resolution); L is set to 30 cm, $\tau = 2$ ns,

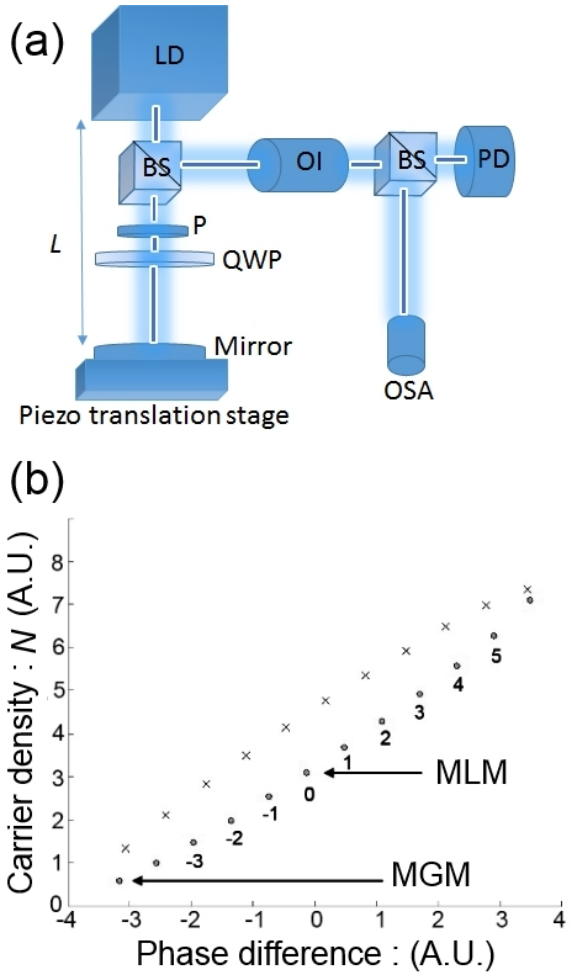

Figure 24: (a) Experimental setup. LD: LD, BS: beam splitter, PD: photodetector, P: polarizer, QWP: quarter-wave plate, OI: optical isolator, OSA: optical spectrum analyzer, L: external-cavity length. LD is an intrinsically single-longitudinal mode InGaAsP distributed feedback laser at 1550 nm with maximum power of 15 mW. (b) Ellipse structure of fixed points in $\Delta\phi$-vs.-N plane. Circles represent ECMs; crosses represent antimodes. Labels indicate mode number.

and $f_\tau = 500$ MHz with f_{RO} in the multi-GHz range. The experimental feedback strength η is proportional to the optical intensity fed back into the LD; η is varied via the angle of the quarter-wave plate (QWP) in the feedback loop.

We control the QWP angle in 0.01 degree increments, giving 4500 possible different η values with a motorized rotation stage under high-stability conditions. Maximum feedback (η=1) is when the QWP angle is such that the electric field is not subjected to any rotation. In that case, the percentage of threshold reduction $(I_{th}-I)/I_{th}$ is $\sim$0.066 and $\sim$20 % of the optical power is fed back onto the collimating lens.

The experimental results are analyzed and compared with the LK model which is widely used to describe the effect of optical feedback and has proven successful in predicting many aspects of the dynamics [69, 115, 123, 145], though some inconsistencies persist [99]. Still, due to its considerable success we use the LK to analyze our experiments. According to LK, as feedback is increased, steady-state CW solutions appear in pairs as a result of saddle-node bifurcationS: ECMs and antimodes that are unstable saddle points [37, 115]. These may be thought of as the nonlinear modes of the ECSL. The ECMs and antimodes are known to lie on an ellipse in the plane formed by the carrier density (inversion) $N(t)$ versus phase difference $\Delta\phi(t) = \phi(t) - \phi(t-\tau)$ plane, with ϕ the slowly-varying phase of the electric field, as shown in Fig. 24(b) [66]. Two ECMs stand out: the minimum linewidth mode (MLM) and the maximum gain mode (MGM). The MGM has the lowest frequency (high-gain end), and is always stable [60, 95, 115]. The MLM is the closest ECM in frequency to the solitary LD mode. ECSL dynamics can be visualized in terms of the trajectory moving amongst the ECMs and antimodes on this ellipse. Simulations of the LK model [69, 97, 124, 132, 198] predict complex routes to chaos which typically start, when f_{RO} is not an integer multiple of f_τ, as quasi-periodic routes but which are also typically interrupted by windows corresponding to periodicity, quasi-periodicity, or to attractor switching.

4.4 Experimental Results

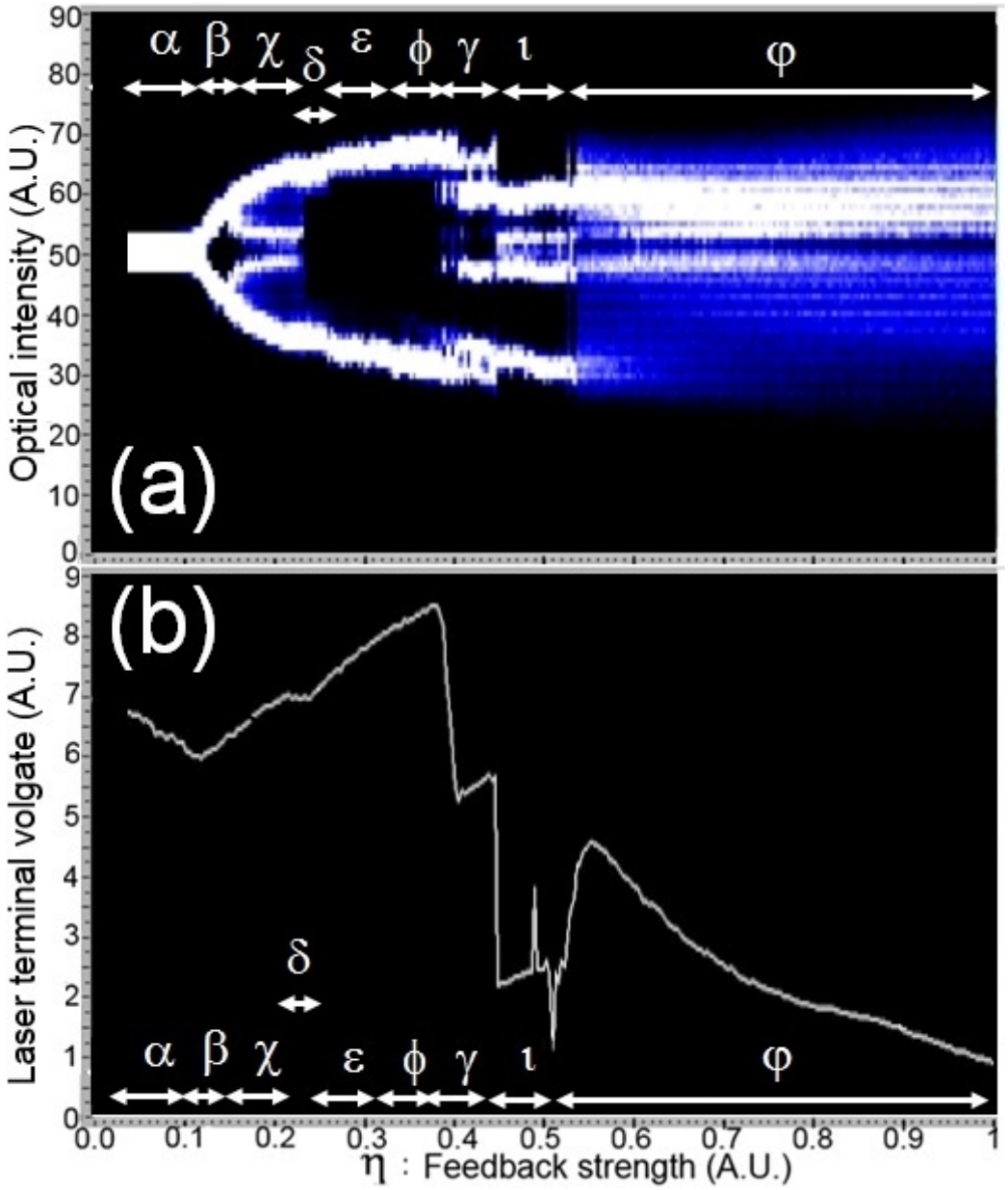

Figure 25: (a) Experimental forward BD for $I = 22.08$ mA and $L = 30$ cm and (b) corresponding V_{LD}.

Figure 25(a) shows the experimental BD (ramping η up) with $I = 22.08$ mA and $L = 30$ cm, giving f_{RO} ∼7.4 GHz and $f_\tau \sim 500$ MHz. This BD is obtained by taking the local extrema of $\mathcal{I}(t)$ at each η. Density is high in white but low in black regions. The corresponding time-averaged voltage drop across the injection leads of

the LD $V_{\rm LD}$ is shown in Fig. 25(b). It has been shown [156, 176] that $V_{\rm LD}$ tracks the changes in N. A reduction (increase) in N caused by η reduces (increases) the difference between quasi-Fermi levels in the p- and n-type quasi-neutral regions of the LD. Thus, the overall reduction (increase) in N in the active region leads to a reduction (increase) in $V_{\rm LD}$. Thus $V_{\rm LD}$ provides information on dynamical variable variable N [176], complementing the more conventionally probed optical intensity.

To further elucidate the ECSL dynamics, experimental RF spectra of $\mathcal{I}(t)$ (left column), optical spectra (right column), and $\mathcal{I}(t)$ (inset) at various η are plotted in Fig. 26 for I=22.08 mA. 0 GHz on the optical-frequency scale corresponds to the ECM at 193.271 THz. We see from Figs. 25 and 26 that the ECSL is initially in ECM 1. In the corresponding region α ($\eta \sim$0.05) of Figs. 25(a), (b) and 26(a1), (a2) only one fixed point (ECM 1) participates in the output, and the ECSL displays CW behavior. From Fig. 25(b), one sees $V_{\rm LD}$ decrease with increasing η in this regime, indicating a decrease in N and an increase in power, consistent with predictions of LK [124].

As η is increased above 0.12, it is clearly seen in the BD and from the shape of $I(t)$ in Fig. 26(b2) that the ECSL undergoes periodic oscillation. This oscillation is manifested as sidebands $\pm$8 GHz from ECM 1, a frequency that also stands out in the RF spectrum [Fig. 26(b1)]. Also, $V_{\rm LD}$ is monotonically increasing in η [region β of Figs. 25(a), (b)]. This transition in the dynamics corresponds to a Hopf bifurcation leading to a limit cycle with frequency close to f_{RO}, as predicted by LK [123, 133].

With increasing η, additional sidebands near $\pm f_\tau$ appear in the optical spectrum [Fig. 26(c2)], revealing the presence of a second frequency in the dynamics. This other frequency is confirmed by the RF spectrum [Fig. 26(c1)], and the corresponding time series of $\mathcal{I}(t)$ exhibits quasi-periodic oscillation. The undamping of a second frequency close to f_τ corresponds to a secondary Hopf bifurcation predicted by LK [97,124] and corresponding to the development, in phase space, of a torus attractor. Note that

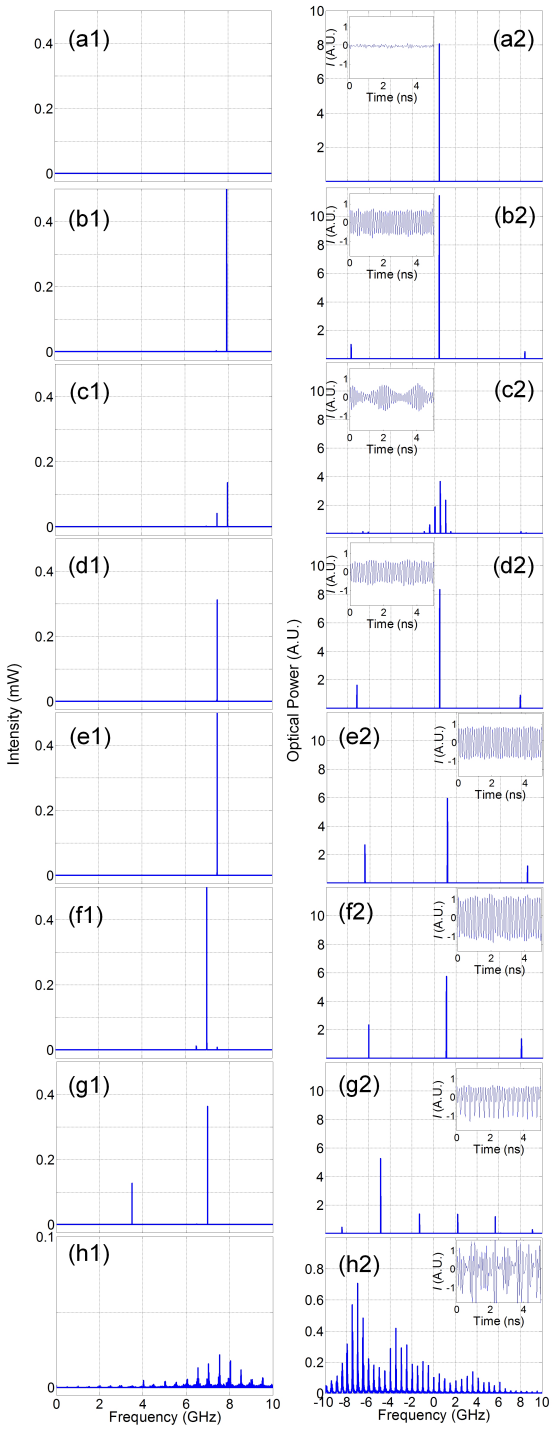

Figure 26: Experimental RF spectra (first column), and optical spectrum with OSA of $\mathcal{I}(t)$ (second column), and associated $\mathcal{I}(t)$ (inset) for (a1)(a2) η=0.05, (b1)(b2) 0.13, (c1)(c2) 0.2, (d1)(d2) 0.26, (e1)(e2) 0.28, (f1)(f2) 0.35, (g1)(g2) 0.5, and (h1)(h2) 0.8.

both the limit cycle and the torus result from the destabilization of ECM 1 and are located around it in phase space. This is the first such experimental observation of this sequence of two Hopf bifurcations to our knowledge providing a fundamental point of comparison with the LK model.

For a further increase in η, another limit cycle appears in the BD. The optical spectrum shows [Fig. 26(d2)] that this cycle is still centered on ECM 1, and has now a frequency of approximately $\pm$7.5 GHz, evidenced both by the RF [Fig. 26(d1)] and optical spectra [Fig. 26(d2)]. Interestingly, the dominant ECM (1) does not change in between Fig. 26(b2) and (d2), thus providing experimental evidence of the existence, at different feedback levels, of two periodic solutions with different frequencies, 8 GHz and 7.5 GHz, whose separation is $\sim f_\tau$. Mork *et al.* [123], Ritter and Haug [162] and Erneux [38] had demonstrated, based on LK, the existence of two limit cycles originating in the same ECM but differing in frequency by approximately the f_τ. The second limit cycle arise from a Hopf bifurcation of the unstable fixed point resulting from the Hopf bifurcation that lead to the first limit cycle. These previous works show that our observation of several limit cycles with different frequencies around the same ECM is compatible with LK. Pieroux *et al.* [147] have shown that, more generally, multiple periodic solutions can occur in class-B lasers subjected to delayed feedback and that their interaction can lead to quasi-periodic solutions. As η is further increased, and region ϵ of Figs. 25(a) is reached, one observes a small discontinuity in the BD, as well as a discontinuity in the slope of V_{LD} [Figs. 25(b)]. The optical spectrum [Figs. 26(e2)] reveals that this discontinuity corresponds to a shift from ECM 1 to 2. As shown by the corresponding $\mathcal{I}(t)$, the ECSL still oscillates periodically, and both the optical [Fig. 26(e2)] and RF spectra [Fig. 26(e1)] confirm that the frequency of the oscillations is still 7.5 GHz. The previous observations indicate that the trajectory moves in the positive-frequency direction and transits to another limit cycle, of the same frequency, on a different ECM. Increasing η further,

another limit cycle at $f_{\mathrm{RO}} \sim 7$ GHz is seen [region ϕ of Figs. 25(a),(b) and 26(f1),(f2)]. The active ECM 2 does not change in the transition from region ε to ϕ of Fig. 25(a), indicating the existence of two different oscillation frequencies, 7.5 GHz and 7 GHz, again separated by $\sim f_\tau$ on ECM 2.

It must also be noted that to this point, a monotonic increase of V_{LD} is seen and V_{LD} is higher than for the initial condition (ECM 1) with $\eta \sim 0.02$. This indicates that the trajectory moves toward higher frequencies [right half in the $\Delta\phi$-vs-N plane in Fig. 24 (b)]. The optical spectrum [Fig. 26(e2) and (f2)] also confirms that the dominant mode is ECM 2, which is at larger frequency. These observations are fundamental to understanding the route to chaos on the basis of the LK model. This is the first time to our knowledge to report experimentally that the trajectory moves toward higher frequency at low η for high I. Our experimental results agree with Masoller and Abraham [115], who calculated that initially, for small η, the dominant peak is shifted by a multiple of the ECM frequency spacing towards positive frequency. They attributed this behavior to the fact that ECMs that are close to the MLM (e.g. ECM -1 and -2) but of lower frequency have very small basins of attraction compared to positive ECMs at low η for high I, while ECMs with large positive frequency shifts are highly unstable.

As η is further increased, two sudden drops in V_{LD} are seen, one at $\eta \sim 0.38$, the other at ~ 0.45. The values reached by V_{LD} are lower than the initial ECM 1 at $\eta = 0.02$ indicating that the trajectory has abruptly moved toward ECMs at lower frequencies than the MLM [left in the $\Delta\phi$-vs-N plane in Fig. 24(b)].

Figure 26(g) shows the behavior of the ECSL just after the second dropout [region ι of Figs. 25 (a),(b)]. The optical spectrum shows that the ECM is now near -10 [Fig. 26(g2)], while the RF spectrum highlights that the frequencies involved in the dynamics are ~ 7 GHz and 3.5 GHz [Fig. 26(g1)]. We interpret this region as a period-doubled limit cycle oscillation around ECM -10. It is interesting to note that

other period-doubling observations reported in the literature [125, 220] correspond to the doubling of a period close to that of relaxations oscillations. Additionally, we interpret the previous region γ of Figs. 29 (a),(b), as corresponding to a region where intermittency is observed between regions ϕ and γ of Figs. 25 (a),(b). This interpretation is corroborated by the experimentally observed non-stationarity of ECSL behavior in this region.

Finally, when η exceeds ~ 0.5, thus reaching the maximum values of η explored here, the trajectory wanders among several ECMs located at lower frequencies than the MLM, as indicated both by the optical spectrum and V_{LD}. $\mathcal{I}(t)$ undergoes rapid chaotic fluctuations on the sub-ns time scale [Fig. 26(h2)] and the broad RF spectrum [Fig. 26(h1)] indicates the excitation of a continuous range of frequencies. This regime is usually called in the literature *fully developed coherence collapse*. This evolution of the laser dynamics around several negatively shifted ECMs is the typical prediction of the LK model under fully developed coherence collapse [115, 132, 184].

We have observed the main features of the BD presented in Fig. 25 for various large range values of L ($f_\tau \ll f_{\mathrm{RO}}$) and for values of $I \gtrsim 1.8 I_{\mathrm{th}}$. When $I \lesssim 1.8 I_{\mathrm{th}}$, qualitative changes occur as windows of stability corresponding to the settling of the trajectory on the MGM typically appear, as reported in [69, 81].

4.5 Conclusion

In this chapter, we report experimental BDs of a semiconductor laser, biased well-above threshold, subjected to external optical feedback. We measured BDs of the optical intensity of an ECSL with large L and I. We observed that initial instabilities correspond to the first steps of a quasi-periodic route to chaos that develops around a single ECM. This ECM loses stability first via a Hopf bifurcation to limit-cycle behavior at a frequency close to f_{RO}, which undergoes a secondary Hopf bifurcation corresponding to the undamping of a second frequency, close to f_τ, and leading to

quasi-periodic oscillations. The quasiperiodic route is then interrupted by various windows of periodicity, as well as by intermittent behavior. In addition, we observe the existence of several limit cycles of different frequencies around the same ECM as well as transitions between two different limit cycles existing around the same or two different neighboring ECMs. Finally, for larger η, the merging of numerous attractors corresponding to different ECMs dictates the dynamics which correspond to a chaotic region of fully developed coherence collapse. To our knowledge our results provide the first detailed experimental observations of the bifurcation of a LD, biased well-above I_{th}, subjected to external optical feedback, and moreover provide detailed confirmation of some of the predictions of the LK model concerning the route to chaos for ECSLs.

In addition to experimental BDs of a semiconductor laser in low injection current case mentioned in Chap. 3, we reiterate: the results map out detailed BDs of ECSLs as function of a feedback strength for various L and I, thus covering a significant portion of parameter space.

CHAPTER V

INITIAL-STATE DEPENDENCE OF THE ROUTE TO CHAOS OF AN EXTERNAL-CAVITY LASER

5.1 Summary

ECSLs are an example of a hybrid engineered-physical system exhibiting emergent properties not evident from the physics of the underlying LD material. A signature feature of chaos is the *butterfly effect* or sensitivity to initial conditions (SIC). Direct observation of SIC in actual systems, however, can be elusive due to the ubiquitous nature of noise as well as difficulties in selecting the initial conditions.

In this chapter, we observe experimentally for the first time, in a high-dimensional dynamical system experiencing generalized multistability, the sensitivity of the route to chaos on the initial state relying on a novel initial-state selection method. As the feedback level determined by the effective mirror reflectivity is increased, chaos develops from a different mode of the external-cavity depending on the initial mode experimentally specified.

This chapter is based on the following publication:

1. Byungchil Kim, Locquet, A., Daeyoung Choi, Citrin, D.S., "Initial-state dependence of the route to chaos of an external-cavity laser," preparing for submission to Phys. Rev. A. (2016).

5.2 Introduction

ECSLs, which utilize an external cavity formed by a mirror to provide time-delayed optical feedback into the gain region of the LD, are known to display a rich variety of dynamical behaviors depending on the operating and device parameters. It is, for example, known that the delayed feedback produces an infinite-dimensional dynamical system–the infinite dimensions are due to the infinite number of initial conditions needed to specify the subsequent dynamics of a differential-delay system–in which hundreds of attractors or attractor ruins can coexist, leading to a wealth of dynamical regimes of varying complexity [132, 153, 184]. Thus, ECSLs serve as a prototype for high-speed (subnanosecond) chaos in high-dimensional time-delayed dynamical systems [21, 115, 123, 204]. Their highly complex dynamics further make them attractive for applications as diverse as chaos communications [17] and ultrahigh rate random-bit generation [201].

Despite years of interest in these systems, experimental investigations on ECSLs have suffered from a lack of detailed and systematic experimental knowledge of the various dynamical regimes that can be accessed as a function of the various operating parameters, such as the feedback strength η, the current I injected into the LD, and the external-cavity length L, which in turn determines the feedback time $\tau = 2L/c$ with c the speed of light. A standard tool for analyzing the dynamical regimes of a complex nonlinear system is the BD, which maps out the dynamical regimes as a parameter of the system is continuously tuned. The BD is a plot of the histogram of local extrema of a dynamical quantity as the single parameter is varied; transitions between qualitatively different dynamical regimes, known as *bifurcations*, are evident in the BD, and the sequence of bifurcations in a system that eventually exhibits chaos is known as the *route to chaos*.

The route to chaos is typically regarded as a fingerprint of a dynamical system, providing deep insight into the nonlinear dynamics. Its prediction, for example, is

an important test of theoretical descriptions of a given system. To the best of our knowledge, before our recent work [81] devoted to an ECSL, no experimental and systematic BDs were available for these devices. Our work at relatively high I of $(2-3)I_{th}$ with I_{th} the LD threshold current, has unambiguously resolved several distinct bifurcations leading to chaos, most notably the first two bifurcations which are of the Hopf type [83], as predicted by [123, 133].

The dimensionality of a dynamical system is important as it plays a key role in determining the types of phase-space trajectories that exist for a given set of system parameters. High-dimensional dynamical systems can exhibit generalized multistability in which several different stable or unstable limit sets, at various stages of development, coexist. The complex topology of phase space leads potentially to a route to chaos that strongly depends on the system's initial conditions.

Before continuing, we distinguish between several aspects of SIC. In its barest form, SIC is demonstrated by selecting specific initial conditions, i.e., the initial values of dynamical quantities sufficient to determine the system's subsequent evolution. By slightly changing the initial condition, one can then track the differences in the evolution. Indeed, at least at the theoretical level, this is how one defines the Lyaponov exponents that characterize the dimensionality of the chaos. While conceptually attractive, this approach fails experimentally for many systems. First, there are frequently severe limits to the ability of choosing the specific initial conditions. Second, ubiquitous noise may obscure what might otherwise be evidence of SIC in the dynamics given two different initial conditions. Third, due to the shear complexity of the dynamics and recording data, a statistical approach may be inescapable. As such, we can identify three key manifestations of SIC: strong SIC, moderate SIC, and weak SIC. *Strong SIC* consists of directly tracking dynamical differences given different SICs. *Moderate SIC* consists of mapping out the coexistence of attractors

(multistability) in phase space. *Weak SIC* consists of finding evidence of hysteresis–differences of where bifurcations occur as a system parameter is ramped up or down. Demonstration of hysteresis relies, however, not on different initial conditions, but on different initial parameters, and thus we assign it the *weak* appellation.

Weak SIC has long been noted in optically chaotic systems, including in fiber lasers [146], CO_2 lasers [12], Fabry-Perot lasers [41], and vertical-cavity surface-emitting lasers [140]. Hysteresis in ECSLs has amply been documented [81, 83]. For the ECSL, strong SIC is unlikely to be measured experimentally for the variety of reasons discussed above.

We therefore focus on moderate SIC. Though falling short of strong SIC, this provides detailed information on the structure of phase space. While coexistence of attractors and the associated multistability is expected based on theoretical considerations, in an experiment, as noted above, one might expect that the selection of initial conditions would have little effect on the BD, since it is reasonable to suppose that noise would cause the phase-space trajectory to converge rapidly toward the same attractor, regardless of initial conditions. Indeed, many experiments would suggest this is the case, but careful consideration–as we discuss below–shows that this experimental difficulty is surmountable. In this study, in addition to different forward (ramping η up) and reverse (ramping η down) BDs, that correspond to the phenomenon of hysteresis, we report *different routes to chaos corresponding to different initial states*, in our case adiabatically ramping η upwards.

Above we raised the point that noise could be expected to obviate the dependence of the BD in the initial conditions. [For our system, *initial conditions* mean lasing at low η on a selected ECM.] In fact, this is what is found; spontaneous-emission noise can make it in practice impossible to select the initial conditions–even in the sense of testing moderate SIC. But what if the effects of noise could be adequately suppressed? One might then expect a marked initial-condition dependence to the

route to chaos. Such a situation can be achieved when the ECSL is biased at high I, since at such injection levels, the ECSL output is dominated by stimulated emission whereas spontaneous emission, the presumed source of noise in careful experiments, plays a small role.

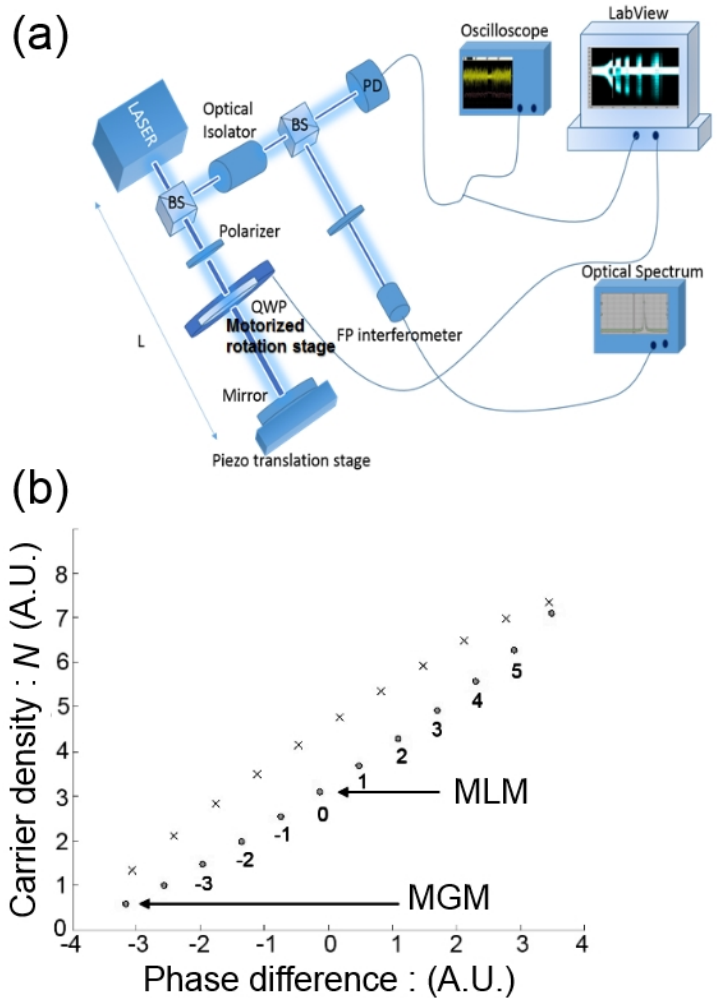

Figure 27: Experimental setup and ellipse structure of fixed points. (a) Schemmatic diagram of experiment showing LD: LD, BS: beam splitter, PD: photodetector, P : polarizer, QWP : quarter-wave plate, OI : Optical isolator, OSA : Optical spectrum analyzer. (b) Ellipse structure of fixed points in the phase-difference-vs.-N plane. Circles represent stable external-cavity modes (ECMs); crosses represent unstable antimodes. The labels indicate the mode number.

Specifically, we report a clear *experimental* moderate SIC in the route to chaos in a distributed-feedback LD ECSL biased at $I \sim (2-3)I_{th}$ in the long-cavity case, in

which L is chosen such that the relaxation-oscillation frequency f_{RO} is higher than the external-cavity free-spectral range $f_\tau = \tau^{-1}$. To do so, we select the initial ECM on which the laser operates at low η and map out the ensuing forward BD. Moreover, we highlight the differences in the bifurcation cascades for forward and reverse BDs.

5.3 Experimental Setup and Theoretical Framework

The experimental setup is shown in Fig. 27(a) (similar to that in Fig. 9 above) and was described in Ref. [81]. The LD free-running threshold current I_{th} is 9.27 mA. The temperature and I are stabilized. A real-time oscilloscope with 12 GHz bandwidth is used to capture the time-dependence optical output intensity $\mathcal{I}(t)$. We also measure the spectrum of $\mathcal{I}(t)$ (RF spectrum) with a spectrum analyzer with 23 GHz bandwidth and the optical spectrum with a high-resolution optical spectrum analyzer with 10 MHz optical resolution. In all cases, we choose $L = 30$ cm, corresponding to $\tau = 2$ ns, amply satisfying the long-cavity criterion. The feedback strength η, controlled by the reflection associated with the external cavity that is allowed to propagate back into the laser, is varied via the angle of the quarter-wave plate (QWP) in the feedback loop. Maximum feedback, corresponding to $\eta = 1$, is reached when the QWP angle is such that electric field is not subjected to any rotation. In that case, $\sim$20 % of the optical power is fed back onto the collimating lens.

Observation of the experimental intensity times series $\mathcal{I}(t)$, RF and optical spectra, as well as the time-averaged voltage V_{LD} across the laser-diode injection terminals are used to analyze the dynamical regimes involved in the BDs. In our previous publication [83], we showed that the forward BD exhibits a complex route to fully-developed coherence collapse interrupted by several windows corresponding to periodic and quasi-periodic behaviors, as well as period-doubling and intermittency phenomena. At low η and high I, the participating ECMs appear with a positive frequency shift with respect to that of the solitary LD, while at high η, closer to

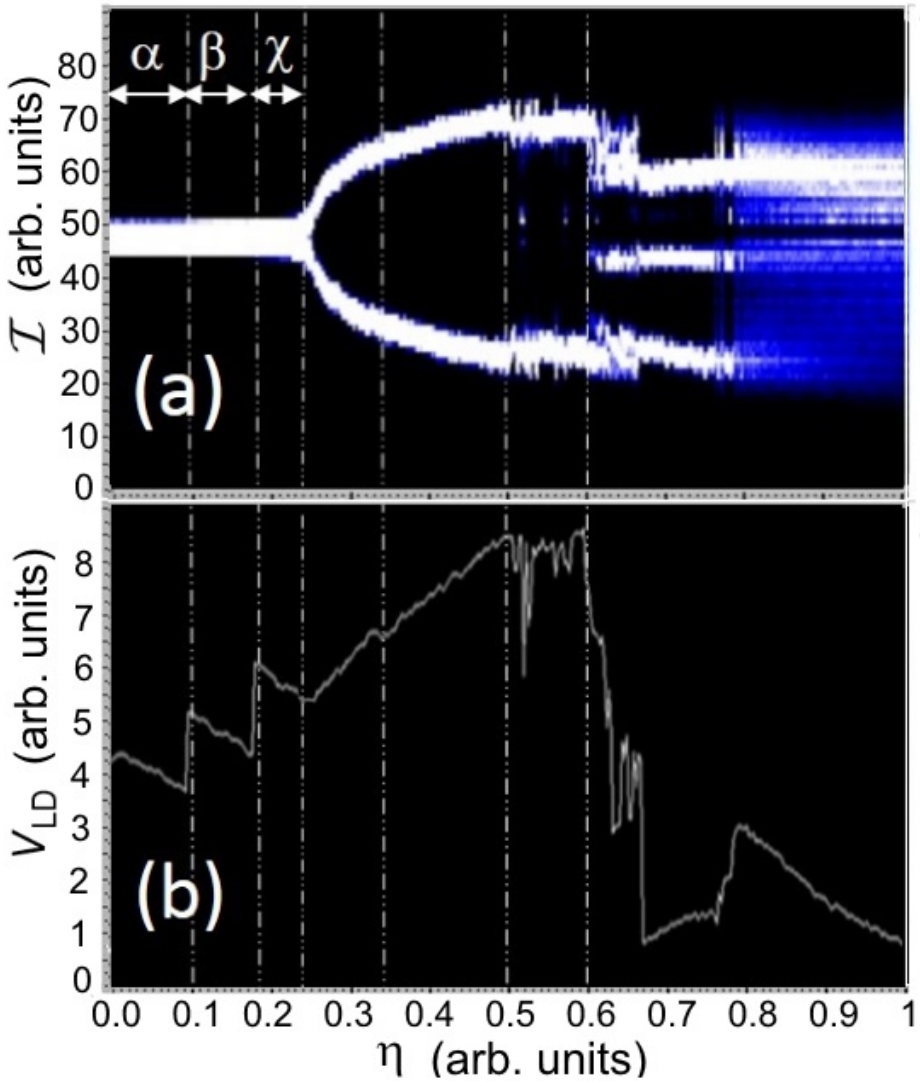

Figure 28: Reverse bifurcations diagrams. (a) Reverse BD and (b) the corresponding V_{LD}. $I = 22.59$ mA and $L = 30$ cm.

the coherence collapse regime, the optical spectra show negative-frequency shifted ECMs. The reverse BD is significantly different and displays mainly windows of periodic behavior, around positive-shifted ECMs, and with periods differing by the external-cavity round-trip time τ.

It is well-known that the delayed optical feedback has a profound impact on the dynamics of the ECSL and that it leads to the creation of two types of in-principal steady-state modes of the ECSL: potentially stable ECMs, separated in frequency by approximately f_τ, and unstable antimodes [115]. Moreover, according to the widely-used LK model [91], the ECMs and antimodes lie on an ellipse in the carrier density N versus phase difference $\Delta\phi(t) = \phi(t) - \phi(t-\tau)$ plane projected from the three-dimensional phase space $(N, \mathcal{I}, \phi)$, as shown in Fig. 27(b) [66]. Among ECMs, two stand out: the minimum linewidth mode (MLM) and the maximum gain mode (MGM). The MGM is the one with the lowest frequency (high-gain end of the ellipse), and is usually stable [60, 115]. The MLM is the closest ECM in frequency to the solitary LD mode. The evolution of the system can be visualized in terms of the trajectory moving amongst the ECMs and antimodes lying on this ellipse.

5.4 Experimental Results

In numerical simulations, one simply chooses initial conditions and computes from there. In experiment, however, this can be quite challenging. We introduce a controlled method to select experimentally the initial ECM at low η where the ECSL otherwise operates cw approximately like the solitary LD. The selection procedure is described as follows. Consider mapping out the forward BD starting with $\eta = 0$. In this case, the ECSL lases on the MLM; this is the initial state. Suppose we proceed ramping η up, and once the forward BD is obtained, map out the reverse BD starting from $\eta = 1$ and ramping it down. A typical example of the reverse BD is shown in Fig. 28(a) and the corresponding V_{LD} is shown in Fig. 28(b). It has been shown [156, 176]

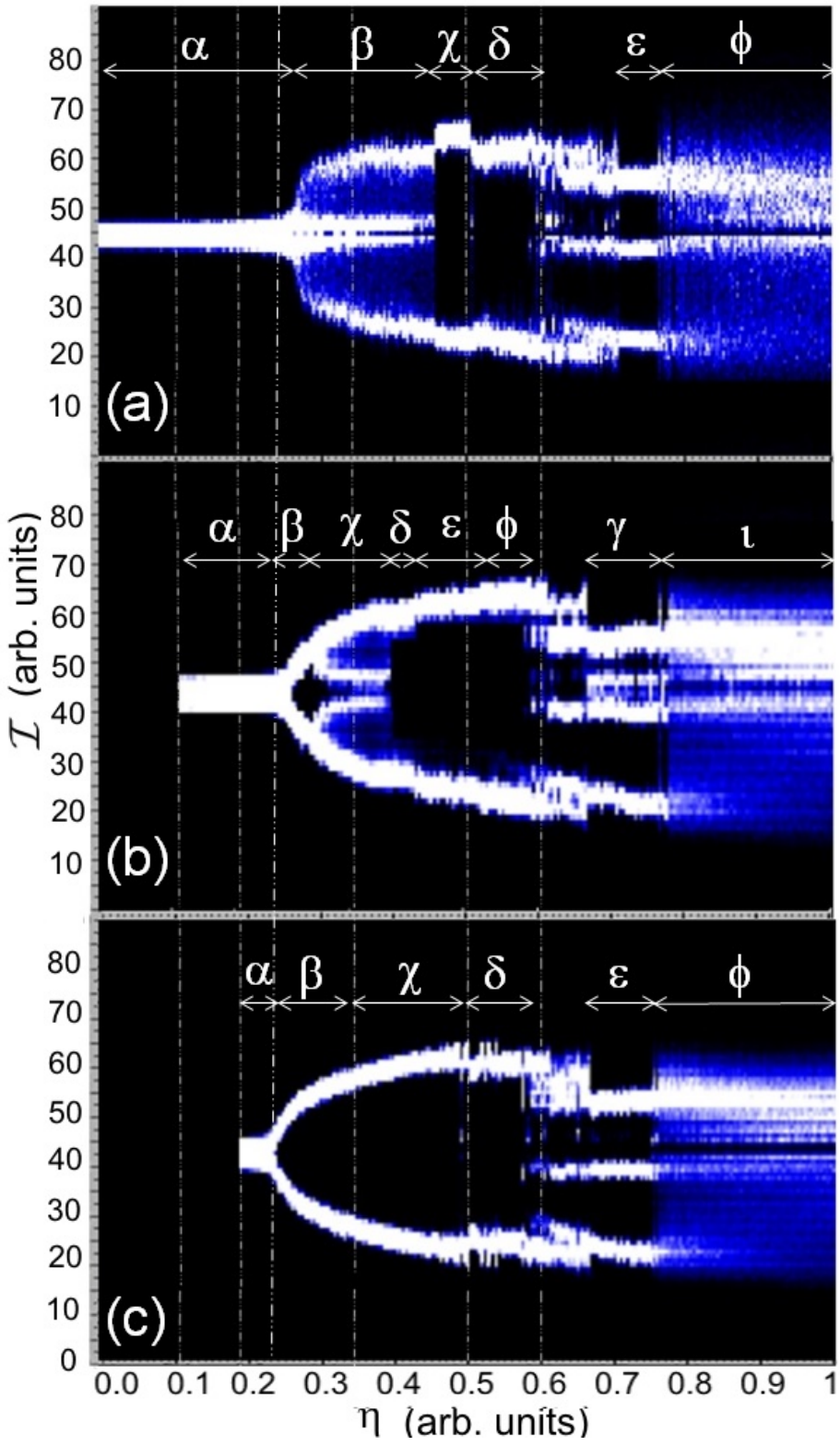

Figure 29: Forward BDs for several initial conditions. BDs with $I = 22.59$ mA and $L = 30$ cm. Initial mode (a) ECM 0, (b) ECM 1, and (c) ECM 2.

that V_{LD} tracks the changes in the time-averaged N. One observes two discontinuities in V_{LD} at $\eta = 0.1$ and 0.18 [Fig. 28(b)] in the horizontal band toward the left of the BD. These discontinuties reveal that different ECMs are participating in the light emission for regions α, β, and χ. As will be discussed later, the discontinuities in V_{LD} can be correlated with the changes in the optical spectrum, which evidence first a shift from ECM 2 to 1, followed by a shift from ECM 1 to 0 as η is ramped from 0.24 down to 0: Fig. 30(a) corresponds to Fig. 28 α , Fig. 31(a) to Fig. 28 β, and Fig. 32(a) to Fig. 28 χ.

Having illustrated the ability to detect the relevant ECM dominating the emission at low η, in Fig. 29(a), (b), and (c) we show forward BDs beginning on *different* ECMs (ECMs 0,1, and 2, respectively). The way we access different initial states is by ramping η *down* to a low value and then using this as the initial state from which we map out the forward BD as discussed in the previous paragraph. Though the lowest η reached in the three BDs is different, the three BDs overlap for η belonging to the interval [0.18,1]. As a result, in this interval, all the system parameters (*including* feedback phase) are identical except for the initial state of the ECSL at $\eta = 0.18$. *As a result, the three BDs represent three different routes to fully developed coherence collapse of the same ECSL starting from three different initial states.* The difference [see Fig. 29] among the three BDs starting from different ECMs is found to be significant in the sense that the route to chaos indeed depends on the initial state, as will be illustrated below.

Figure 29(a) shows the forward BD starting from ECM 0, and Fig. 30 shows the corresponding optical spectrum. It is clear from the optical spectrum that in region α of Figs. 29(a) only one ECM (ECM 0) of the solitary laser (MLM) participates to the dynamics. As shown in Fig. 29(a), this stable mode survives over a large feedback interval ($\eta < 0.24$) and remains in a cw regime. When η is increased above that level, the optical spectrum [Fig. 30(b)] reveals that several ECMs (-3 to 3) start

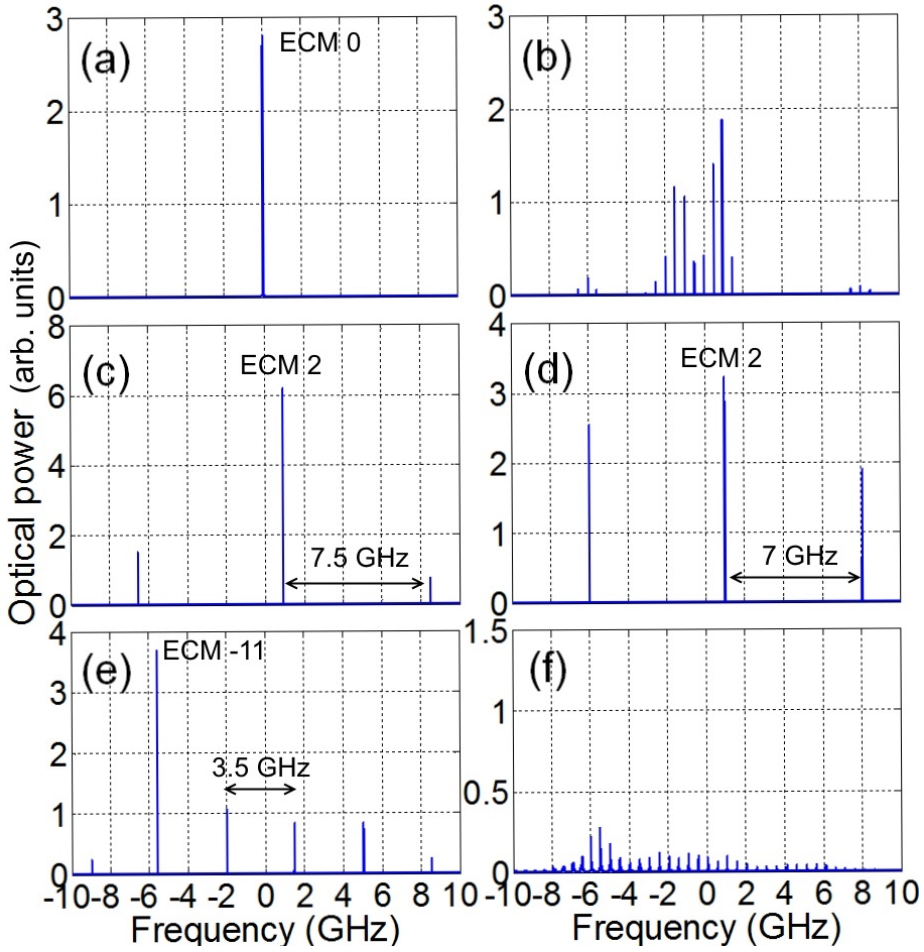

Figure 30: Optical spectra with the initial condition ECM 0. (a) $\eta = 0$, (b) 0.35, (c) 0.39, (d) 0.45, (e) 0.75, and (f) 0.9.

to participate in the emission. An analysis of the corresponding $\mathcal{I}(t)$ (not shown here), shows that the dynamical behavior is of a quasi-periodic nature. For a further increase in η (around 0.47), a discontinuity appears in the BD [region χ of Figs. 29(a)] that corresponds to an abrupt change of the dynamical behavior toward a limit-cycle oscillation. The optical spectrum [Fig. 30(c)] shows that the oscillation occurs around ECM 2, and the frequency of the oscillation 7.5 GHz as it corresponds to the distance between ECM 2 and its sidebands.

As we further increase η, at ~ 0.5, another limit cycle oscillating at $f_{\mathrm{RO}} \sim 7$ GHz is observed [region δ of Fig. 29(a)]. The optical spectrum of Fig. 30(d) further confirms that the oscillation is manifested as sidebands at around ± 7 GHz from ECM 2. Interestingly, the dominant mode (ECM 2) does not change in the transition from region χ to δ of Fig. 29(a), indicating two different frequencies at 7.5 GHz and 7 GHz on ECM 2. Previous works [38, 123, 162] show that our observation of two limit cycles with different frequencies around the same ECM is compatible with the LK prediction.

For a further increase in η, at ~ 0.6, intermittency between the dynamical behaviors of regions δ and ϵ of Fig. 29(a) is seen.

Region ϵ, which corresponds to $\eta \gtrsim 0.74$, displays a periodic oscillation with a fundamental frequency of ~ 3.5 GHz and a harmonic at ~ 7 GHz, centered around ECM -11 [Fig. 30(e)]. The presence of the harmonic indicates that the 3.5 GHz limit cycle originates probably from a period-doubling bifurcation of a 7GHz cycle that must have existed, at lower η, around ECM-11.

If η is further increased, the limit-cycle oscillation disappears, giving rise to fully-developed coherence collapse, (region ϕ) which involves multiple ECMs negatively-shifted in frequency [Fig. 30 (f)].

Figure 29(b) shows the forward BD starting from ECM 1 and Fig. 31 shows the corresponding optical spectrum. As expected, the ECSL initially displays cw behavior

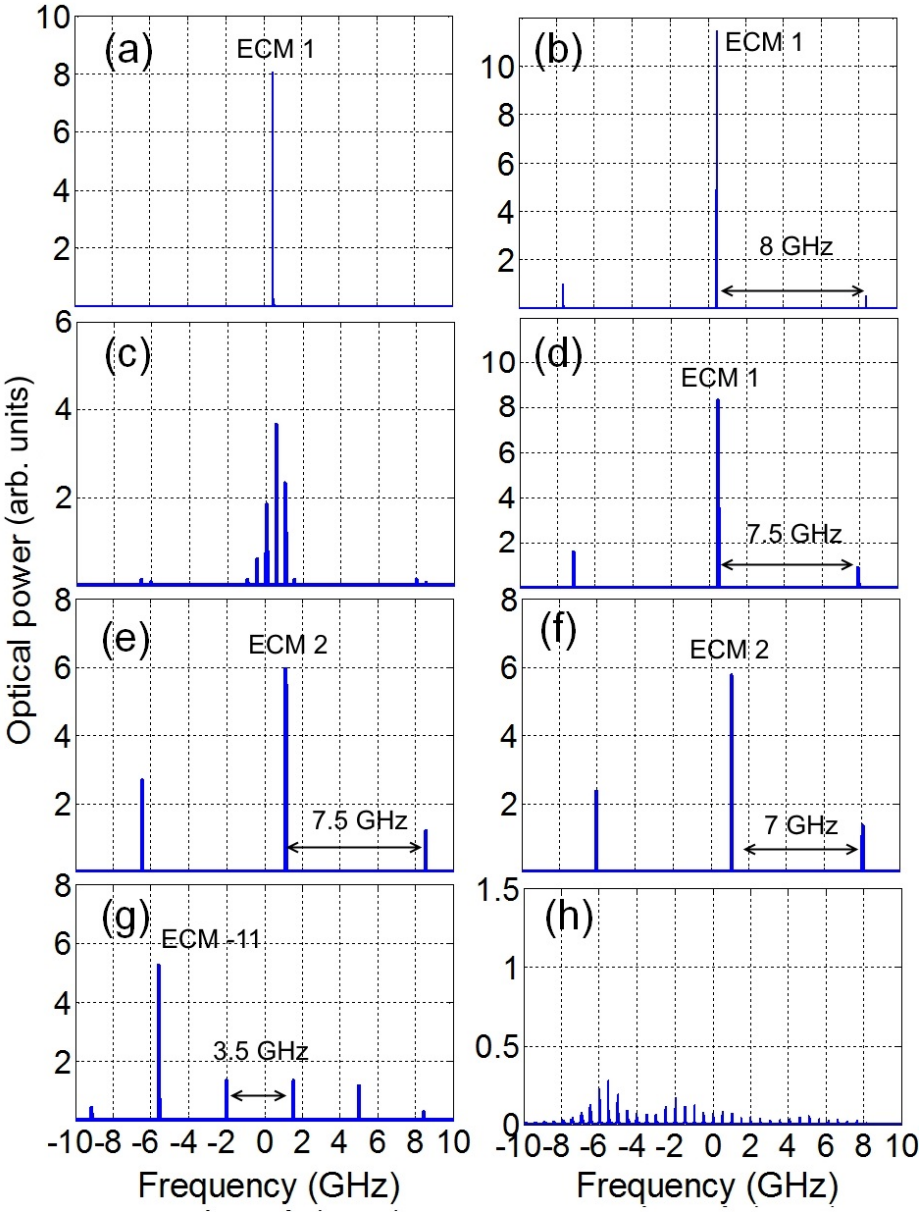

Figure 31: Optical spectra with the initial condition ECM 1. (a) $\eta = 0.15$, (b) 0.24, (c) 0.35, (d) 0.42, (e) 0.47, (f) 0.55, (g) 0.75, and (h) 0.9.

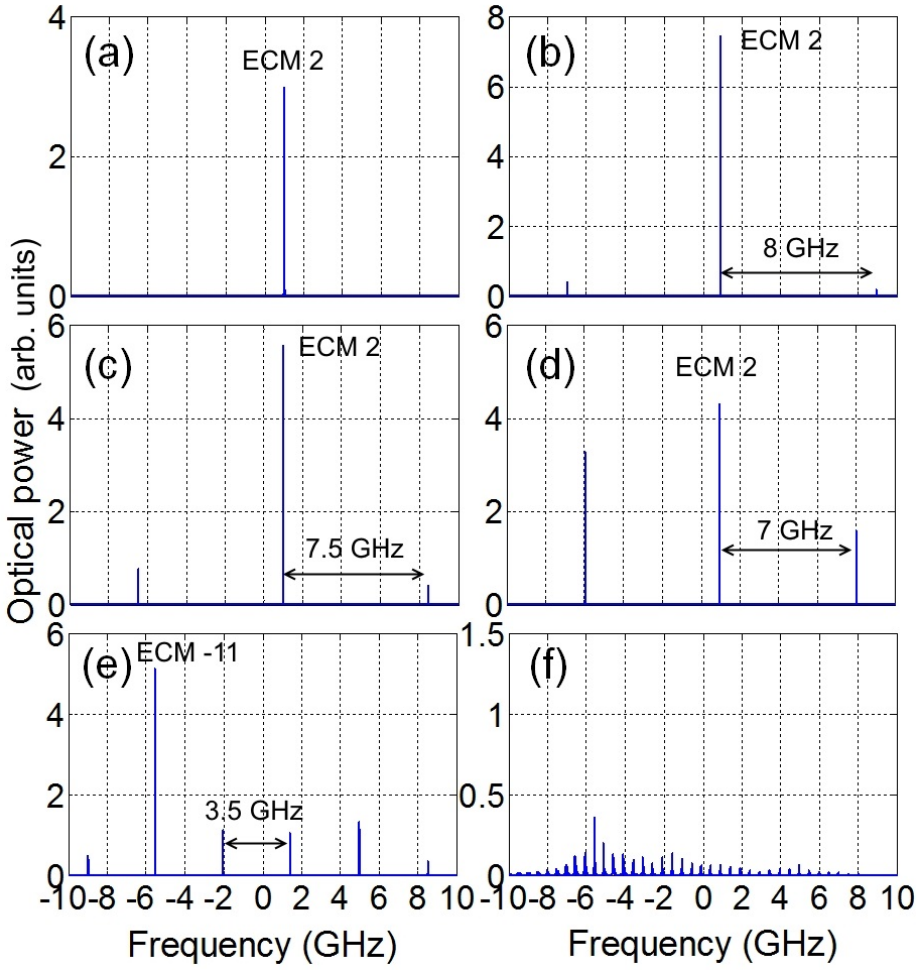

Figure 32: Optical spectra with the initial condition ECM 2. (a) η=0.2, (b) 0.3, (c) 0.39, (d) 0.55, (e) 0.7, and (f) 0.9.

[Fig. 31(a)] (region α ($\eta \sim 0.22$) of Fig. 29(b)] because only one fixed point (ECM 1) participates in the output. As η is increased above 0.22, it is clearly seen in the BD that the ECSL undergoes a periodic oscillation. This oscillation is manifested as sidebands ± 8 GHz from ECM 1 [Fig. 31 (b)]. This transition in the dynamics corresponds to a Hopf bifurcation leading to a limit cycle with frequency close to f_{RO}, as predicted by LK [123, 133].

With increasing η, additional sidebands near $\pm f_\tau$ appear in the optical spectrum [Fig. 31(c)], revealing the presence of a second frequency in the dynamics. The undamping of a second frequency close to f_τ corresponds to a second Hopf bifurcation and signals the development, in phase space, of a torus attractor. Note that both the limit cycle and the torus result from the destabilization of ECM 1 and are located around it in phase space [Figs. 31(b) and (c)].

For a further increase in η, another limit cycle appears in the BD. The optical spectrum shows [Fig. 31(d)] that this cycle is still centered on ECM 1, and has now a frequency of approximately ± 7.5 GHz. One notes that the dominant ECM 1 does not change in between Figs. 31(b) and (d), thus providing experimental evidence of the existence, at different η, around the same ECM, of two periodic solutions with different frequencies, 8 GHz and 7.5 GHz, whose separation is $\sim f_\tau$. As η is further increased, and region ϵ of Fig. 29(b) is reached, a small discontinuity is observed in the BD. The optical spectrum [Fig. 31(e)] reveals that this discontinuity corresponds to a shift from ECM 1 to 2. The ECSL still oscillates periodically, and the optical spectrum confirms that the frequency of the oscillations is still 7.5 GHz. Increasing η yet further, another limit cycle at $f_{\mathrm{RO}} \sim 7$ GHz is seen [region ϕ of Figs. 29(b)]. The active ECM 2 does not change in the transition from region ε to ϕ of Fig. 29(b), indicating again the existence of two different oscillation frequencies, 7.5 GHz and 7 GHz, again separated by $\sim f_\tau$ around a single ECM.

As η is increased even further, the scenario is similar to the one observed for Fig.

29(a): the trajectory moves toward negatively-shifted ECMS: first, a period-doubled limit cycle around ECM -11 is observed (region γ) and then a regime of fully-developed coherence collapse (region η).

Figure 29(c) shows the forward BD starting from ECM 2 and Fig. 32 the corresponding optical spectrum. In the initial region α ($\eta \sim 0.22$) of Fig. 29(c), only one fixed point (ECM 2) participates in the output, and the ECSL displays a cw behavior [Fig. 32 (a)]. As η is increased above 0.22 and region β is reached, the ECSL undergoes a periodic oscillation [Fig. 32 (b)], manifested as sidebands $\pm$8 GHz from ECM 2. Increasing η, the optical spectrum reveals the existence of two regions, χ and *delta*, corresponding to the appearance of two other limit cycles, of frequencies $\pm$7.5 GHz [Figs. 32 (c)] and $\pm$7 GHz [Figs. 32 (d)], still centered on ECM 2. It is noteworthy that the active ECM (2) does not change between Figs. 32(b),(c), and (d), thus providing evidence of the existence, at different η, of three periodic solutions with different frequencies, 8 GHz, 7.5 GHz and 7 GHz, whose separation is $\sim f_\tau$. For larger feedback regions, the behavior of the BD is similar to that of the two previous cases.

5.5 Conclusion

To conclude, we show that the initial conditions chosen have a profound impact on the route to chaos exhibited by ECSLs otherwise sharing identical parameters. In this sense, we demonstrate experimentally moderate SIC, *viz.* the coexistence of attractors in phase space We note in particular that the qualitative behavior of the route to chaos changes considerably at small η; however, the chaotic windows in Figs. 29 (a), (b), and (c) are of roughly the same size and are reached from almost the same η. These observations can be interpreted by the fact that at moderately low η, various attractors have developed around several ECMs, but have not yet merged or only a few neighboring attractors have merged [115]. As as result, the system is an

configuration of generalized muntistability in which the initial state will be crucial in determining the dynamics experienced by the ECSL, confirming the predictions by Mork and Masoller [115, 124]. For larger η, most attractors have merged and, independent of the initial state of the BD, the trajectories end being attracted by a group of merged attractor ruins located around ECMs with a large negative frequency detuning, as is typical in a regime of fully-developed coherence collapse. These are also the first experimental observations of the sensitivity to initial conditions of the BD of a high-dimensional dynamical system experiencing generalized multistability.

CHAPTER VI

LASER TERMINAL VOLTAGE CHANGE

We show that the bifurcations between dynamical states originating in the nonlinear dynamics of an ECSL at constant current can be detected by its terminal voltage. We experimentally vary the intensity fed back into the gain medium by the external cavity and show that the dc component V_{dc} of V tracks the optical intensity-based BD. It is shown using computational results based upon the LangKobayashi model that whereas optical intensity accesses the dynamical-state variable $|E|$, V is related to population-inversion carrier density N. The change in feedback strength affects N and thereby the quasi-Fermi energy level difference at the p-i-n junction band-gap of the gain medium. The change in the quasi-Fermi energy-level thereby changes the terminal voltage V. Thus, V is shown to provide information on the change in the dynamical-state variable N, which complements the more conventionally probed optical intensity.

This chapter is based on the following publication:

1. A. A. Sahai, B. Kim, D. Choi, A. Locquet, and D. S. Citrin, "Mapping the nonlinear dynamics of a laser diode via its terminal voltage," Opt. Lett. 39, 5630-5633 (2014).

6.1 Introduction

Laser diodes (LDs) driven at constant current are often exposed to optical feedback from external optical components. This time-delayed feedback triggers nonlinear dynamics observed as instability of emitted light with extreme sensitivity to operating parameters. Conventionally, the dynamics is studied for various applications [184] by sampling the optical output. In this Letter we present an effect where the voltage V across an ECSL complements the study of chaotic dynamics accessed by the time resolved optical output. We vary the intensity fed back into the gain medium by the external cavity and show that V tracks the optically measured bifurcations between different dynamical states. Applications of terminal voltage V across a LD [79, 120] have been explored in the negligible feedback linear-regime of the ECSL phase-space. However, the nonlinear dependence of the terminal voltage on the feedback level due to abrupt transitions of the dynamical state across different regions of the phase-space has been ignored. It is shown here that in the nonlinear regime, for a negligible instantaneous change in optical feedback, N changes significantly at the bifurcations corresponding to jumps of phase-space trajectory across several ECM. The quasi-Fermi level band-gap potential difference across the p-i-n active-medium changes proportional to change in N. An understanding of nonlinear instability of the dynamical state of the ECSL is critical because the effects of feedback are not understandable in terms of perturbation about a given ECM. It is well known both experimentally [21, 115, 123, 133, 204] and theoretically [92] that ECSLs exhibit a rich variety of nonlinearity, including fullydeveloped chaos, when varying operating parameters such as the feedback strength. The feedback-tovoltage physics in Refs. [79, 120, 121, 178] does not take account of the rich dynamics. We show that the dynamical regimesas well as the bifurcations between themare reproduced in the dc component V_{dc} of V while tracing the more typically detected optical output. The changes in feedback intensity modify the stimulation-rate controlling the population

inversion that affects the quasi-Fermi energy-levels and thereby V. In other words, we directly access a key dynamical-state variable, the inversion density N, which complements the knowledge of the system from conventionally probed state variable $|E|$, accessed through optical intensity. Importantly, V is an electrical signal, and thus a photodetector is not required in contrast to accessing the optical intensity I. The experimental results based on the terminal voltage are shown to be in excellent agreement with the optically detected signal and explained by the simple physical model presented here. Our results, therefore, encompass observations discussed in Refs. [6, 73, 156] where V was used to characterize certain dynamical characteristics. But, in our work we show the significance of terminal voltage as a dynamical state detector over the entire phase-space.

Also, the laser's current threshold reduction due to the feedback is the one of way to measure the feedback strength in many papers. However, the threshold reduction is not clear by different kinds of lasers. However, measuring the laser terminal voltage is the simple alternative way to measure the feedback strength in an ECSL.

Measuring the change in voltage across the LD terminal is considered a very good tool for indicating the carrier density variation [73]. Also, we show that the LD terminal voltage is directly related to the signal on an optical feedback such as a reflection. The intensity level of the external feedback is shown to affect the carrier density in the conduction band in direct band-gap of a compound semiconductor active region of the LDs. Feeding light back into the gain region of LD should accelerate the stimulated emission and depress the inversion. The reduced carrier concentration in the active region should lead to greater diffusion currents trying to resupply those carriers, and the constant current source will reduce the applied bias to prevent the overall current from increasing. With decreasing the carrier concentration in conduction band, the voltage difference of two terminal is decreasing.

Figure 33 shows increasing the feedback level at a fixed external cavity length, the

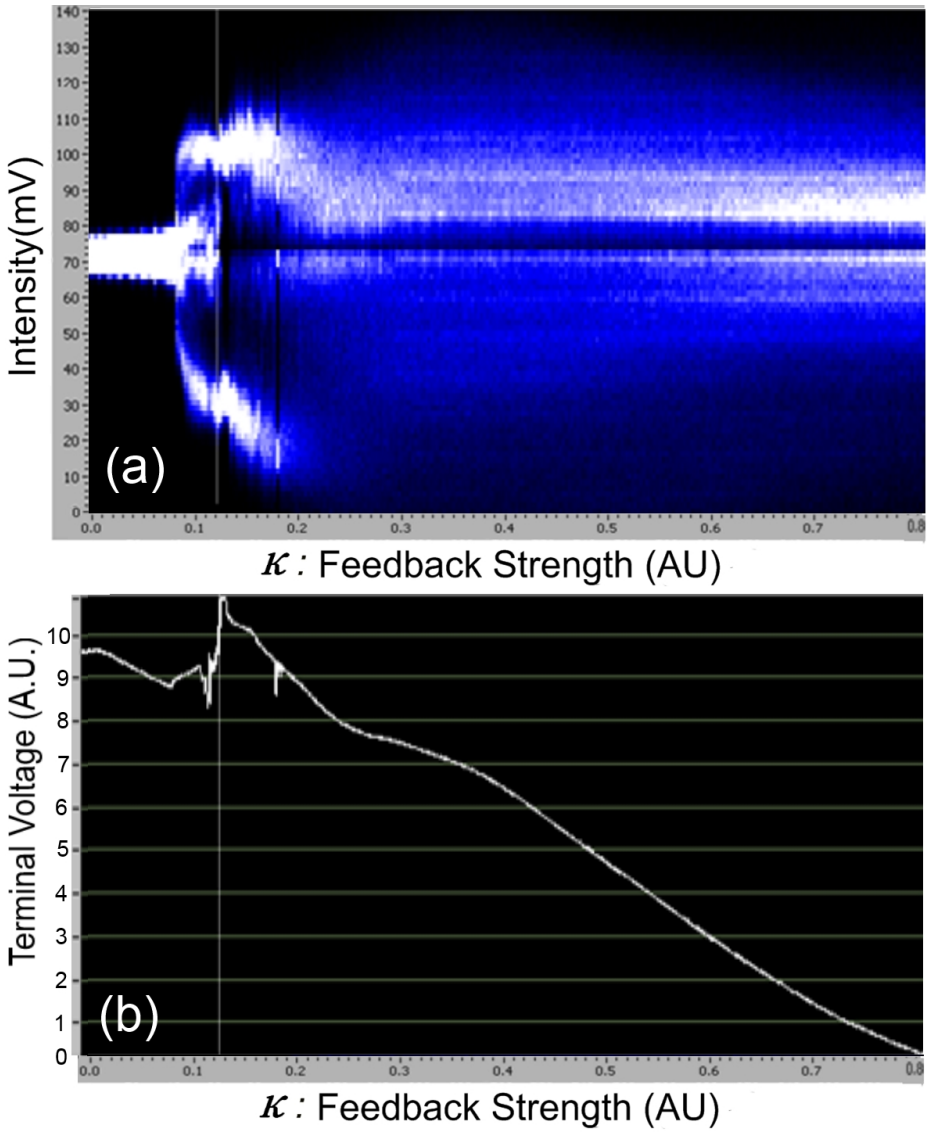

Figure 33: (a) Experimental Bifurcation diagram for $I = 18.63$ mA and $L = 30$ cm and (b)its corresponding the laser terminal voltage.

LD terminal voltage, $V_{\rm LD}$ reduces. So, under the maximum feedback configuration the LD terminal voltage is at its minimum. During these experiments, we fix $I =$ 18.63 mA and $L = 30$ cm. Then we change the intensity of the external feedback light into the diode cavity by changing the relative angle between the external polarizer and a QWP. The LD is driven using a constant current power supply. Also, the diode package is maintained at a constant temperature using an externally controlled thermoelectric cooler. It is the first time that the LD terminal voltage can be used to determine the dynamical regime of the laser and the feedback strength in ECSL dynamics.

In this Capter, we explore an effect where the voltage V across an ECSL evidences its underlying chaotic dynamics in the time-dependent optical output. Namely, we vary the strength associated with the intensity fed back into the gain medium by the external cavity and show that V tracks the BD (BD) measured optically.

Refs. [79,120] studied V in a LD with optical feedback. However, it has been only studied in the linear regime of the ECSL phase-space and an understanding accounting for the ECSL's dynamical state has been ignored. Optical feedback increases the instantaneous intensity, $\mathcal{I}(t)$ in the gain medium resulting in a reduction in carrier density $N(t)$ due to higher stimulation rate in the active medium ($-\dot{N} \propto |E|^2 \propto \mathcal{I}$). It is shown in our model and experiments that an increase in the optical feedback reduces N which results in a significant reduction of the potential difference of the *p-i-n* quasi-Fermi levels in the active medium. Since the change in N can be significant it can cause the phase-space trajectory itinerancy over many spatial modes of the external cavity.

Nonetheless, an understanding accounting for the ECSL's dynamical state is critical. Since the *change* in N due to feedback can be significant compared with N, the resulting nonlinear effects can involve phase-space trajectories spanning several external-cavity modes. In other words, the effects of feedback may not necessarily be

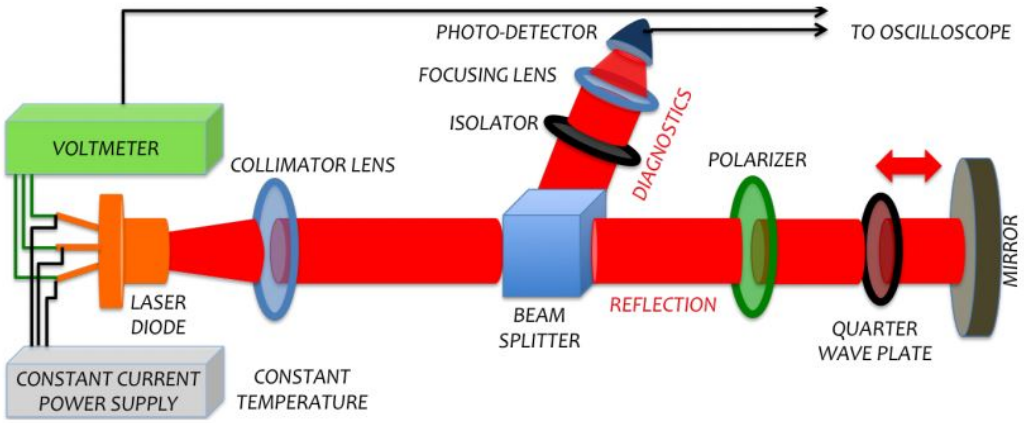

Figure 34: Experimental setup. A distributed feedback LD is powered with a constant-current power supply (maintained at a constant temperature) and its dc terminal voltage $V_{\rm dc}$ is monitored on a voltmeter and oscilloscope. The laser output is linearly polarized and split with one path being for external reflection to form an external cavity and the other arm being for diagnostics. The diagnostics are isolated from the dynamical system using an optical isolator.

understandable in terms of perturbation about a given external-cavity mode.

6.2 Experimental Setup and Theoretical Framework

The experimental setup is shown in Fig. 34. The intrinsically single-longitudinal-mode InGaAsP distributed feedback laser used as the gain medium oscillates at 1550 nm and maximum cw power 15 mW. The free-running threshold current I_{th} is 9.27 mA. T and I controllers make it possible to maintain constant T (drift <0.002 K/dy) and I (drift <100 μA/dy). In order to detect changes in $V_{\rm dc}$, a multimeter and an oscilloscope (12-GHz cutoff) are connected to the voltage terminals of the distributed feedback laser. The external cavity length L is set to be 15 and 65 cm, equivalent to external-cavity round-trip time $\tau = 1$ and 4.3 ns, respectively. With the help of a motorized piezo-actuation stage, the angle of the quarter-wave plate (QWP) is controlled in small steps. In this Letter, ∼16 % of the optical power is fed back onto

the collimating lens at maximum experimental feedback $\eta = 0.8$. The optical signal on the diagnostics path is sent to a photodetector and is recorded as $\mathcal{I}(t)$.

6.3 Experimental Results

Figure 35 shows the experimental BD and dc terminal voltage $V_{\rm dc}$ as functions of the experimental feedback strength η for a given L and injection current I. The BD is obtained by collecting the time series $\mathcal{I}(t)$ and plotting the histogram of local extremal values for a given η; density is high in white (blue in the color figure) but low in black regions.

Bifurcation cascades between apparently stable and unstable regions are observed as qualitative changes in $\mathcal{I}$ as η varies in Figs. 35(a) and (c). Because of the relatively low value of I, $\mathcal{I}$ is weak and does not always stand out from system noise. Consequently, the thinner regions $\mathcal{I}$, that we call *stable*, do not necessarily correspond to textbook stable CW behavior but also contain regimes in which phase-space trajectories have small excursions around an island of stability resulting in low-amplitude instabilities around a single ECM have developed. The wider regions in $\mathcal{I}$, referred to as *unstable* regions, typically correspond to regimes in which phase-space trajectories wander around several ECMs and thus clearly stand out above the noise.

The differences between Figs.35 (a), (b) and (c), (d) can largely be attributed to the frequency separation between ECMs. When L is long (65 cm), the spectral separation between ECMs is reduced (for $L = 15$ cm, the external-cavity free spectral range is 1 GHz, for $L = 65$ cm, 233 MHz) in the optical spectrum. Therefore, each participating mode being close in phase space, large-amplitude itinerancy between several modes is easily observed. Indeed, numerical simulations of the trajectories on the ellipse in phase space projected on the N-*vs.*-phase plane show that the proximity of the ECMs for longer cavities impedes the development of independent attractors

and thus prevents the existence of a bifurcation cascade. Conversely, increased distance between the ECMs for shorter L means that larger η is needed before attractor merging occurs, thus explaining the longer stable regions.

In Figs. 35 (b) and (d) $V_{\rm dc}$ is plotted as η is varied corresponding to the intensity, $\mathcal{I}$ BD's in Figs. 35(a) and (c), respectively. We note an overall (though clearly not monotonic) decrease in $V_{\rm dc}$ with increasing η; various bifurcations that occur in $\mathcal{I}(t)$ in Figs. 35(a) and (c) at specific values of η are clearly reflected at the same η in the terminal voltage $V_{\rm dc}$ in Figs. 35 (b) and (d). This juxtaposition of $\mathcal{I}$ with $V_{\rm dc}$ illustrates the ability to tap into additional dimensions of phase space with high-fidelity but without a photo-detector.

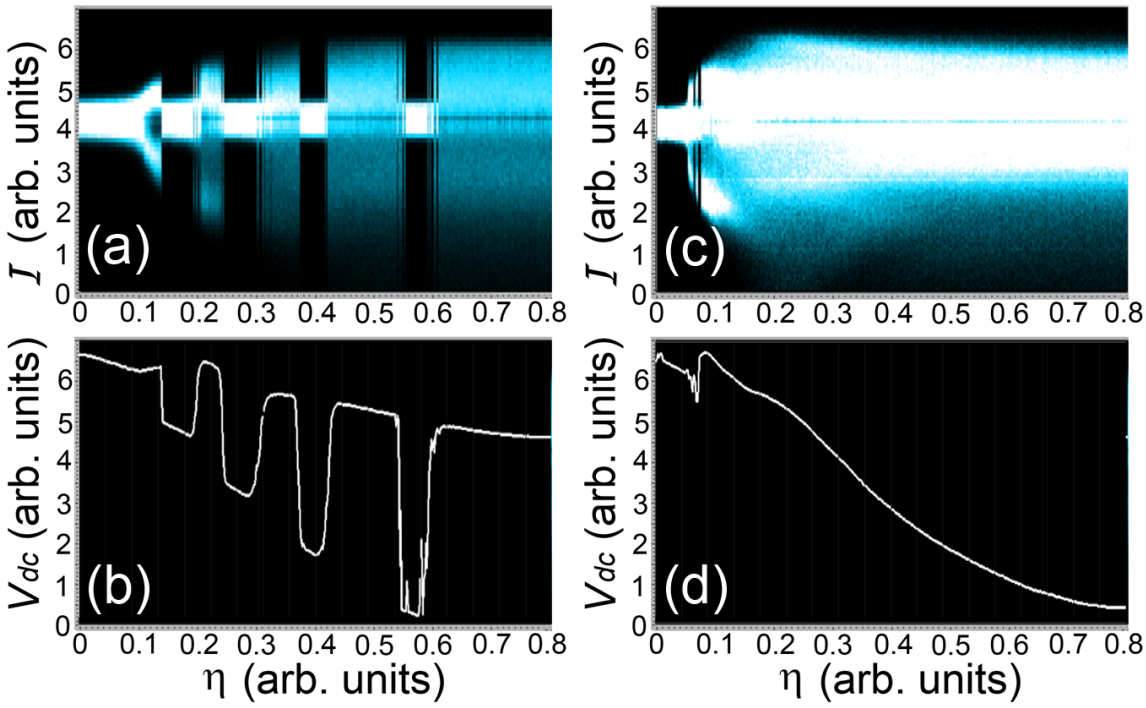

Figure 35: (a) Experimental BD and (b) and corresponding $V_{\rm dc}$ for $I = 11.42$ mA and $L = 15$ cm, resulting in a frequency spacing between ECMs of $\sim$1 GHz. (c) Experimental BD and (d) corresponding $V_{\rm dc}$ for $I = 11.42$ mA and $L = 65$ cm, resulting in a frequency spacing between ECMs of $\sim$233 MHz.

We next turn to a theoretical description of the dynamics of the various dynamical variables associated with the ECSL. The LK (LK) model provides a single-longitudinal-mode description of an ECSL in terms of rate equations [92]. It must be borne in mind that this approach integrates out spatial degrees of freedom; nonetheless, while obtaining perfect agreement between theory and experiment is not expected, the LK equations reliably predict dynamical trends as a function of various parameters [92]. The LK equations are

$$\frac{dE}{dt} = \frac{1}{2}(1+i\alpha)(\mathcal{G}-\tau_p^{-1})E(t) + \frac{\kappa}{\tau_{in}}E(t-\tau)e^{-i\omega_0\tau} + F_E, \tag{22}$$

$$\frac{dN}{dt} = pJ_{th} - \frac{N(t)}{\tau_s} - \mathcal{G}|E|^2. \tag{23}$$

The units are defined in Ref. [123]; $E(t)$ the slowly-varying envelope of the complex optical field (E is normalized such that $|E|^2$ is the number of photons in the active region per active-region volume v), $N(t)$ is the carrier density in the active region, $\mathcal{G} = g[N(t) - N_0]$ is the modal gain (in s^{-1}) where g is the differential modal gain coefficient (in m^3/s), and N_0 the carrier density at transparency. In addition, τ_p is the photon lifetime, τ_s is the carrier lifetime, τ_{in} is the round-trip time in the gain medium, $\tau = 2L/c$ is the optical round-trip time in the cavity (the time delay) with c the speed of light, α is the linewidth-enhancement factor, p is the pumping factor, and I_{th} is the threshold current divided by the absolute value of the electron charge multiplied by v (thus in units of $\mathrm{m}^{-3}\mathrm{s}^{-1}$), i.e., $J = pJ_{th}$ is the pumping injection current areal density where p provides a measure of injection current referenced to the threshold value; it is thus the carrier density per unit time supplied by the injection current. Note that the *theoretical* feedback strength κ is proportional to the *experimental* feedback strength η, but the constant of proportionality is not accurately determined. The spontaneous-emission noise is modeled by an additive term $F_E = \sqrt{2\beta N}\xi$, where β is a spontaneous-emission noise factor, and ξ is a complex Gaussian white noise of zero

mean and autocovariance function $C_x(t) = 2\delta(t)$. We numerically integrated Eqs. (22) and (23) with parameters $g = 8.1 \times 10^{-13}$ m^3/s, $N_0 = 1.1 \times 10^{24}$ m^{-3}, $\tau_p = 1$ ps, $\tau_{in} = 8$ ps, $\tau_s = 1$ ns, $\alpha = 3$, and $\omega_0\tau = 2\pi\nu$ for some integer ν [81]. Other parameters will be specified in the context.

Figures 36(a) and (c) show the theoretical (a) BD (subtracting off the time-averaged $\mathcal{I}$) and (b) and (d) the time-averaged carrier density $N_{\rm dc}$ as a function of κ for L=15 and 65 cm, respectively. Note that the BDs bear a close resemblance to those of Fig. 35. This is discussed at length in Ref. [81]. As we discuss just below, $N_{\rm dc}$ is directly connected to $V_{\rm dc}$ as measured experimentally.

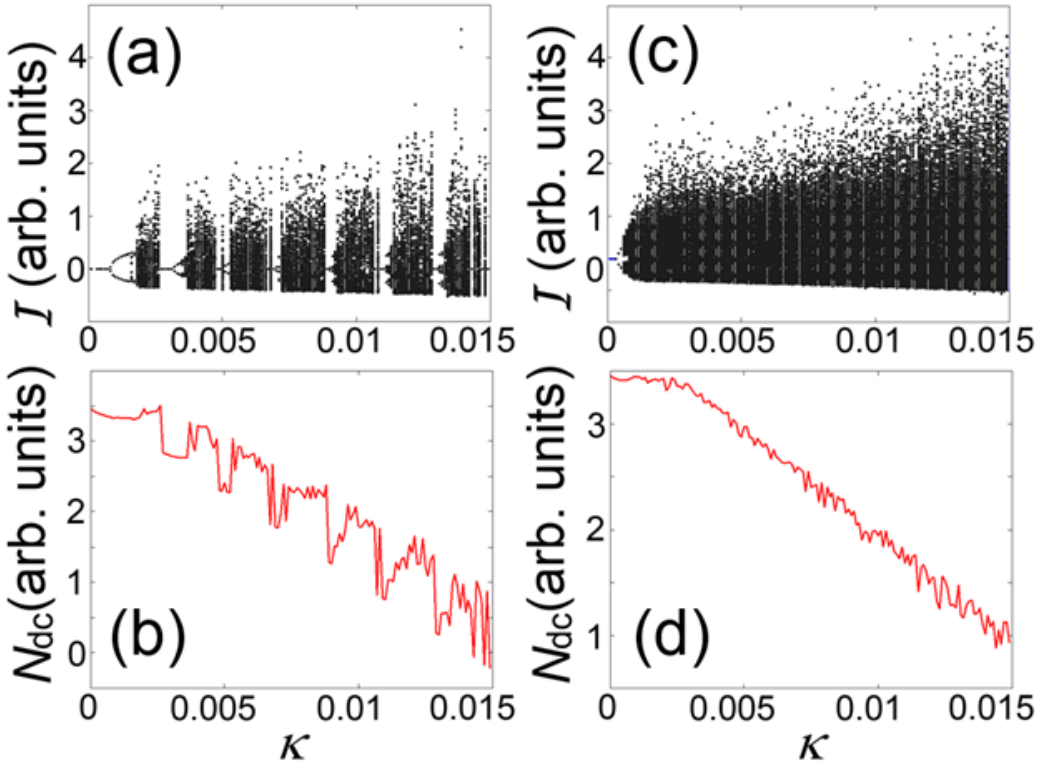

Figure 36: (a) Theoretical BD and (b) corresponding $N_{\rm dc}$ ($\propto V_{\rm dc}$) for $p = 1.3$ and L = 15 cm. (c) Theoretical BD and (d) $N_{\rm dc}$ for $p = 1.3$ and $L = 65$ cm.

The voltage across a p-i-n structure of the LD, V is the product of the electron charge $-e$ and the difference Φ(t) between the quasi-Fermi levels $\mathcal{E}_F^j$ on the $j = p$

and n side. Thus, assuming flat bands in the quasi-neutral regions,

$$V(t) = \mathcal{E}_F^n(t) - \mathcal{E}_F^h(t) = \left[\ln\left(\frac{N_e(t)}{N_e^i(T)}\right) - \ln\left(\frac{N_h(t)}{N_h^i(T)}\right)\right] k_B T, \tag{24}$$

where N_e, N_h, $N^i(T)$ are the electron, hole (in the n and p-type regions, respectively), and intrinsic concentrations [79]. We assume I and T are constant, and the ECSL fluctuates around one ECM. The change in the carrier concentration is assumed to be small compared with the carrier concentration N_{ECM} in the quasi-neutral intrinsic region (gain medium), giving $N(t) = N_e(t) = N_h(t) = N_{\mathrm{ECM}}$. By measuring Φ as N changes, we can determine the voltage change in V in response to the the change in N due to the optical-feedback induced dynamical state. It should be noted that when the ECSL undergoes a bifurcation, N undergoes a discontinuity; however, the expression (taking the time-dependent variations to be smaller on average than the dc components) relating the change in V_{dc} due to the change in the dc value of N starting with Eq. (24) is

$$\delta V_{\mathrm{dc}} = e\delta\Phi_{\mathrm{dc}} = \frac{e}{N_{\mathrm{ECM}}}\left(\frac{\partial \mathcal{E}_F^e}{\partial \ln N_e} - \frac{\partial \mathcal{E}_F^h}{\partial \ln N_h}\right)\delta N_{\mathrm{dc}}. \tag{25}$$

holds where $\delta N_{\mathrm{dc}} = N - N_i$ in the gain medium within a given dynamical regime. Since $\partial \mathcal{E}_F^e / \partial \ln N_e > 0$ and $\partial \mathcal{E}_F^h / \partial \ln N_h < 0$ [20], δV_{dc} is proportional to and of the same sign as δN_{dc}.

The voltage fluctuation $-e\delta\Phi_{\mathrm{dc}}$ (and hence δV_{dc}) is proportional to δN_{dc}. Optical feedback induces a rise in the photon number $\propto |E|^2$ in the active region, which results in reduced N_{dc}. Externally feeding light back into the gain region in turn increases the rate of stimulated emission. This thereby reduces the population inversion. Consequently, the overall reduction in N_{dc} in the active region leads to a reduction in Φ_{dc} and therefore in V_{dc}. While the analysis above is expected to remain approximately valid to describe the time-dependence of the quantities, our experiment only monitors the the time-averaged voltage V_{dc} since our volt meter is relatively slow. Nonetheless,

the dc analysis provides rich insight into the physics–at a level comparable to the BD associated with $\mathcal{I}$. Clearly, signatures of the various bifurcations are observed both in the experiment [Fig. 35(b) and (d)] as well as in the theory [Fig. 36(b) and (d)], the latter being computed by means of the LK equations; based on Eq. (24) in the dc limit, we see that these latter curves are proportional to $V_{\rm dc}$. Namely, the overall downward trend in $V_{\rm dc}$ with increasing feedback (experiment κ; theory η) is interrupted by abrupt jumps at bifurcations, as can be seen by comparing with the corresponding BDs [Fig. 35(a) and (c); Fig. 36(a) and (c)]. With the understanding of the theoretical model by comparing Figs. 35(a), (c), and (b), (d), respectively, we can clearly see a distinct advantage of the terminal-voltage approach. While $N_{\rm dc}$ reduces, the BD fails to provide information on the itinerancy of the phase-space trajectories about the ECMs. For the case of $L = 65$ cm, at fairly low κ the ECSL enters a chaotic regime with no clearly discernible bifurcations apart from the initial one upon entering the chaotic regime. In contrast, $V_{\rm dc}$ undergoes a steady decrease in the unstable region revealing a drift in phase space in the direction of the maximum gain mode.

The ECSL, at the level of the LK model, is described by three dynamical variables, *viz.* the electric-field amplitude $|E(t)|$ (or $\mathcal{I}(t) \propto |E(t)|^2$), the optical phase $\varphi(t) = \arg E(t)$, and the carrier density $N(t)$. $\mathcal{I}(t)$ is the quantity probed in the vast majority of published work. The present work provides information on the dynamical dependence of N, though only the dc value N_{dc} here. Nonetheless, such information is indeed valuable and provides insight into the dynamics on a level comparable to the BD constructed from $\mathcal{I}(t)$. The steady-state solutions of the LK equations (22) and (23) are the stable ECMs and unstable antimodes. Plotted in the N-*vs.*-ϕ plane, these are points lying on an ellipse [115]. Thus, measuring $V_{\rm dc}$ provides information on those ECMs that dominate the phase-space trajectory. Such measurements can

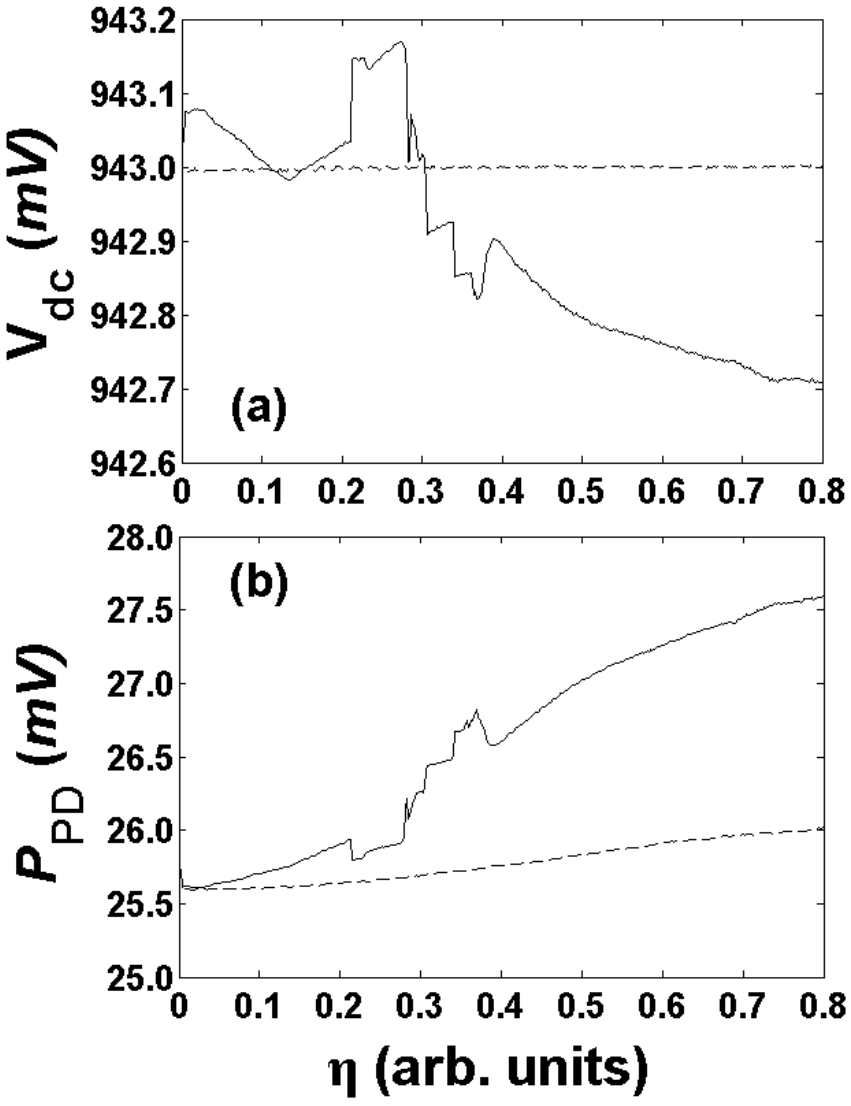

Figure 37: (a) $V_{\rm dc}$ and (b) voltage $P_{\rm PD}$ across PD detecting light at back facet of LD for $I = 21.14$ mA and $L = 30$ cm. The solid curves show the voltage for the optimally aligned external cavity; the dashed curves with the external cavity intentionally misaligned. The dashed curve in (b) shows that $P_{\rm PD}$ changes with nominal η even when the light fedback into the LD is negligible.

be directly be coupled with measurements of the optical spectrum of the ECSL output [81]. While the dc measurement here does not directly reveal the underlying detailed dynamics, it is clear that when the system undergoes a bifurcation, the relevant ECMs can be identified by measuring $V_{\rm dc}$. Future work will focus on resolving the dynamics of $N(t)$. The remaining dynamical variable, $\varphi(t)$ has attracted less attention, and indeed requires an interferometric approach, which is beyond the scope of the current work.

In addition to studying the dynamics, we show that the physics of $\delta V_{\rm dc}$ can be used to determine the coupling between the LD and the external cavity. Changing the angle between the QWP and polarizer that controls η and monitoring the LD packaged internal photodiode is not always a good indicator of the light fed back onto the LD active region. In this context we show that $V_{\rm dc}$ can be used as reliable metric for understanding the ratio of feedback into the active medium. As we show below, while the *nominal* value of η might be changed considerably, if there is significant misalignment in the external cavity, the real feedback strength onto the LD active region might actually be negligible.

In Fig. 37 (a) is plotted $V_{\rm dc}$ for $I = 21.14$ mA and $L = 30$ cm for various apparent η. The solid curves show experimental (a) $V_{\rm dc}$ and (b) the laser-package internal photodiode voltage $P_{\rm PD}$ due to optical power incident collected directly from the LD back facet. In the solid curves, the external cavity is optimally aligned so that the overlap of the feedback light with the LD is maximum; the dashed curves show corresponding data when there is intentional significant misalignment. Note that in Fig. 37 (a) (dashed curve) $V_{\rm dc}$ remains constant when the fed back light does not reach the LD; however, Fig. 37 (b) (dashed curve) shows that $P_{\rm PD}$ increases ~ 1.54 % as the nominal η increases over the same range when the external cavity is intentionally misaligned. This occurs due to stray light impinging on the back-facet PD. In practice, adequate isolation of this PD may be quite difficult. Therefore, use

of $V_{\rm dc}$ may provide a more reliable window into the internal dynamics of the ECSL, but also provides a more practical way to ensure that the external cavity is optimally aligned, and therefore that *apparent* changes in η correspond to *actual* changes.

6.4 Conclusion

We show that the bifurcations between dynamical states originating in the nonlinear dynamics of an ECSL at constant current can be detected by its terminal voltage. We experimentally vary the intensity fed back into the gain medium by the external cavity and show that the dc component V_{dc} of V tracks the optical intensity-based BD. It is shown using computational results based upon the LangKobayashi model that whereas optical intensity accesses the dynamical-state variable $|E|$, V is related to population-inversion carrier density N. The change in feedback strength affects N and thereby the quasi-Fermi energy level difference at the p-i-n junction band-gap of the gain medium. The change in the quasi-Fermi energy-level thereby changes the terminal voltage V. Thus, V is shown to provide information on the change in the dynamical-state variable N, which complements the more conventionally probed optical intensity. Indeed, we can view the current work in the broader context in which even under significant feedback well into the chaotic regime the LD in acts as a photodetector as well [45, 104]. But we emphasize that the significance of our work lies in the access provided to a dynamical variable hitherto rarely if ever studied, *viz.* N. This chapter explores the application of this approach in a specific regime, namely moderate cavity lengths and moderate injection, but over a wide range of feedback strengths. Clearly, the approach has application over diverse operating and design regimes, which will be the subject of future studies.

CHAPTER VII

STATISTICAL PROPERTIES OF CHAOTIC TIME SERIES FROM ECSLS

An ECSL can be used to exhibit chaotic behavior. The corresponding statistical properties might be influenced by the variation of control parameters, such as the pump current and the feedback strength. An ECSL operating in the LFF regime demonstrated experimentally [74] that the statistical distribution of the laser intensity has strong asymmetry about its maximum because of sporadic intensity-dropout events. It is still unclear in which way the probability density function (PDF) of the optical intensity of an ECSL operating in a chaotic regime, including the LFF and fully developed coherence collapse regimes, will qualitatively change with varying I and/or feedback strength. Therefore, we experimentally and numerically study the statistical properties of the time-dependent intensity of an ECSL. We compare the probability density distribution of the raw time series and investigate the mean and the variance as the first order statistics. We also compare the peak of the autocorrelation around the delay time (peak size), and the width (3 dB peak width) of the autocorrelation at first peak (the time shift is equal to zero) as a function of the current, for different feedback strengths as the second order statistics.

We study experimentally and theoretically based on the LK model first- and second-order statistical measures of the optical intensity of a chaotic ECSL in fully-developed coherence-collapse. The second-order statistic is characterized by the autocorrelation function, for which we achieve consistent experimental and theoretical results over the entire parameter range considered. For the first-order statistic, we

find that the experimental probability-density function is significantly more concentrated around the mean optical power and robust to parameter changes than the density functions obtained from the LK model.

This chapter is based on the following publications:

1. Nianqiang Li, Byungchil Kim, A. Locquet, Daeyoung Choi, Wei Pan, and D. S. Citrin,"Statistics of the optical intensity of a chaotic external-cavity DFB laser," Opt. Lett. 39, 5949-5952 (2014).

2. N Li, B.C. Kim, A. Locquet, D.S. Citrin, and W. Pan, "Numerical Characterization of Probability Density Function of the Optical Intensity of Chaotic External-Cavity Semiconductor Lasers", IS-PALD, P7, Paris, France (2013).

7.1 Introduction

The dynamics of semiconductor lasers with delayed optical feedback [ECSL], are of interest in nonlinear science and for applications [21,78,158,158,184,204]. Much work has been devoted to elucidating the nonlinear dynamics of ECSLs [81, 115, 123, 132]. The LK model is useful to understand feedback-related dynamics of ECSLs [92], though it is not successful in accounting for all observations; it considers only one spatial dimension and thus does not describe the overlap of the optical mode with the gain medium nor does it account for multiple round-trips in the external cavity (EC). Still, the LK model accounts qualitatively and sometimes quantitatively [197] for many experimentally observed dynamical regimes [184] as well as certain dynamical tendencies depending on injection current J, cavity length L, and feedback rate [81]. In view of LKs successes, it is important to determine how well it reproduces statistical properties associated to ECSL dynamics. In addition to being an important way to characterize chaotic processes, precise knowledge of the statistics of a random variable is fundamental in random-bit generation (RBG) applications as it determines both the random-bit rate and the post-processing techniques that should be used to generate random bits [86]. Due to the complexity of the dynamics and the broad and multidimensional nature of the parameter space, a systematic statistical comparison of observed behaviors and that predicted by LK model is called for .

Previous studies of the statistics of the time-dependent intensity *I(t)* focused on the LFF regime in single- and multi-longitudinal mode lasers [74, 75, 192], typically seen near threshold J_{th} for low-to-moderate feedback [71, 124, 174]. LFF is characterized by rapid (< 1 ns) *I(t)* dropouts followed by a slow (several ns) recovery during which the laser experiences a pulsating behavior, and can be explained as chaotic itinerancy with drift [42, 205] . Pulsing occurs not only in LFF but also for slightly higher J [42], as well as determines to some extent the statistics of *I(t)* [177]. At even larger J, a chaotic regime of fully-developed coherence-collapse can be observed, in

which *I(t)* typically undergoes sub-ns fluctuations around its mean value, but seldom reaching zero and without experiencing dropouts.

Experimental studies of the probability-density function (PDF) of *I(t)* with high-bandwidth apparatuses show, for truly-single-longitudinal mode emission, PDFs peaked just above the spontaneous-emission level and decreased monotonically with increasing *I(t)* [74,192]. Besides, these investigations also show that numerical simulation of the LK model can reproduce the main features of the experimental PDFs. Differences between previous experiments might result also from inadequate characterization of the laser operating parameters as well as limitations of the physical detection used.

While the statistics of *I(t)* in LFF have been studied and compared to the LK model, statistical studies for well-developed chaos, corresponding to coherence collapse, are sparse [18]. It is known that traditional LFF exists only slightly above or below the threshold current J_{th} of the solitary laser [115]; the associated dropouts rapidly disappear in experiment at J just a few percent above J_{th} as coherence collapse is entered.

In this section, we explore the agreement between experimental and numerical first- (FO) and second-order (SO) statistics of an ECSL operated in coherence collapse. The FO statistic of the chaotic process is characterized by means of the PDF of *I(t)* while its SO statistic is studied by means of the autocorrelation function (ACF). Specifically, the injection current is set to J=1.4$J_{\mathrm{th}} \sim 2.4J_{\mathrm{th}}$. We find that residual pulsing persists in theoretical calculations as J is increased well above the value where it no longer appears in experiment; part of the discrepancy between theoretical and experimental PDFs is associated with this effect.

7.2 Experimental Setup and Theoretical Framework

The experimental setup for an EC distributed feedback laser was similar to that in [81]. It consists of the intrinsically single-longitudinal-mode MQW InGaAsP distributed feedback laser that oscillates at 1550 nm and has maximum cw power of 15 mW. The free-running $J_{\rm th}$ is ∼9.27 mA. The EC length L is 65 cm (EC round-trip time τ = 4.3 ns). With the help of a motorized piezo-actuation stage, the angle of the quarter-wave plate (QWP) is controlled in small steps. The maximum feedback (experimental feedback rate η = 1.0) is reached when the QWP is such that the polarization is not subject to any rotation. In our experiment, ∼20 % of the optical power is fed back onto the collimating lens for η = 1.0. To detect *I(t)*, the output of the distributed feedback laser is first coupled to a 12-GHz photodiode, and then captured by a 12-GHz oscilloscope with 40 GS/s sampling rate.

The LK model consists of rate equations for the slowly varying envelope of the complex electric field E and the carrier density N as in [92, 164]. Parameters are defined as in [164]. Namely, *G(t)*=g[*N(t)*-$N_{\rm o}$] is the optical gain g, with the differential gain coefficient, $N_{\rm o}$ the carrier density at transparency, α the linewidth-enhancement factor, $\omega_{\rm o}$ the angular frequency of the solitary laser, $\tau_{\rm p}$ the photon lifetime, $\tau_{\rm p}$ the carrier lifetime, $\kappa_{\rm f}$ the theoretical feedback rate, τ the feedback time delay, and q the pump factor ($J = qJ_{\rm th}$). We take α = 3, $\tau_{\rm p}$= 2.65 ps, $\tau_{\rm e}$ = 2.5 ns, $g = 2.5 \times 10^{-8}$ ps, $N_{\rm o} = 1.3 \times 10^{8}$, $\omega_{\rm o}\tau = 0$, giving $J_{\rm th} \approx 9.27$ mA, corresponding to $J_{\rm th}$ of the distributed feedback laser. The delay is not varied in this section and is set equal to the experimental value; $\kappa_{\rm f}$ and q are varied according to experimental conditions. Nevertheless noise has been neglected here as we found that moderate noise does not significantly change the statistics for the relatively large J considered here. When η = 1, we take $\kappa_{\rm f} = 25$ ns^{-1} as will be shown below.

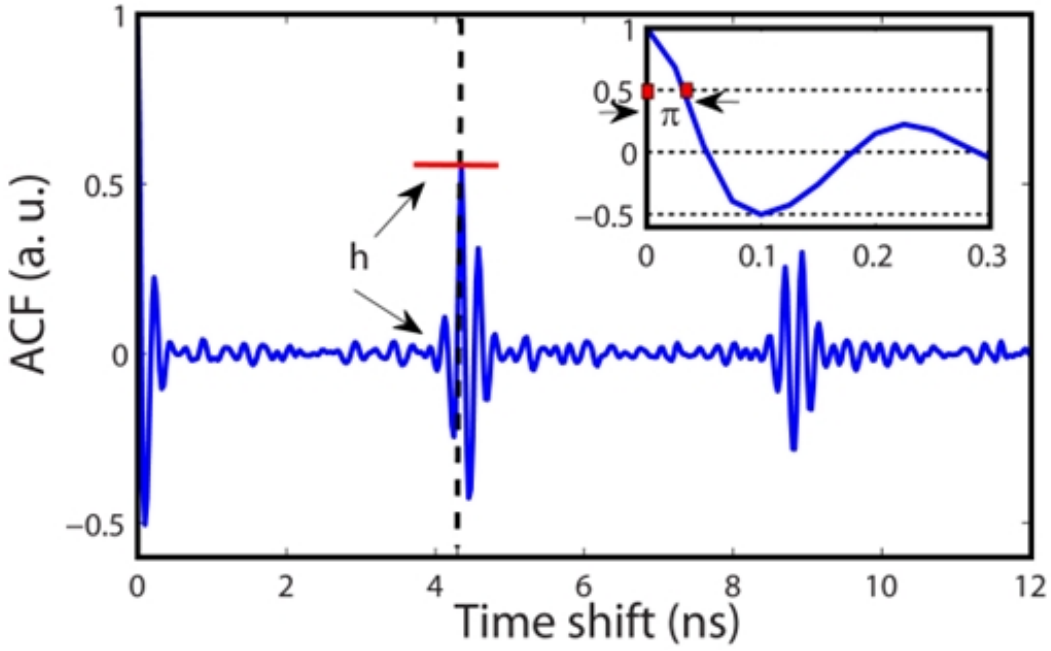

Figure 38: ACF for $\tau = 4.3$ ns, $J = 1.4J_{\text{th}}$ and $\kappa_{\text{f}} = 18$ ns^{-1}. The vertical dashed line indicates τ. The inset is the ACF arond zero delay.

7.3 Experimental and Numerical Results

The statistics are studied by the PDF of *I(t)*, characterizing the FO statistic, and the ACF for the SO statistic by quantifying the correlation between two intensity values separated in time [164]. We first focus on the comparison between the experimental and numerical ACFs as functions of $\eta(\kappa_{\text{f}})$ for four values of J in coherence collapse: $1.4J_{\text{th}}$, $1.7J_{\text{th}}$, $2.0J_{\text{th}}$, and $2.4J_{\text{th}}$. To mimic the filtering imposed by the photodiode and oscilloscope, the theoretical time traces were subsequently filtered using a cascade of two third- and ninth-order Butterworth filters with a bandwidth of 12 GHz, corresponding to frequency responses of the photodiode and oscilloscope used.

To help interpret the results, a typical ACF of *I(t)* obtained from the LK equations is shown in Fig. 38 with $J = 1.4J_{\text{th}}$ and $\kappa_{\text{f}} = 18$ ns^{-1}. A peculiarity of delay systems is the existence of a local maximum h of the ACF near the EC delay (vertical dashed line) [164]. This gives useful information on the chaotic dynamics as changes in its

value can be used to identify transition from weak to strong chaos [65, 152, 196].

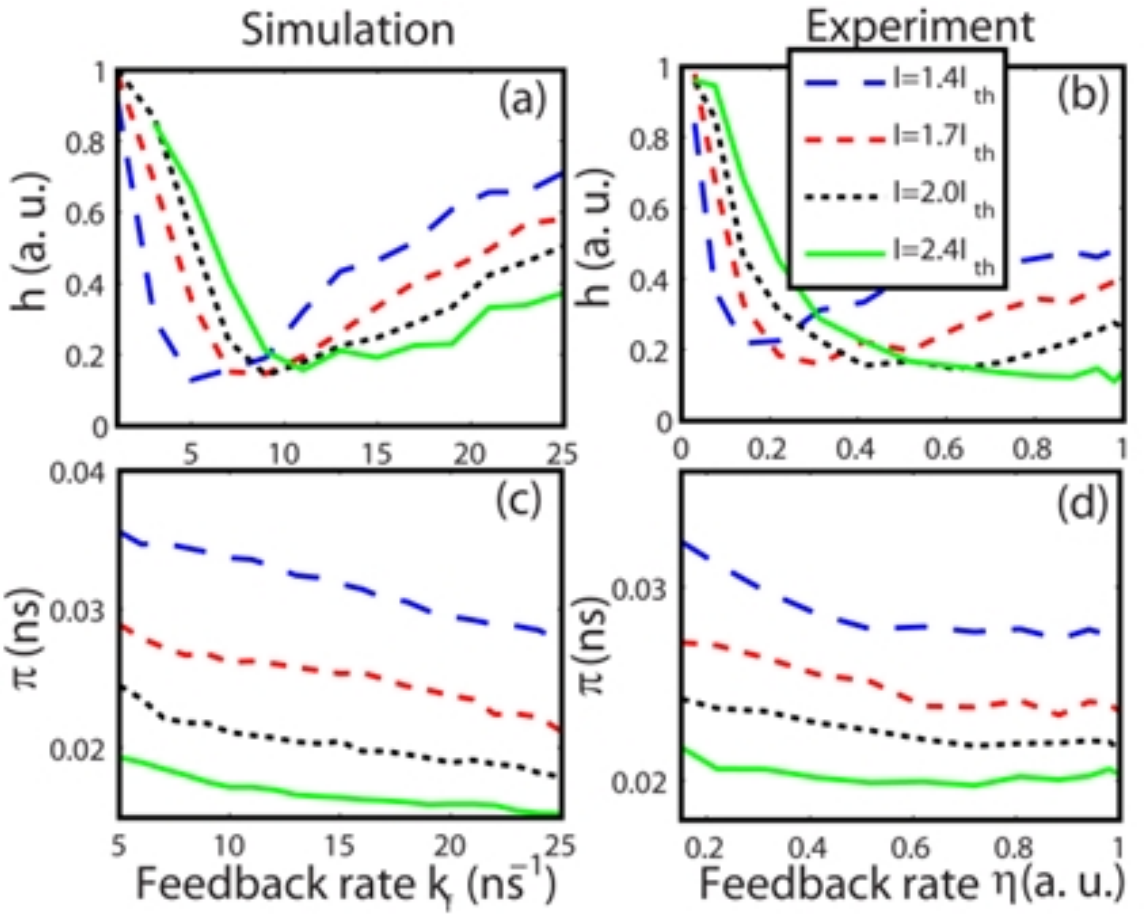

Figure 39: Numerical (a, c) and experimental (b, d) results for h and π at four J : $1.4J_{\rm th}$, $1.7J_{\rm th}$, $2.0J_{\rm th}$, and $2.4J_{\rm th}$

Figure 39 (a) shows numerical and (b) experimental results for h at various J and $\eta(\kappa_{\rm f})$: at all J shown, as $\eta(\kappa_{\rm f})$ increases, first falls, becoming a dip for a critical intermediate η or $\kappa_{\rm f}$, J and then increases. We see that the numerical results are in good agreement with experiments, both in the terms of curve shape and its variation with increasing J (dip moves to larger η or κ as J increases), and it also suggests that the parameter ranges considered in simulations are reasonable to reproduce experimental observations. These results also confirm numerical results in [29] in which the identifiability of the EC delay based on an analysis of *I(t)* was explored. Additionally, it is interesting to investigate the half-width π of the zeroth ACF peak that is a standard

indicator of the correlation decay time (see inset in Fig. 38), and is also a good indicator of the bandwidth of chaotic processes (Wiener-Khinchin theorem states that the Fourier transform of the ACF is equal to the power-spectral density.). In chaos-based RBG, sampling typically cannot be performed faster than this decorrelation time, thus restricting the sampling rate [78, 102, 201].

In chaos-based communications, the decorrelation time sets an upper bound in the speed at which a chaotic carrier can be modulated [185]. Fig. 39(c) shows numerical and (d) experimental results of π for various J and $\eta(\kappa_{\mathrm{f}})$. At all J shown, experiments and simulations show good agreement as decreases monotonically when increasing $\eta(\kappa_{\mathrm{f}})$. Moreover, in both cases, larger J results in smaller π, leading to a larger chaotic bandwidth.

We consider the FO statistic of *I(t)*, characterized by its PDF. Fig. 40 shows numerical and experimental PDFs. Each is derived from $4{\times}10^4$ samples of *I(t)* separated by 25 ps. The horizontal axis is scaled to its average value $<I>$, while the PDFs are plotted as functions of $\kappa_{\mathrm{f}}(\eta)$ for four well above ($1.4J_{\mathrm{th}}$, $1.7J_{\mathrm{th}}$, $2.0J_{\mathrm{th}}$, and $2.4J_{\mathrm{th}}$); also, for all $\kappa_{\mathrm{f}}(\eta)$ considered the ECSL operates in coherence collapse.

Figures 40 (e)-(h) show the measured PDFs. These are peaked near $<I>$ and fall off both at low and high *I(t)* over a wide range of parameters. The shape of the experimental PDFs is well fitted for all η and J, by an exponential around the maximum, located at $<I>$, but with different decay rates on each side of the maximum. This exponential shape of the PDF is consistent with our independent experimental work utilizing a different distributed feedback laser and fiber-optic components (not shown) [33], as well as with various published PDFs obtained from chaotic distributed feedback lasers with delayed optical feedback [34-36].

Figures 40 (a)-(d) show the corresponding PDFs of the filtered time traces obtained from the LK equations. As in experiment, the numerical PDFs appear to be unimodal for all κ_{f} and J. Another similarity with experiments is that at high J, the

PDFs exhibit a maximum near $<I>$ [Figs. 40 (b)-(d)].

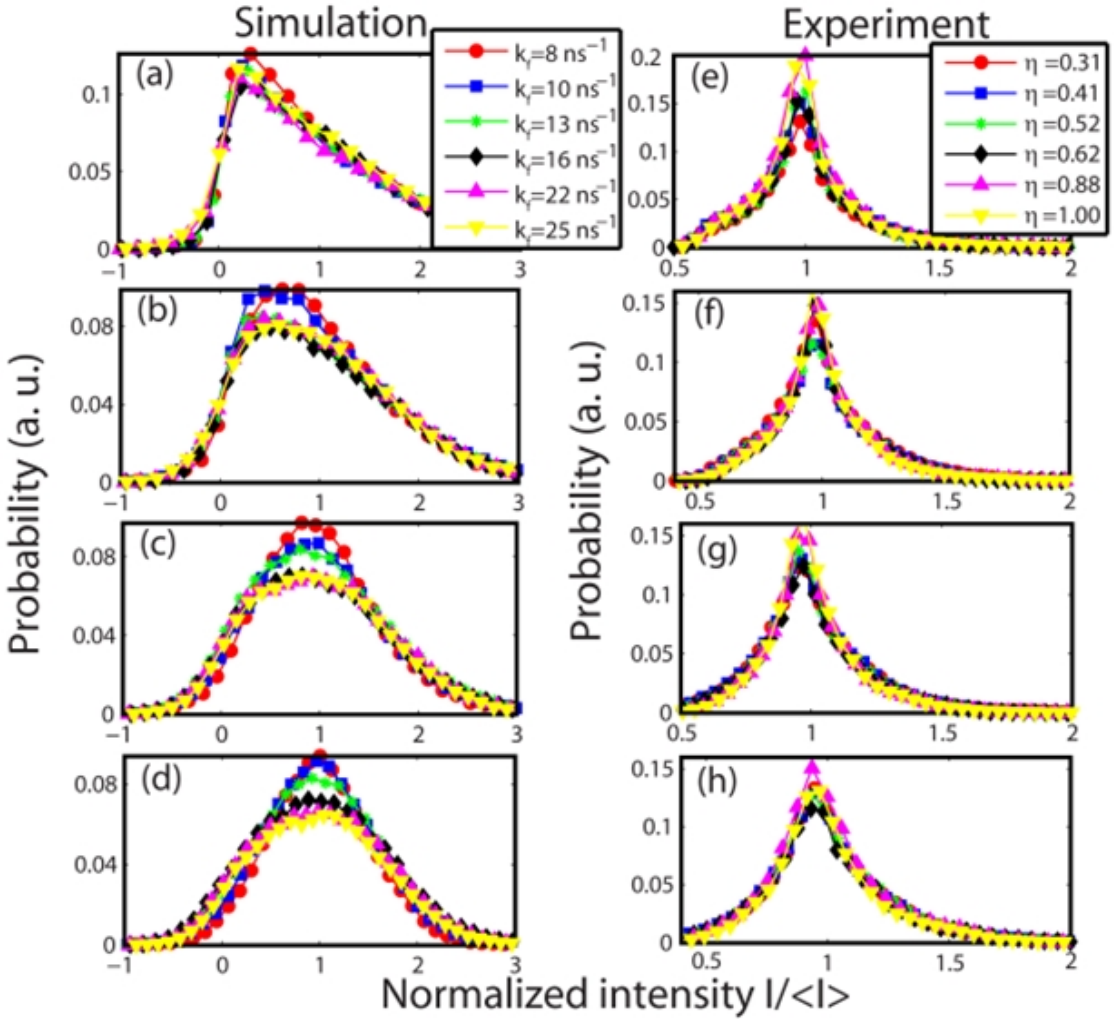

Figure 40: Numerical (a-d) and experimental PDFs (e-f) of *I(t)* for various κ_f and J : $1.4J_{th}$ (a, e), $1.7J_{th}$ (b, f), $2.0J_{th}$ (c, g), and $2.4J_{th}$ (d, h)

Significant differences also exist between experimental and numerical PDFs. Simulated PDFs show, at all J , more dispersion than experiments. We see that the experimental PDF shape, at J considered, is weakly influenced by η. By contrast, simulations show a change in the dispersion of the PDFs with increasing κ_f. Moreover, the numerical PDFs tend toward Gaussian for large J, while the experimental ones are exponential at all J. Also, the numerical PDFs in Fig. 40 (a), for low J, are peaked at low *I(t)*, while the corresponding experimental PDFs are centered close to $<I>$.

The discrepancies in terms of the location of the PDF maximum may be associated with stronger pulsing in the LK model [177], at low J, compared to experimental results [Fig. 40 (a), (e)]. It has been shown theoretically and experimentally in truly-single-mode ECSLs [74, 192] that in LFF, the PDFs display a maximum close to zero *I(t)*. This shape is attributed to the pulsation of the *I(t)* dynamics and thus to the associated larger dwell time of *I(t)* near zero, between two pulses. These pulsations are predicted by the LK model [205], and have been observed experimentally in LFF but also for J larger than those leading to LFF [42]. This difference is illustrated by Figs. 41 and 42, which represent experimental and filtered simulated intensities. We observe that 40 % above J_{th}, the simulated *I(t)* still exhibits a clear tendency to pulse and to keep a small value between pulses. This is not the case of the experimental time series, consistent with the differences in maximum locations in the PDFs. At larger J, both the numerical [Figs. 41(c) and 42(c)] and experimental [Figs. 41(d) and 42(d)] time series experience fluctuations around their averages, as reflected by the corresponding PDFs in Fig. 40. In the LK model at low J, *I(t)* tends to keep a close-to-zero value after a pulse has occurred due to a depleted reservoir of carriers; at large J, the rate at which carriers are supplied by the current source is larger and thus *I(t)* recovers faster, preventing *I(t)* from maintaining a small value for a long time and thus explaining the change in the PDFs. The difference between experiments and simulations might thus be due to more efficient recovery in experiment than in the model.

Figures 42(c) and (d) also illustrate the strong difference in the dispersion between the model and the experiment. Indeed, Fig. 42(c) displays much wider fluctuations around the mean than in Fig. 42(d). Lower experimental dispersion of *I(t)* is observed for all the values of J and $\eta(\kappa_{\mathrm{f}})$, therefore indicating stronger damping of oscillations between carrier and photon populations than accounted for by the LK

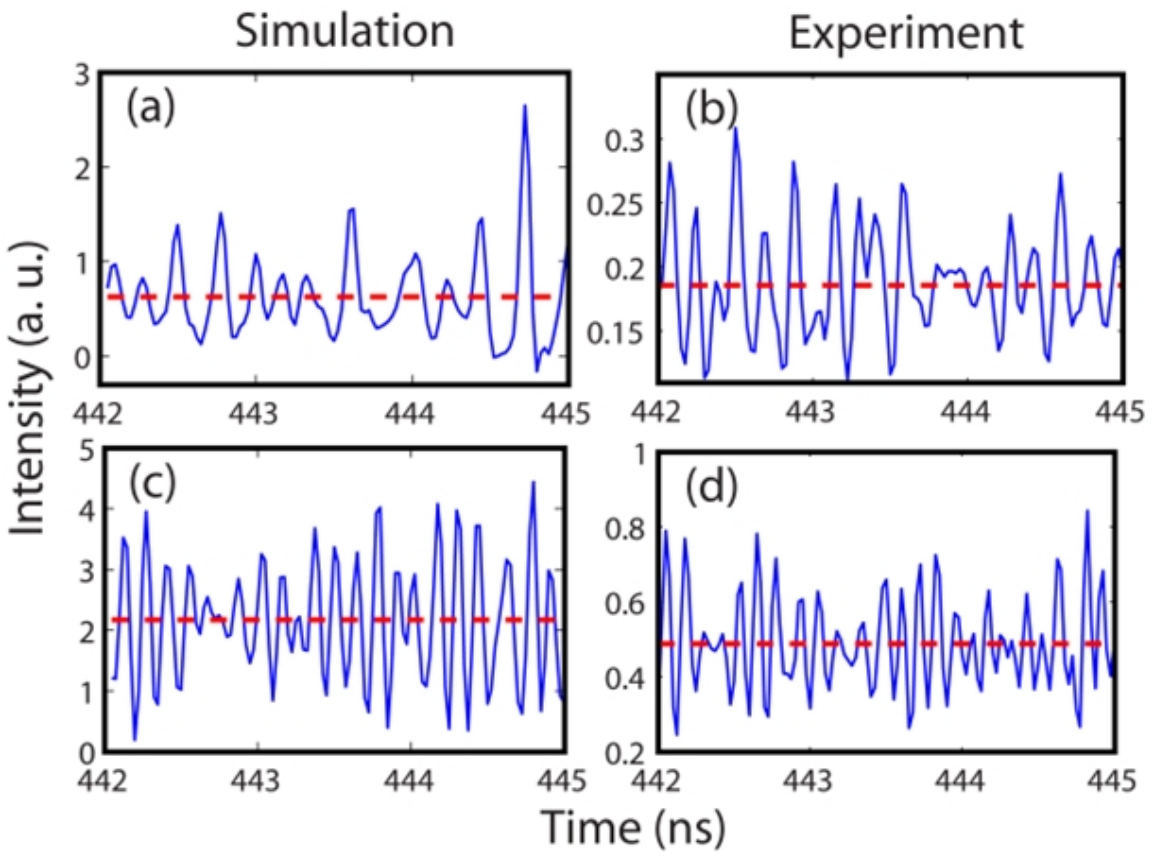

Figure 41: $<I(t)>$ for small $\kappa_{\rm f}(\eta)$. (a, b) low J : $1.4J_{\rm th}$; (c, d) high J : $2.4J_{\rm th}$. (a, c) simulation, $\kappa_{\rm f}$) = 8 ns^{-1}; (b, d) experiment, η=0.31. The horizontal dashed line indicates $<I>$.

model. We were not able to obtain a better fit between experimental and numerical PDFs by adjusting the LK parameters or by tuning the model itself, *e.g.*, by introducing phenomenologically gain saturation with [177, 184, 192].

Another difference between theory and experiment is that the experimental PDFs are robust to changes in J and η, while the LK-based PDFs vary with J, and to a smaller extent with $\kappa_{\rm f}$. To understand this, we compared the active ECMs predicted by the LK equations with the active modes from measured optical spectra. We see that, for moderate $\kappa_{\rm f}$, the LK model predicts that, as J increases, the active modes undergo significant right-shift from a spectral range close to maximum-gain mode toward frequencies much closer to the minimum-linewidth mode (MLM) [184]. The

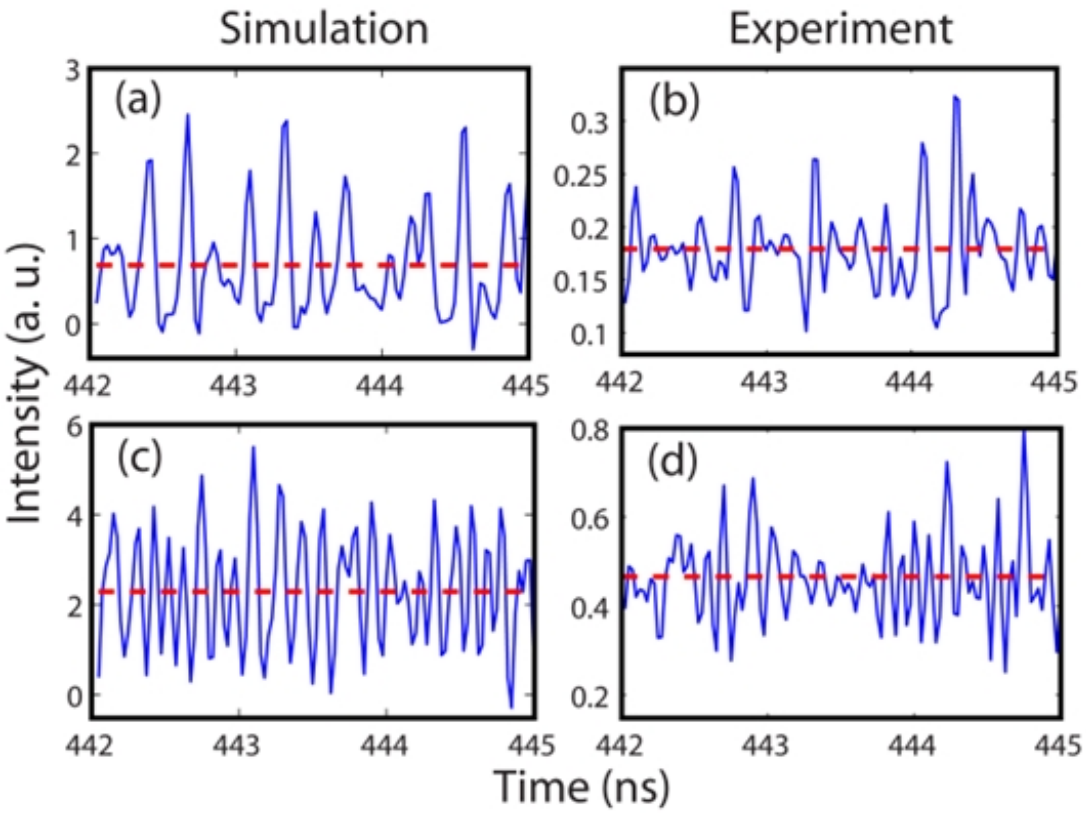

Figure 42: $<I(t)>$ for small $\kappa_{\mathrm{f}}(\eta)$. (a, b) low $J : 1.4J_{\mathrm{th}}$; (c, d) high $J : 2.4J_{\mathrm{th}}$. (a, c) simulation, $\kappa_{\mathrm{f}}) = 25$ ns^{-1}; (b, d) experiment, η=1.0.

difference in the dynamical properties of the selected ECMs (stability, basin) [115] may explain the variability of the PDFs. In contrast, experimental spectra show a relative invariance of the active modes, tending to be close to the MLM, for all η and J considered. This robust selection of active modes may contribute to the relative robustness of the experimental PDFs.

7.4 Conclusion

An ECSL can be used to exhibit chaotic behavior. The corresponding statistical properties might be influenced by the variation of control parameters, such as the pump current and the feedback strength. An ECSL operating in the LFF regime demonstrated experimentally [74] that the statistical distribution of the laser intensity has strong asymmetry about its maximum because of sporadic intensity-dropout

events. It is still unclear in which way the probability density function (PDF) of the optical intensity of an ECSL operating in a chaotic regime, including the LFF and fully developed coherence collapse regimes, will qualitatively change with varying I and/or feedback strength. Therefore, we experimentally and numerically study the statistical properties of the time-dependent intensity of an ECSL. We compare the probability density distribution of the raw time series and investigate the mean and the variance as the first order statistics. We also compare the peak of the autocorrelation around the delay time (peak size), and the width (3 dB peak width) of the autocorrelation at first peak (the time shift is equal to zero) as a function of the current, for different feedback strengths as the second order statistics.

We study experimentally and theoretically based on the LK model first- and second-order statistical measures of the optical intensity of a chaotic ECSL in fully-developed coherence-collapse. The second-order statistic is characterized by the autocorrelation function, for which we achieve consistent experimental and theoretical results over the entire parameter range considered. For the first-order statistic, we find that the experimental probability-density function is significantly more concentrated around the mean optical power and robust to parameter changes than the density functions obtained from the LK model.

To conclude, we studied the statistics of *I(t)* from an ECSL in coherence collapse. Substantial agreement between theory and experiment was found for the autocovariance, both for h and π as functions of $\eta(\kappa_{\mathrm{f}})$. This indicates a good reproduction by the LK model of linear correlations between successive dynamical states. Discrepancies are observed, however, in the PDFs. Theory is more skewed to low *I(t)*, but this diminishes for higher J, appearing increasingly Gaussian. While inclusion of noise in simulations (not shown) slightly reduces the effect, it does not account for its size. We attribute this effect to residual intensity pulsations that are not present in experiments. Experimental PDFs for all parameters show consistently exponential-like

shape, for all $\eta(\kappa_{\mathrm{f}})$ and J, with smaller dispersion than simulations. Thus the LK model may overestimate, in the coherence collapse regime, the size of the chaotic fluctuations with respect to $<I>$ and the variability of the dynamics as a function of $\eta(\kappa_{\mathrm{f}})$ and operating J.

CHAPTER VIII

TWO APPROACHES FOR ULTRAFAST RANDOM BIT GENERATION BASED ON THE CHAOTIC DYNAMICS OF A SEMICONDUCTOR LASER

This chapter reports the experimental investigation of two different approaches to random bit generation based on the chaotic dynamics of a semiconductor laser with optical feedback. By computing high-order finite differences of the chaotic laser intensity time series, we obtain time series with symmetric statistical distributions that are more conducive to ultrafast random bit generation.

The first approach is guided by information-theoretic considerations and could potentially reach random bit generation rates as high as 160 Gb/s by extracting 4 bits per sample. The second approach is based on pragmatic considerations and could lead to rates of 2.2 Tb/s by extracting 55 bits per sample. The randomness of the bit sequences obtained from the two approaches is tested against three standard randomness tests (ENT, Diehard, and NIST tests), as well as by calculating the statistical bias and the serial correlation coefficients on longer sequences of random bits than those used in the standard tests.

This chapter is based on the following publications:

1. Nianqiang Li, Byungchil Kim, V. N. Chizhevsky, A. Locquet, M. Bloch, D. S. Citrin, and Wei Pan,"Two approaches for ultrafast random bit generation based on the chaotic dynamics of a semiconductor laser," Opt. Express 22, 6634-6646 (2014).

2. N. Li, B. Kim, V.N. Chizhevsky, A. Locquet, D.S. Citrin, and W. Pan, "Ultra-fast random bit generation based on the chaotic dynamics of a semiconductor laser", submitted to Opt. Express (2013).

3. N Li, B.C. Kim, V. N. Chizhevsky, A. Locquet, M. Bloch, D. S. Citrin, and Wei Pan,"Fast random bit generation with a single chaotic laser subjected to optical feedback ", SPIEs Photonics Europe 2014, Proceedings of SPIE paper 9134-75, Brussels, Belgium.

8.1 Introduction

Semiconductor lasers are very sensitive to perturbations from the outside environment [115, 123]. Even very weak optical feedback may significantly increase both the intensity noise and lasing linewidth, which is undesirable in most applications. Consequently, many conventional laser-diode systems are commonly prepared with optical isolators to impede feedback from surface reflections. Recently, however, in view of the technological importance of these devices, the rich nonlinear dynamics of semiconductor lasers with delayed feedback/injection have been widely investigated [132, 184]. Among them, a form of chaotic dynamics, termed coherence collapse, has been exploited for several applications, such as chaos-based communications [130, 193], chaotic lidar/radar [105], reservoir computing [93], and chaos-based random bit generation(RBG) [78, 158, 201]. Our focus here is on chaotic laser-diodes for RBG.

Generally speaking, there exist two approaches to generate random bits. The first is based on deterministic mathematical algorithms and is known as pseudo RBG [84]; unfortunately, the quality and generation rate may be inadequate, for applications such as cryptography and large-scale Monte Carlo numerical computations in which it is crucial to have nearly unpredictable bits [44, 72]. The second approach consists in extracting randomness from physical phenomena, such as radioactivity, noise, turbulence, and electrical chaos in nonlinear circuits, and is known as physical RBG [31, 52, 70, 103, 113, 155, 166, 187, 216]; the generation rate of most physical random-number generators is typically on the order of a couple of Gb/s or lower [25]. Following the first demonstration of physical RBG based on broadband optical chaos [201], chaotic semiconductor lasers have gained interest as physical sources of randomness because of the high potential generation rate and the ease of implementation [15, 56, 78, 134, 136, 158, 221]. It should also be mentioned that there is debate about the role of noise in chaotic systems with regard to RBG [39, 58, 118].

Progress has recently been made in improving the generation rate using high-order derivatives [78], coupled chaotic lasers [68, 101, 102, 217], as well as advanced post-processing techniques, such as the bit-order-reversed method [5]. Experimental implementations have been demonstrated based on photonic integrated circuits [15, 56], as well as numerical implementation using various schemes, such as RBG based on all-optical components [103] and a single ECSL [56]. Higher generation rates have been obtained thanks to large sampling rates and to complex post-processing that artificially increase the allowed number of retained bits from each high-resolution analog-to-digital converted sample. As an example, Kanter et al. have demonstrated ultrafast chaos-based RBG with a rate of 300 Gb/s based on the use of the high-order derivatives using a sampling rate of 20 GHz and extracting 15 random bits per sample, although the raw data were digitized with 8-bit resolution [78]. Very recently, Oliver et al. have highlighted that the fundamental limits of maximum RBG rate imposed by information theory depend on the analog bandwidth of the chaotic laser and cannot be improved by simply increasing the sampling rate or by creating additional bits through post-processing [134]. In fact, in earlier works, the number of bits extracted from per sample from the chaotic laser intensity has been chosen heuristically. In [68, 130, 134], this number has been estimated by plotting histograms of the truncated values until a flat histogram, [i.e., probability density distribution (PDF)], is obtained. The heuristics were validated by testing the generated bit stream against existing statistical tests of randomness. Nevertheless, intuitively, to extract almost-uniform and independent bits from a source, the source should initially contain at least bits of randomness in it; this can be formally quantified with information-theoretic measures, such as the Shannon entropy and min-entropy [134, 179, 209]. In particular, if one were to extract more than the number of quantization bits from each sample, the generator should be considered as a pseudo random-number generator based on physical phenomena or called a physical-based pseudo random-number

generator, rather than a true physical random- number generator.

The majority of existing schemes for fast chaos-based RBG in the literature require bitwise exclusive-or (XOR) operation [One of the examples using XOR - Appendix A] to amplify inherent randomness to remove residual correlations, in addition to the selection of several least significant bits (LSBs) [67, 101, 201, 217]. In this section, we explore two approaches to fast RBG based on the processing of the chaotic laser intensity time series of an ECSL. In the first approach, the number of retained bits is conservatively selected according to the limits set by information theory. In the second approach, the number of extracted random bits is merely chosen to pass standard randomness tests. Accordingly, we name the first approach physical RBG, and the second physical-based pseudo RBG. Proving that our conservative first approach does indeed ensure information-theoretic RNG requires an in-depth analysis of our post-processing, which is beyond the scope of the present section and will be the subject of a subsequent work. Some previous works show that the interplay of dynamical properties, acquisition conditions, and post-processing plays a critical role in the performance of RBG [67,134,219]. We apply the procedure described in [24] which is based on the calculation of the high-order finite differences (HFD) of the initial data, which results in symmetric statistical distributions. It must be noted that this method is similar to the independently developed high-order derivatives method presented in the pioneering [78]. The post-processing proposed in [24] and [78] reduces the dependence on the dynamical properties and acquisition conditions at the expense of additional numerical processing. For this reason, the strict adjustment of the feedback strength, the injection current, and the external-cavity length is not needed. Throughout the study, the post-processing employed only includes the calculation of HFD and the selection of LSBs. Moreover, unlike many existing reports of chaos-based RBG [15, 56, 78, 134, 136, 158, 201, 221], the randomness in the present experimental study is not only verified by three standard randomness tests, for which the required

size of the sequence of random bits is only of the order of 1 Gbit, but is also checked by calculating the statistical bias and correlation coefficient, for very long (10-50 Gbits) random bit sequences.

This section is organized as follows. Sub-section 3 briefly describes the experimental setup employed for ultrafast RBG, which is a semiconductor laser subject to time-delayed optical feedback. Sub-section 4 presents the experimental results; we first focus on physical RBG and then investigate physical-based pseudo RBG. Sub-section 5 provides concluding remarks.

8.2 Experimental Setup

The schematic diagram of the experimental setup for RBG is shown in Fig. 43. The setup consists of a semiconductor laser with optical feedback, which generates intensity chaos and provides the physical source, and of a post-processing unit, which extracts randomness. This processing is performed offline as in most previous studies [130, 217].

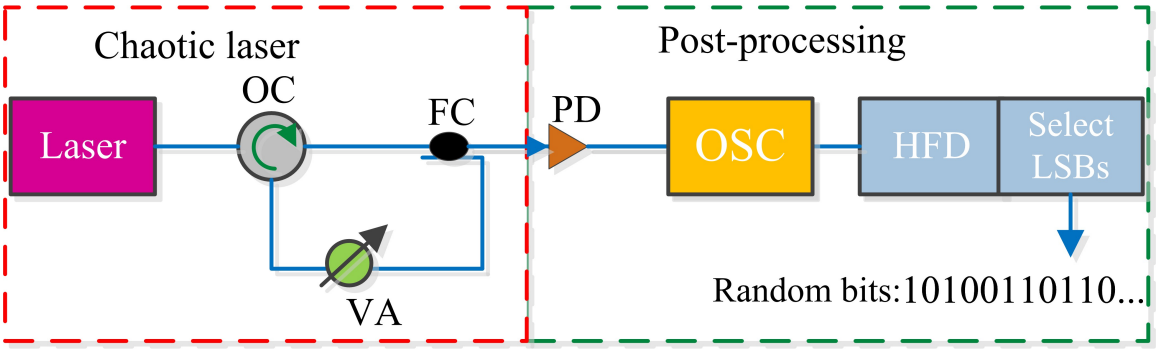

Figure 43: Schematic diagram of ultrafast RBG based on optical chaos. Laser: a distributed feedback LD; OC: optical circulator; VA, variable optical attenuator; FC, 85: 15 fiber coupler; PD, photodiode; OSC, 40 GHz real-time oscilloscope; HFD, high-order finite differences; LSBs, least significant bits.

8.2.1 Chaos Generation

The generation of complex chaotic signals is realized by perturbing a semiconductor laser using an external-cavity to feed light back into the gain medium. The semiconductor laser used in our experiments is an intrinsically single-longitudinal mode distributed feedback laser that operates at a nominal wavelength of $\lambda = 1550$ nm and has a threshold current of $I_{\text{th}} \approx 10$ mA. The output light is fed back into the laser facet after it passes through a fiber ring cavity that consists of an optical circulator (OC), a variable optical attenuator (VA), and a fiber coupler (FC). The distributed feedback laser is easily destabilized by adjusting the VA to change the feedback power. The laser is driven by an ultra-low-noise current source (ILX-Lightwave, LDX-3620B) and controlled by a thermoelectric controller (ILX-Lightwave, LDT-5412).

The laser was pumped well above threshold to ensure operation in the coherence collapse regime: the injection current was set to ~ 20 mA so that the chaotic fluctuations dominate the background noise. The external-cavity formed by the abovementioned components results in a large roundtrip delay time of 57.68 ns. The feedback strength, defined as the ratio of the optical feedback power fed back into the laser to the laser power in the absence of feedback was set to 8%. As we will not focus on the dynamical properties, finding the optimum operating conditions for the RBG by a careful adjustment of the feedback strength or the injection current is beyond the scope of the present work. However, we stress that one can optimize the statistical properties of chaotic dynamics by carefully controlling the feedback level.

8.2.2 Post-processing

The dynamics of the laser intensity were detected at a photodiode (PD), and then acquired by a real-time oscilloscope (LeCroy WaveMaster 813zi, 13 GHz bandwidth). The experimental data was digitized by the 8-bit analog-to-digital converter (ADC)

in the oscilloscope. As mentioned above, the post-processing employed for the chaos-based RBG consists of the calculation of the HFD and followed by the retention of the LSB. For the first approach, we point out here that we do not extract more bits than the limit set by information theory, leading to physical RBG; for the second approach, we attempt to extract as many bits for each sample as possible, so as to realize ultra-high speed physical-based pseudo RBG.

In our experiments, unlike many previous optical RBG schemes summarized in the introduction, we choose a high sampling rate of 40 GHz. The chaos bandwidth obtained from such an ECSL is on the order of several GHz, and the bandwidth of the oscilloscope is 13 GHz. The detection bandwidth and sampling rate are sufficient to capture all relevant dynamics in the intensity time series. In addition, our two schemes of chaos-based RBG only involve limited post-processing. Moreover, as also explained in [78, 158], a single laser is necessary contrary to [67, 101, 127, 201, 217], and contrary to [208, 217], we do not need to use and adjust a delay line to generate a second, uncorrelated, bit stream from the measured stream. Thanks to the use of HFD, the rigorous, and experimentally difficult, threshold voltage adjustment, as well as the selection of the retained range of output intensities, described in [67, 201, 219] are also avoided.

8.3 Experimental Results

8.3.1 Statistical properties of laser chaos

True random bit sequences lack any pattern in their appearance and, in principle, are completely unbiased and unpredictable. The quality of the generated random bits depends upon the statistical properties of the sources of randomness.

Entropy sources with a close to uniform distribution are good candidates for high-quality RBG; however, the physical sources known to us do not have an ideally symmetric PDF, to say nothing of being uniformly distributed at each digitization

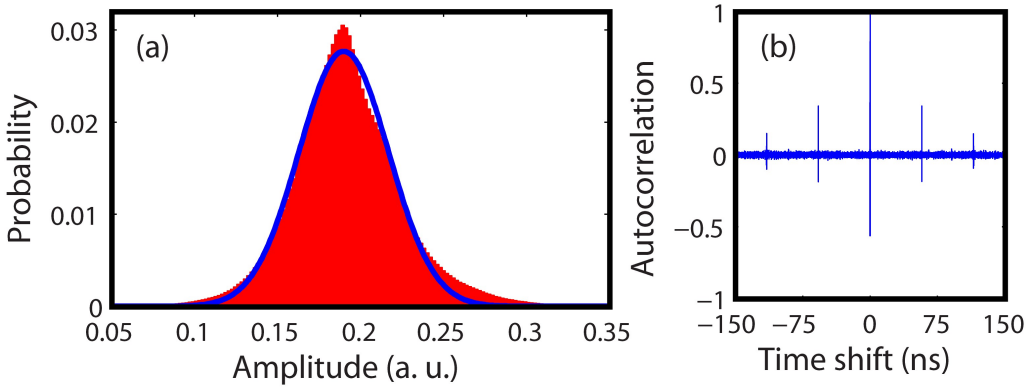

Figure 44: Statistical properties of laser chaos. (a) PDF and (b) autocorrelation function of the chaotic waveforms. The blue curve in (a) denotes the fitted Gaussian.

level. For example, Fig. 44(a) presents the calculated PDF for the chaotic laser intensity generated by the experimental setup displayed in Fig. 43. The PDF is directly obtained from 3×10^7 digitized samples. Although the PDF resembles a Gaussian distribution, the asymmetry of the PDF is clearly identified by comparing it with the fitted Gaussian [blue curve in Fig. 44(a)], which is a common feature of chaotic semiconductor lasers. In our case, the coefficient of skewness and kurtosis are about 0.27 and 4, respectively, which substantially deviate from a Gaussian distribution. This means that keeping all LSBs of the 8-bit data cannot pass the statistical tests of randomness since the non-uniformity of the initial distribution influences the randomness of the bits generated. Moreover, neither are consecutive bits independent.

The autocorrelation trace for the full 8-bit signal is shown in Fig. 44(b). It can be clearly seen that peaks appear at integer multiples of the delay time, e.g., a pronounced peak with a correlation coefficient about 0.34 is located at a delay time of 57.68 ns, which corresponds to the roundtrip time in the external-cavity. Therefore, to extract random bits from the chaotic sources, post-processing techniques should be employed.

Selection of LSBs is a common, simple post-processing procedure for improving the uniformity of the bit distributions and for destroying the residual correlations

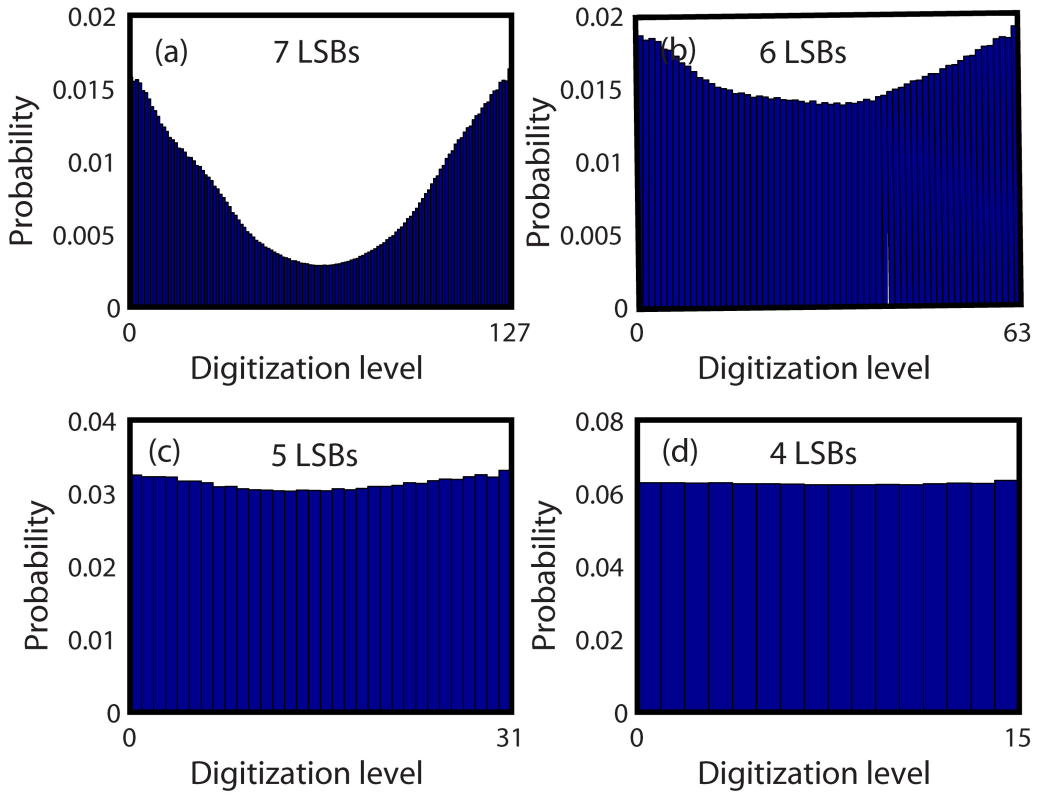

Figure 45: PDFs over the range of digitization levels for (a) 7 LSBs, (b) 6 LSBs, (c) 5 LSBs, and (d) 4 LSBs retained from each 8-bit sample.

in the original dynamics [68, 130, 134, 136, 217]. Here, this technique is applied to our experimental signal. Figures 45(a)-45(d) show the distributions for down to 4, respectively. In Fig. 45(a) only the most significant bit (MSB, m = 7) is excluded and the corresponding PDF significantly differs from a uniform distribution. When more MSBs are discarded the uniformity of the PDF is improved, as shown in Figs. 45 (b) and 45(c).

Furthermore, if one selects only 4 LSBs (m = 4) for each 8-bit sample, the resulting PDF is close to uniform, as is illustrated in Fig. 45(d). In addition, the residual correlations are gradually eliminated as the number of discarded MSBs increases even though the original dynamics exhibit obvious short-term correlation. For this reason, the signature of the feedback delay time is not important for RBG when such

post-processing is introduced. We will explore the residual correlation feature for our chaos-based RBG in the following sections.

Note that in the experiment, for the fixed injection current and feedback strength given above, random bits obtained by keeping the 4 LSBs of the 8-bit data cannot pass all the statistical tests of randomness. This is because there still exist significant biases or correlations in the generated random bits. To further distill the randomness, as mentioned above, additional post-processing is needed. In this study, we therefore only employ the selection of LSBs as the second post-processing step after calculating the HFD of the experimental signal.

8.3.1.1 High-quality physical RBG

In order to achieve efficient generation of random bits, we adopt the nth-order finite differences (HFD) procedure described in [24], which allows one to extract random bits from any source of randomness with nonsymmetric distribution. A similar method for increasing the speed of chaos-based RBG was previously discussed in [78,158]. To generate random bit sequences, we need not choose the optimal conditions regarding the chaotic dynamics and acquisition process. This is because the calculation of HFD reduces dependence on these properties.

The working point of the laser is fixed as given in Fig. 43, unless otherwise stated. In the HFD method, the generation of random bit sequence consists of the following two steps. The first step involves collecting integer samples $\alpha_\kappa(\kappa = 1, 2,...N)$ with 8-bit resolution from the measured output intensities of a chaotic laser. They are transformed into floating-point numbers with M-bit resolution (M>>8), and then the nth-order differences of the floating-point data are calculated. It is worth noting that one cannot aim to extract all significant bits from each obtained sample since strong correlations appear in the bit stream after the calculation of HFD. Therefore, one should discard certain MSBs to eliminate these correlations. To this end, in

the second step, one just retains LSBs of each new variable in the floating-point representation and consecutively concatenates all the retained bits to obtain a long random bit sequence.

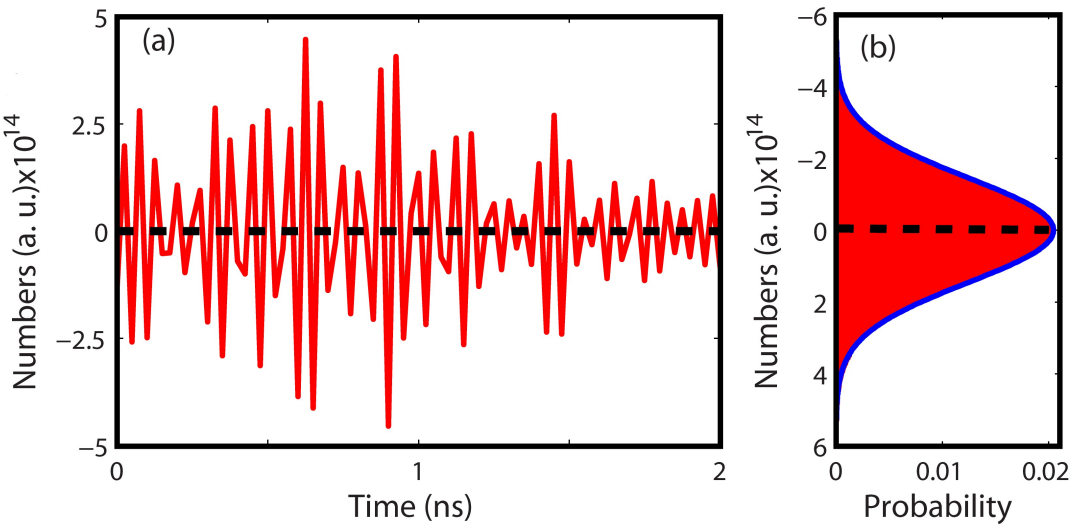

Figure 46: (a) Characteristics of the calculated floating-point numbers based on 50th-order finite differences. (a) Time series and (b) its associated statistical distribution. The dashed lines stand for the mean value of the time series. The blue line in (b) represents a fitted perfect Gaussian distribution.

As a point of comparison, we evaluate the potential rate of randomness extraction in the first approach, by properly quantifying the amount of randomness in the obtained sequences $\{\alpha_\kappa\}$. While, the Shannon entropy and min-entropy may have operational information-theoretic meaning in the present context we opt to evaluate the min-entropy, which is the most conservative way to measure then randomness that could be extracted from a discrete random variable [113, 209].

The min-entropy is defined as H_∞ = - log$\{max(P_i)\}$ with $max(P_i)$ being the probability of the most likely event and is defined to be the probability of the ith value of the alphabet of the discrete variable. In our experiments, the real-time oscilloscope recorded 10^7 samples at a time of 8-bit data at 40 GHz sampling rate; We calculated the min-entropy values of 200 sets of samples and then made an average over 200 values of min-entropy.

For our experimental data, the final min-entropy is ∼4.4 bits per sample, which indicates that, even the best method for extracting randomness cannot lead to more than 4.4 information-theoretically random bits from each raw 8-bit resolution sample. In addition, random bit sequences obtained by directly keeping 4 LSBs per sample cannot pass the entire statistical randomness tests because the generated random bit sequences may still contain certain biases and correlations, which can stem for example from long term correlations associated with the external-cavity length of the chaotic laser [154, 163] as illustrated in Fig. 44(b). (Thus, in the first approach, the technique of calculating nth-order finite differences is utilized.)

Firstly, all the random integers of 8-bit resolution obtained from our oscilloscope were transformed into floating-point numbers according to the procedure described in [24, 25]. Secondly, the HFD of these numbers were calculated. Specifically, the maximal number of bits that represents each sample is chosen to be 52, since numbers represented in the double format have a maximum precision of 52 bits. The maximal difference order n_{th} allowed for the experimental data can be determined by the condition (1) in [24], where the author demonstrated the violation of that condition leads to appearance of strong correlations in the generated bit stream. However, in our case, we aim to extract only 4 LSBs for each sample to avoid exceeding the min-entropy. The first step of our procedure is to calculate the 50th-order finite differences of a sequence of the floating-point numbers. It is worth noting that the use of lower-order differences leads to 4 LSB-based random sequences that pass the standard statistical tests (as mentioned below) but not the three-standard-deviation criteria. This highlights the beneficial role of HFD post-processing in the extraction of randomness, as well as the limitations of the three tests cited above.

Figure 46(a) presents the fluctuation evidence for such floating-point numbers. One can see that these numbers symmetrically fluctuate around their mean. As a result, a highly symmetric distribution is obtained with a coefficient of skewness of

the order of $\approx 10^{-7}$, as shown in Fig. 46(b), where a perfect Gaussian distribution fit is also depicted, indicating that one can achieve RBG based on the data after this post-processing. Before extracting random bits, all new after calculating the HFD were transformed into positive numbers by adding 2^{51} and mapped into the binary format. Finally, the random bits obtained by keeping 4 LSBs for each sample after the use of HFD have a distribution that is significantly closer to uniform than that of Fig. 45(d). Moreover, the serial correlation coefficients are also significantly closer to zero, as will be shown below. In that regard, we consider that the use of HFD combined with a restriction to the number of LSBs corresponding to the min-entropy may have the potential to generate information-theoretic random bits at a rate of 160 GHz (= 4LSBs $\times$ 40 GHz).

We verified the quality of the generated bit sequences utilizing three collections of standard statistical tests. These are the pseudorandom bit sequence test program (ENT) [207], the Diehard tests [114], and the National Institute of Standards and Technology test suite (NIST Special Publication 800-22) [172]. First, a sequence of 1 Gbit length was tested in ENT program. The ENT results are as follows: Entropy=1.000 000 bits per bit (the optimum compression would reduce the bit file by 0 percent), distribution χ^2 is 0.39 (randomly would exceed this value 50% of the times), arithmetic mean value of data bits is 0.5000, Monte Carlo value for π is 3.142211186, and serial correlation coefficient is 0.000015. Second, we carried out the Diehard tests according to the description in [114], which outlines that the Diehard battery consists of 17 tests, and p-values obtained in each test (269 in total for a sequence of 2.5×10^9 bits used in our case) should not be 0 or 1 up to 6 decimal places and are supposed to be uniform in [0, 1). The overall p-value (p_0) characterizes the uniformity of this distribution. We obtained with minimal and maximal from the total number of 269 (KS denotes the Kolmogorov-Smirnov test). Finally, the NIST tests were performed using 1000 instances of 1Mbit sequences and are shown in Table 1. The bit sequences

Table 2: Results of NIST statistical tests for physical random bits. The results have been performed using 1000 samples of 1 Mbit data and a significance level $\alpha = 0.01$, for "Success", the P value (uniformity of p values) should be larger than 0.0001 and the proportion should be in the 0.99 $\pm$0.0094392 range [172]. For the tests that produce multiple P values and proportions, the worst case is shown.

Statistical test	P value	Proportion	Result
Frequency	0.450297	0.9890	Success
Block frequency	0.610070	0.9910	Success
Cumulative sums	0.211144	0.9890	Success
Runs	0.911413	0.9830	Success
Longest runs	0.406499	0.9900	Success
Rank	0.234373	0.9910	Success
FFT	0.701366	0.9900	Success
Nonoverlapping templates	0.302058	0.9850	Success
Overlapping templates	0.090388	0.9870	Success
Universal	0.812905	0.9850	Success
Approximate entropy	0.308561	0.9900	Success
Random excursions	0.137487	0.9888	Success
Random excursions variant	0.164071	0.9888	Success
Serial	0.285427	0.9930	Success
Linear complexity	0.738534	0.9850	Success

generated by the chaotic dynamics of a semiconductor laser with optical feedback at the bit rate of passed all three standard randomness tests of ENT, Diehard, and NIST.

It is worth noting that the standard tests above operate on bit sequences that are limited to a couple of Gbits, such as 1 Gbit in ENT and NIST tests, as well as 2.5 Gbits in Diehard tests. It is important to check the statistical properties on longer sets that are more in line with the large bit rates obtained here. Therefore, to further evaluate the randomness of the long random-bit sequences, we calculate the statistical

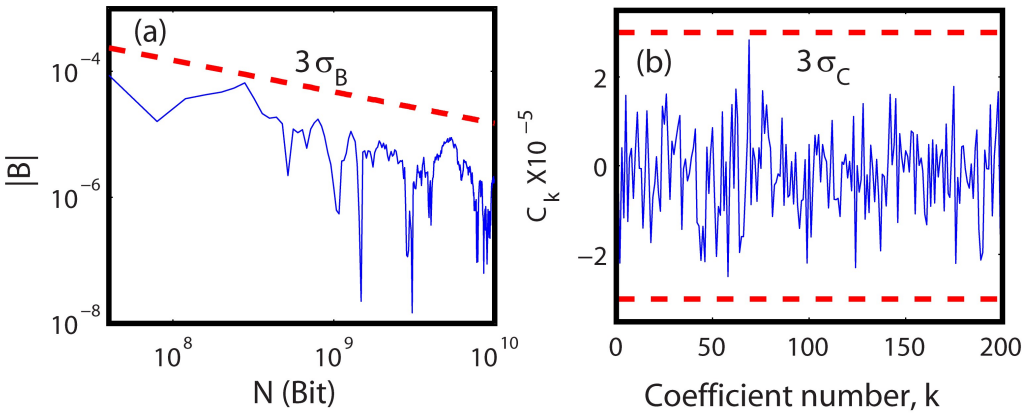

Figure 47: The results of the statistical bias and serial autocorrelation coefficient C_k for the physical RBG at a speed of 160 Gb/s. (a) B as a function of the number of generated bits N; (b) first 200 serial autocorrelation coefficients for the binary sequence of 10 Gbit length. The values of C_k were calculated by ensemble averaging over 1×10^4 sequences of 1 Mbit length each.

bias and the serial autocorrelation coefficients C_k. C_k and B are defined as [24].

where b_i (i = 1,2,,...) takes the values "0" or "1" is the delay in bits and the averaging $< \cdots >$ is performed over the index i. Note that the statistical bias B and the serial autocorrelation coefficients C_k are random variables which vary from one sequence to another and depend on its length. For high-quality random bit sequence of length N, both the statistical bias B and the absolute value of the serial autocorrelation coefficients C_k should be smaller than the three-standard-deviations: $3\sigma_B = 1.5N^{-0.5}$ for and for with a probability of 99.7% [12]. Figure 47(a) shows on a log-log scale the dependence of the statistical bias on the sequence length . It is apparent that the statistical bias always lies below the -criterion (dashed line). Figure 45(b) shows the first 200 autocorrelation coefficients for a sequence with a length of 10 Gbits. One can see that, all values are within the range that is bounded by dashed lines corresponding to the -criterion. Therefore, both criteria are well satisfied for the random bit sequence of 10 Gbits.

8.3.1.2 Ultrafast physical-based pseudo RBG

Let us now consider the randomness extraction in the second approach. Concretely, information theory shows us that if one samples at a rate R_s GHz and quantizes on$M$ bits, the entropy rate of the resulting discrete-time stochastic process cannot exceed $R_s \cdot M$ b/s. As an example, [78] reported a generation rate of 300 Gb/s with and R_s=20 GHz and M=8 bits, which violates the above reasoning. Here, in this second approach, we aim to extract as many bits as possible from the chaotic dynamics of a single ECSL that pass the three standard tests and satisfy the three standard-deviation criteria. To this end, the calculation of HFD of the initial data was also implemented. In contrast to [24, 25], where all the random integers were transformed into floating-point numbers of 52-bit resolution, in our implementation here the initial data of 8-bit resolution were transformed into a 64-bit integer data type (int64). Moreover, we found that the maximal difference order n_{max}=58 determined by condition (1) in [24] may be not the optimal one, and we obtained better performance for generating random bits when n_{max} was slightly increased to 62. Therefore, the 62th-order finite differences were used. The need for such a high order of difference may be caused by the sharpness and asymmetry of initial distribution, as shown in Fig. 44(a). All α_κ were then transformed into positive numbers by adding 2^{62} and converted in binary.

Next, the randomness extraction was carried out. To reiterate, even though all numbers contain 64 bits, again, one cannot extract all significant bits from each of them because keeping the full bits results in appearance of strong correlations in the generated bit sequences. To eliminate these correlations several of the MSBs have to be discarded. One can estimate the number of bits that need to be removed by plotting PDFs of the truncated values as is done in Fig. 45. Thanks to HFD, the removal of only a few bits leads to flat PDFs. Then one has to further check the ENT, Diehard, and NIST tests to determine the number of bits that should be retained. Based on extensive tests, we found that an extraction of 55 LSBs from each sample

Table 3: Results of NIST statistical tests for ultrafast physical-based pseudo random bits.

Statistical test	P value	Proportion	Result
Frequency	0.651693	0.9830	Success
Block frequency	0.275709	0.9900	Success
Cumulative sums	0.186566	0.9830	Success
Runs	0.079051	0.9850	Success
Longest runs	0.680755	0.9880	Success
Rank	0.587274	0.9930	Success
FFT	0.676615	0.9910	Success
Nonoverlapping templates	0.011709	0.9810	Success
Overlapping templates	0.074330	0.9850	Success
Universal	0.158133	0.9850	Success
Approximate entropy	0.552383	0.9870	Success
Random excursions	0.256333	0.9823	Success
Random excursions variant	0.184128	0.9871	Success
Serial	0.500279	0.9900	Success
Linear complexity	0.662091	0.9890	Success

may pass all the statistical tests for randomness. We carried out the same procedure of the randomness tests as that for the physical RBG in the first approach. The ENT results are as follows: Entropy=1.000 000 bits per bit (the optimum compression would reduce the bit file by 0 percent), χ^2 distribution is 0.27 (randomly would exceed this value 50% of the times), arithmetic mean value of data bits is 0.5000, Monte Carlo value for π is 3.141596402 and serial correlation coefficient is -0.000014. For the Diehard tests, it was obtained that $p_0 = 0.068578[KS]$ with minimal $p = 0.9897$ and maximal from the total number of 269. Table 3 presents the NIST results. For this second approach, the statistical bias B and the serial autocorrelation coefficients C_k of the random bit sequences were tested as well. As 55 LSBs were extracted from each sample, one can easily obtain a long bit-sequence from the chaos-based RBG. The bias was evaluated versus the length of the sequence N. It is clearly shown in Fig. 48(a) that the statistical bias B of the random bit sequence always keeps below

the significance level of $3\sigma_B$ up to 50 Gbits. In the meantime, the first 200 serial autocorrelation coefficients C_k of 50 Gbits random bit stream is presented in Fig. 48(b). One can see that, all values C_k are kept within the range, which is bounded by dashed lines corresponding to the $3\sigma_C$-criterion. These results further confirm the uncorrelatedness of the sequences, indicating that the chaos-based RBG can also be used to produce random bit sequences of ultra-long length at the same time the corresponding generation rate is increased up to the order of a couple of Tb/s.

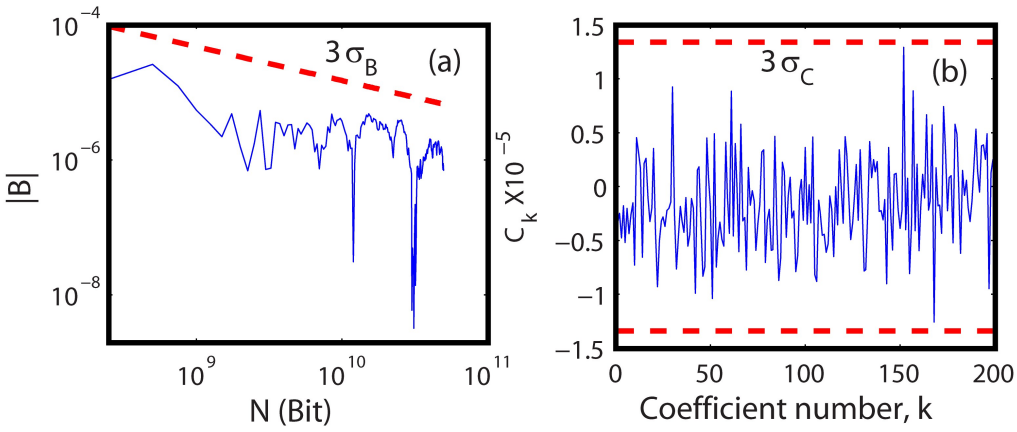

Figure 48: The results of the statistical bias and serial autocorrelation coefficient for the physical-based pseudo RBG at a speed of 2.2 Tb/s. (a) B as a function of the number of generated bits N; (b) first 200 serial autocorrelation coefficients for the binary sequence of 50 Gbit length. The values of were calculated by ensemble averaging over sequences of 1 Mbit length each.

The results given above suggest that the generated bit sequences passed all the statistical tests for randomness, in the sense that the inclusion of 55 consecutive LSBs leads to RBG at a rate of 2.2 Tb/s (= 55 LSBs $\times$ 40 GHz) , which is the fastest generation rate based on the chaotic dynamics of semiconductor lasers known to us. However, as it violates the limit set by information theory, we have to consider the corresponding generator as an ultrafast physical-based pseudo random-number generator. A further increase of the generation rate of random bits could possibly be achieved by a transformation of the initial data into a class of integers such as “int128” or “int256”, which may result in a generation rate of 4 Tb/s or 8 Tb/s. Such types

of integers can be implemented in hardware by employing field programmable gate array (FPGA), but a discussion of the experimental realization of such approaches is beyond the scope of this section. Finally, we would like to make several remarks on our work. The two approaches discussed here do not require extensive post-processing. In the two, the post-processing only involves the calculation of HFD and the selection of LSBs. Moreover, what we discuss requires neither the use of several lasers as in [67, 101, 102, 217] nor of delay lines as in [208, 217, 221]. Because of the post-processing chosen, we need not worry about the details of the acquisition nor of selecting a specific chaotic regime for the laser. Indeed, we checked (results not given here) that the randomness tests are passed for a wide range of operating parameters and for various acquisition conditions. That is, the two approaches are insensitive to these parameters, which is obviously another major advantage in addition to the ultrafast bit rate. Moreover, the two approaches introduced in the present study can also be carried out in a more compact photonic integrated circuit [15, 56].

8.4 Conclusion

This chapter reports the experimental investigation of two different approaches to random bit generation based on the chaotic dynamics of a semiconductor laser with optical feedback. By computing high-order finite differences of the chaotic laser intensity time series, we obtain time series with symmetric statistical distributions that are more conducive to ultrafast random bit generation. In the first approach, we only have retained 4 LSBs for each sample according to the min-entropy and demonstrated a possibility of an high-quality physical random-number generator with a generation rate of 160 Gb/s; in the second approach, starting with the use of a transformation of initial data obtained with 8-bit resolution into a 64-bit integer type, we have succeeded in extracting 55 LSBs and shown a feasibility of ultrafast physical-based

pseudo RBG at a rate of 2.2 Tb/s. As mentioned above, post-processing requires additional computational resources. These might be based on parallel arrays of suitable ultrahigh-speed FPGAs or ASICs, though the actual implementation is beyond the scope of the present study. Our work not only highlights an approach to physical RBG that satisfies the bounds set by min-entropy, but also demonstrates the high potential for ultrafast physical-based pseudo RBG based on the chaotic lasers.

CHAPTER IX

CONCLUSION

This thesis aimed to investigate the nonlinear dynamics of ECSLs subject to delayed feedback and focused on the chaotic dynamics of an ECSL and their application for the high-bit-rate generation of random-number sequences.

The investigations of high-dimensional chaotic dynamics was motivated by two reasons. On the one hand, fundamental insight into dynamical phenomena of high-dimensional chaotic dynamics was desired. On the other hand, understanding and utilization of the nonlinear dynamical properties of ECSLs promised high potential for realization of novel applications such as random-number generation. We have pursued this concept by studying three attractive examples:

- Tailoring the emission properties of semiconductor lasers by controlling their nonlinear dynamics properties.
- The realization of a physical system based on ECSLs, modeling and analysis of its random properties, and the determination of the theoretical limit of the RNG rate.
- The design of algorithms leading to high-speed RNG with provable quality.

The thesis consists of two closely coupled components: fundamental properties and applications. In the first integral part of this thesis, we have experimentally investigated the emission dynamics of chaotically emitting semiconductor lasers with time delayed feedback. Our investigations focused on high-dimensional broadband chaotic

dynamics. For characterization and analysis, we have applied state-of-the-art measurement technology and methods from nonlinear dynamics to gain first deep insight into the fundamental dynamical phenomena within this regime. Despite the numerous studies of ECSLs, we have seen that the detailed dynamics for ECSLs remain an open question. Our work examined several aspects of fundamental importance for dynamics of an ECSL using a tool from bifurcation theory. This offers perspectives for an ECSL to understand of the various operating parameters, such as the feedback strength, the injection current I, and the external cavity length L (creating a delay τ). We reiterate: the results map out, for the first time to our knowledge, detailed BDs of ECSLs as function of a feedback strength for various L and I, thus covering a significant portion of parameter space.

We have showed on the case of a distributed feedback laser biased up to 1.6 times the threshold current [low injection current case] and subjected to feedback from a distant reector. We observe bifurcation cascades resulting from the destabilization of external-cavity modes that appear successively when the feedback is increased, and explain, in light of the LK model, how the cascading is influenced by various laser operating parameters (current, delay,feedback phase) and experimental conditions. The experimental observation of a reduction in the number of stable regions with increasing I is consistent with the LK model. Indeed, LK predict that, at low I, the unstable regions correspond to the LFF regime, involving a drift toward the MGM, while at larger I, fully-developed coherence collapse occurs, with no drift toward the MGM. The observation of a gradual disappearance of the cascade with increasing L is also consistent with the model which shows an increase in attractor merging as a result of the increased proximity of ECMs in phase space.

In addition to experimental BDs of a semiconductor laser in low injection current case, we reported experimental BDs of a semiconductor laser, biased well-above threshold, subjected to external optical feedback. We observed that initial instabilities

correspond to the first steps of a quasi-periodic route to chaos that develops around a single ECM. This ECM loses stability first via a Hopf bifurcation to limit-cycle behavior at a frequency close to f_{RO}, which undergoes a secondary Hopf bifurcation corresponding to the undamping of a second frequency, close to f_{τ}, and leading to quasi-periodic oscillations. The quasiperiodic route is then interrupted by various windows of periodicity, as well as by intermittent behavior. In addition, we observe the existence of several limit cycles of different frequencies around the same ECM as well as transitions between two different limit cycles existing around the same or two different neighboring ECMs. Finally, for larger η, the merging of numerous attractors corresponding to different ECMs dictates the dynamics which correspond to a chaotic region of fully developed coherence collapse.

These are also the first experimental observations of the sensitivity to initial conditions of the BD of a high-dimensional dynamical system experiencing generalized multistability. We have showed that the initial conditions chosen have a profound impact on the route to chaos exhibited by ECSLs otherwise sharing identical parameters. In this sense, we demonstrated experimentally moderate SIC, *viz.* the coexistence of attractors in phase space. We noted in particular that the qualitative behavior of the route to chaos changes considerably at small η; however, the chaotic windows are of roughly the same size and are reached from almost the same η. These observations can be interpreted by the fact that at moderately low η, various attractors have developed around several ECMs, but have not yet merged or only a few neighboring attractors have merged. As as result, the system is an configuration of generalized muntistability in which the initial state will be crucial in determining the dynamics experienced by the ECSL. For larger η, most attractors have merged and, independent of the initial state of the BD, the trajectories end being attracted by a group of merged attractor ruins located around ECMs with a large negative frequency detuning, as is typical in a regime of fully-developed coherence collapse.

Also, we have shown that the bifurcations between dynamical states originating in the nonlinear dynamics of an ECSL at constant current can be detected by its terminal voltage. We experimentally vary the intensity fed back into the gain medium by the external cavity and show that the dc component V_{dc} of V tracks the optical intensity-based BD. It is shown using computational results based upon the LangKobayashi model that whereas optical intensity accesses the dynamical-state variable $|E|$, V is related to population-inversion carrier density N. The change in feedback strength affects N and thereby the quasi-Fermi energy level difference at the p-i-n junction band-gap of the gain medium. The change in the quasi-Fermi energy-level thereby changes the terminal voltage V. Thus, V is shown to provide information on the change in the dynamical-state variable N, which complements the more conventionally probed optical intensity. Indeed, we can view the current work in the broader context in which even under significant feedback well into the chaotic regime the LD in acts as a photodetector. Therefore, we shown that measuring the laser terminal voltage is the simple alternative way of measuring the feedback strength in an ECSL.

In the second integral part of this thesis, with regard to fundamental properties, we have shown the statistical nature of chaotic intensity time series from ECSLs and their use for RNG. We studied the statistics of $I(\mathrm{t})$ from an ECSL in coherence collapse. We compared the probability density distribution of the raw time series and investigate the mean and the variance as the first order statistics. We also compared the peak of the autocorrelation around the delay time (peak size), and the width (3 dB peak width) of the autocorrelation at first peak (the time shift is equal to zero) as a function of the current, for different feedback strengths as the second order statistics. For the first-order statistic, we found that the experimental probability-density function was significantly more concentrated around the mean optical power and robust to parameter changes than the density functions obtained from the LK model. Theory is more skewed to low $I(\mathrm{t})$, but this diminishes for higher J, appearing

increasingly Gaussian. While inclusion of noise in simulations slightly reduces the effect, it does not account for its size. We attributed this effect to residual intensity pulsations that are not present in experiments. For second-order statistic, substantial agreement between theory and experiment was found for the autocovariance, both for h and π as functions of $\eta(\kappa_{\mathrm{f}})$.

Based on the statistical properties of ECSLs, we reported the experimental investigation of two different approaches to random bit generation based on the chaotic dynamics of a semiconductor laser with optical feedback. By computing high-order finite differences of the chaotic laser intensity time series, we obtain time series with symmetric statistical distributions that are more conducive to ultrafast random bit generation. In the first approach, we only have retained 4 LSBs for each sample according to the min-entropy and demonstrated a possibility of an high-quality physical random-number generator with a generation rate of 160 Gb/s; in the second approach, starting with the use of a transformation of initial data obtained with 8-bit resolution into a 64-bit integer type, we have succeeded in extracting 55 LSBs and shown a feasibility of ultrafast physical-based pseudo RBG at a rate of 2.2 Tb/s. As mentioned above, post-processing requires additional computational resources. These might be based on parallel arrays of suitable ultrahigh-speed FPGAs or ASICs, though the actual implementation is beyond the scope of the present study. Our work not only highlights an approach to physical RBG that satisfies the bounds set by min-entropy, but also demonstrates the high potential for ultrafast physical-based pseudo RBG based on the chaotic lasers.

The thesis have consisted of two closely coupled components: fundamental properties and applications. As such, it bridges topics of applied mathematics, electrical engineering, and physics as well as information theory and computer science. We grounded our discussion in extensive theoretical studies based on the Lang-Kobayashi (LK) equations thus providing a means to attain physical insight into the observed

dynamics. Also, with regard to fundamental properties, we have observed the BD tracking the intensity time series of the output light as the feedback strength. We tracked at the dynamical regimes of an ECSL as key parameters are varied in order to determine conditions most propitious to high-rate RNG. This beneficial link between semiconductor laser and information theory can serve as a fruitful basis for future progress in both scientific fields.

APPENDIX A

SIMPLE RANDOM NUMBER GENERATION WITH AN ECSL

The need for high-speed encryption and for circuit-embedded random-number sources has driven advances in RNGs. Moreover, recent developments have made urgent the need for rigorous mathematical criteria to characterize and algorithms to generate RNG as opposed to employing standard randomness tests (e.g. NIST and Diehard). Due to the dynamics of ECSLs and their extreme sensitivity to initial conditions, the numerous positive Lyapunov exponents (LE), the noise-like power spectrum, and the irregular subnanosecond behavior, these systems lend themselves to high-speed RNG. For us, random here means that a bit sequence passes the NIST and Diehard random-number tests referred to above.

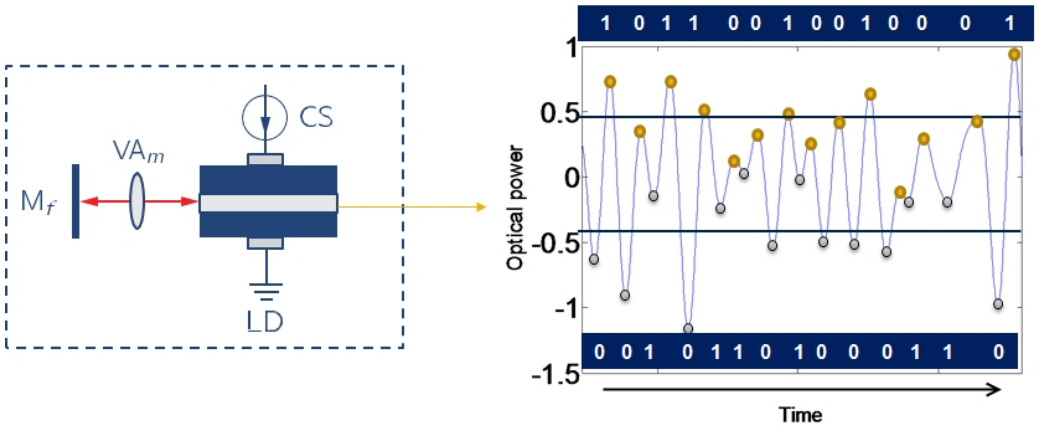

Figure 49: Apply basic post-processing techniques (eg. XOR operation) to the experimental chaotic intensity of ECSL.

We investigated the characteristics of fast RNG with a chaotic LD, which was a single-mode distributed feedback LD with TFD. The aim was to find a simple method for generating chaos and extracting random bits from the oscillations, which would

Table 4: Results of NIST randomness tests for a total of 20 samples of 1 Mbit sequences generated from intensity time series of an ECSL. The P-value (uniformity of p-value) obtained for each test should be larger than 0.0001, which indicate the corresponding test is passed.

Statistical Test	Uniformity of P-value	Propotion	Result
Frequency	0.122325	1.0000	SUCCESS
Block-frequency	0.350485	1.0000	SUCCESS
Cumulative-sums	0.911413	1.0000	SUCCESS
Runs	0.834308	1.0000	SUCCESS
Longest-run	0.534146	1.0000	SUCCESS
Rank	0.066882	1.0000	SUCCESS
FFT	0.350485	0.9500	SUCCESS
Overlapping-templates	0.834308	1.0000	SUCCESS
Universal	0.911413	1.0000	SUCCESS
Approximate-entropy	0.275709	0.9500	SUCCESS
Serial	0.000954	1.0000	SUCCESS
Linear-complexity	0.991468	1.0000	SUCCESS

be suitable for implementation as a practical fast physical RNG. To obtain random binary data from a continuous-time chaotic system, we take two sequences, the local maxima $S_{\max,\,\mathrm{i}}$ and minima sequence $S_{\max,\,\mathrm{i}}$ of the chaotic laser with intensity induced by optical time-delayed feedback. We generated the binary data $B_{\max,\,\mathrm{i}}$ and $B_{\min,\,\mathrm{i}}$ from the following equations :

$$B_{\max,\,\mathrm{i}} = sgn(S_{\max,\,\mathrm{i}} - T_{\max}), \qquad B_{\min,\,\mathrm{i}} = sgn(S_{\min,\,\mathrm{i}} - T_{\min}) \tag{26}$$

where $T_{\max}$ and $T_{\min}$ are appropriately chosen thresholds given as the medians of $S_{\max,\,\mathrm{i}}$ and $S_{\min,\,\mathrm{i}}$. To overcome periodicity in the (imperfectly) random sequence due to the external-cavity round-trip time, the two binary sequences are combined based on an exclusive-OR (XOR) logical operation to obtain a single sequence $S_{\mathrm{XOR},\,\mathrm{i}}$ by $S_{\mathrm{XOR},\,\mathrm{i}} = B_{\max,\,\mathrm{i}} \otimes B_{\min,\,\mathrm{i}}$, where $\otimes$ denotes the XOR operation. The combination of sequences using XOR is a common way to enhance randomness [201]. It is noteworthy that the XOR operation is a simple post-processing step. The chaotic signal was sampled to a binary sequence with at a rate of up to 8 Gb/s [Fig. 49]. The bit sequence generated at 8 Gb/s is verified to pass the NIST statistical tests of randomness as

shown in Table 1.

Note that these are preliminary results with the LD in a specific chaotic dynamical regime under relatively weak feedback strength. In most cases, even with the LD in a chaotic dynamical regime, the generated bit sequence does not pass the test. Our results are intriguing, and it is one aim of the future work to understand how various parameters, in particular the injection current, the external cavity length, and the feedback strength affect the ability of the generated sequences to pass the test. The results will provide clear empirical guidelines for tuning the chaotic LD parameters to achieve random bit sequences.

REFERENCES

[1] Abbe, E., "Polarization and randomness extraction," in *Information Theory Proceedings (ISIT), 2011 IEEE International Symposium on*, pp. 184–188, 2011.

[2] Abraham, N. B., Mandel, P., and Narducci, L. M., "I dynamical instabilities and pulsations in lasers," vol. 25 of *Progress in Optics*, pp. 1 – 190, Elsevier, 1988.

[3] Agrawal, G., "Line narrowing in a single-mode injection laser due to external optical feedback," *IEEE Journal of Quantum Electronics*, vol. 20, pp. 468–471, May 1984.

[4] Agrawal, G., *Long-Wavelength Semiconductor Lasers*. Van Nostrand Reinhold Electrical/Computer Science and Engineering Series, Springer Netherlands, 2012.

[5] Akizawa, Y., Yamazaki, T., Uchida, A., Harayama, T., Sunada, S., Arai, K., Yoshimura, K., and Davis, P., "Fast random number generation with bandwidth-enhanced chaotic semiconductor lasers at 8 x 50 gb/s," *IEEE Photon. Tech. Lett.*, vol. 24, no. 12, pp. 1042–1044, 2012.

[6] Al-Hosiny, N. M., Henning, I. D., and Adams, M. J., "Correlation of electron density changes with optical frequency shifts in optically injected semiconductor lasers," *IEEE Journal of Quantum Electronics*, vol. 42, pp. 570–580, Jun 2006.

[7] Alligood, K., Sauer, T., and Yorke, J., *Chaos: An Introduction to Dynamical Systems*. Chaos: An Introduction to Dynamical Systems, Springer, 1997.

[8] Alred, G. J., Brusaw, C. T., and Oliu, W. E., *Handbook of Technical Writing*. New York: St. Martin's, 2003 (seventh edition).

[9] Annovazzi-Lodi, V., Donati, S., and Scire, A., "Synchronization of chaotic injected-laser systems and its application to optical cryptography," *IEEE Journal of Quantum Electronics*, vol. 32, pp. 953–959, Jun 1996.

[10] Aoki, K., *Nonlinear Dynamics and Chaos in Semiconductors*. Series in condensed matter physics, Institute of Physics Publishing, 2001.

[11] Appeltant, L., Soriano, M. C., Van der Sande, G., Danckaert, J., Massar, S., Dambre, J., Schrauwen, B., Mirasso, C. R., and Fischer, I., "Information processing using a single dynamical node as complex system," *Nat. Commun.*, vol. 2, p. 468, 2011.

[12] Arecchi, F. T., Meucci, R., Puccioni, G., and Tredicce, J., "Experimental evidence of subharmonic bifurcations, multistability, and turbulence in a q-switched gas laser," *Phy. Rev. Lett.*, vol. 49, no. 17, pp. 1217–1220, 1982.

[13] Argyris, A., Hamacher, M., Chlouverakis, K. E., Bogris, A., and Syvridis, D., "Photonic integrated device for chaos applications in communications," *Phys. Rev. Lett.*, vol. 100, no. 19, 2008.

[14] Argyris, A., Deligiannidis, S., Pikasis, E., Bogris, A., and Syvridis, D., "Implementation of 140 gb/s true random bit generator based on a chaotic photonic integrated circuit," *Opt. Express*, vol. 18, no. 18, pp. 18763–18768, 2010.

[15] Argyris, A., Deligiannidis, S., Pikasis, E., Bogris, A., and Syvridis, D., "Implementation of 140 gb/s true random bit generator based on a chaotic photonic integrated circuit," *Opt. Express*, vol. 18, pp. 18763–18768, Aug 2010.

[16] Argyris, A., Grivas, E., Hamacher, M., Bogris, A., and Syvridis, D., "Chaos-on-a-chip secures data transmission in optical fiber links," *Opt. Express*, vol. 18, no. 5, pp. 5188–5198, 2010.

[17] Argyris, A., Syvridis, D., Larger, L., Annovazzi-Lodi, V., Colet, P., Fischer, I., García-Ojalvo, J., Mirasso, C. R., Pesquera, L., and Shore, K. A., "Chaos-based communications at high bit rates using commercial fibre-optic links," *Nature*, vol. 438, no. 7066, pp. 343–346, 2005.

[18] Argyris, G. and Annovazzi-Lodi, V., "Error analysis of a digital message impaired by optical chaos," *IEEE Photonics Technology Letters*, vol. 24, pp. 903–905, June 2012.

[19] Berge, P., Pomeau, Y., and Vidal, C., "Order within chaos: Towards a deterministic approach to turbulence [russian translation]," *Mir, Moscow*, 1991.

[20] Bhattacharya, P., *Semiconductor optoelectronic devices*. Prentice Hall, 1994.

[21] Brunner, D., Porte, X., Soriano, M. C., and Fischer, I., "Real-time frequency dynamics and high-resolution spectra of a semiconductor laser with delayed feedback," *Sci. Rep.*, vol. 2, 2012.

[22] Brunner, D., Soriano, M. C., Mirasso, C. R., and Fischer, I., "Parallel photonic information processing at gigabyte per second data rates using transient states," *Nature communications*, vol. 4, p. 1364, 2013.

[23] Chen, H. F. and Liu, J. M., "Open-loop chaotic synchronization of injection-locked semiconductor lasers with gigahertz range modulation," *IEEE Journal of Quantum Electronics*, vol. 36, pp. 27–34, Jan 2000.

[24] Chizhevsky, V. N., "Symmetrization of single-sided or nonsymmetrical distributions: The way to enhance a generation rate of random bits from a physical source of randomness," *Phys. Rev. E*, vol. 82, p. 050101, Nov 2010.

[25] Chizhevsky, V. N., "Fast generation of random bits based on polarization noises in a semiconductor vertical-cavity laser," *Opt. Spectrosc.*, vol. 111, no. 5, pp. 689–694, 2011.

[26] Colet, P. and Roy, R., "Digital-communication with synchronized chaotic lasers," *Opt. Lett.*, vol. 19, no. 24, pp. 2056–2058, 1994.

[27] Cuomo, K. M. and Oppenheim, A. V., "Circuit implementation of synchronized chaos with applications to communications," *Phy. Rev. Lett.*, vol. 71, no. 1, pp. 65–68, 1993.

[28] Cuomo, K. M. and Oppenheim, A. V., "Circuit implementation of synchronized chaos with applications to communications," *Phys. Rev. Lett.*, vol. 71, pp. 65–68, Jul 1993.

[29] D. Eastlake, J. S. and Croker, S., "Randomness requirements for security," 2005. Available at http://tools.Ietf.Org/html/rfc4086.

[30] Dangoisse, D., Glorieux, P., and Hennequin, D., "Laser chaotic attractors in crisis," *Phys. Rev. Lett.*, vol. 57, no. 21, pp. 2657–2660, 1986.

[31] Durt, T., Belmonte, C., Lamoureux, L.-P., Panajotov, K., Van den Berghe, F., and Thienpont, H., "Fast quantum-optical random-number generators," *Phys. Rev. A*, vol. 87, no. 2, 2013.

[32] Dutta, G. and Agrawal, N., *Semiconductor Lasers*. Kluwer Academic Press, 1993.

[33] Dynes, J. F., Yuan, Z. L., Sharpe, A. W., and Shields, A. J., "A high speed, postprocessing free, quantum random number generator," *Appl. Phys. Lett.*, vol. 93, no. 3, 2008.

[34] Ermakov, I. V. and others, "Semiconductor ring laser subject to delayed optical feedback: Bifurcations and stability," *Commmun. Nonlinear Sci. and Numer. Simulat.*, vol. 17, no. 12, pp. 4767–4779, 2012.

[35] Erneux, T. and others, "Stable microwave oscillations due to external-cavity-mode beating in laser diodes subject to optical feedback," *Phys. Rev. A*, vol. 66, p. 033809, Sep 2002.

[36] Erneux, T., Gavrielides, A., and Sciamanna, M., "Stable microwave oscillations due to external-cavity-mode beating in laser diodes subject to optical feedback," *Phys. Rev. A*, vol. 66, p. 033809, Sep 2002.

[37] Erneux, T. and Glorieux, P., *Laser Dynamics*. Cambridge University Press, 2010.

[38] Erneux, T., "Asymptotic methods applied to semiconductor laser models," *Proc. SPIE*, vol. 3944, pp. 588–601, 2000.

[39] Fang, X., Wetzel, B., Merolla, J.-M., Dudley, J., Larger, L., Guyeux, C., and Bahi, J., "Noise and chaos contributions in fast random bit sequence generated from broadband optoelectronic entropy sources," *Circuits and Systems I: Regular Papers, IEEE Transactions on*, vol. 61, pp. 888–901, March 2014.

[40] Feigenbaum, M. J., "Quantitative universality for a class of nonlinear transformations," *J. Stat. Phys.*, vol. 19, no. 1, pp. 25–52, 1978.

[41] Fischer, A. P. A., Andersen, O. K., Yousefi, M., Stolte, S., and Lenstra, D., "Experimental and theoretical study of filtered optical feedback in a semiconductor laser," *IEEE J. Quantum Electron.*, vol. 36, no. 3, pp. 375–384, 2000.

[42] Fischer, I., van Tartwijk, G. H. M., Levine, A. M., Elsässer, W., Göbel, E., and Lenstra, D., "Fast pulsing and chaotic itinerancy with a drift in the coherence collapse of semiconductor lasers," *Phys. Rev. Lett.*, vol. 76, pp. 220–223, Jan 1996.

[43] Frisch, U., Sulem, P. L., and Nelkin, M., "A simple dynamical model of intermittent fully developed turbulence," *J. Fluid Mech.*, vol. 87, no. 4, pp. 719–736, 1978.

[44] Gisin, N., Ribordy, G., Tittel, W., and Zbinden, H., "Quantum cryptography," *Rev. Mod. Phys.*, vol. 74, pp. 145–195, Mar 2002.

[45] Giuliani, G., Norgia, M., Donati, S., and Bosch, T., "Laser diode self-mixing technique for sensing applications," *Journal of Optics A: Pure and Applied Optics*, vol. 4, no. 6, p. S283, 2002.

[46] Goedgebuer, J. P., Larger, L., and Porte, H., "Optical cryptosystem based on synchronization of hyperchaos generated by a delayed feedback tunable laser diode," *Phy. Rev. Lett.*, vol. 80, no. 10, pp. 2249–2252, 1998.

[47] Goossens, M., Mittelbach, F., and Rahtz, S., *The LaTeX Companion*. Reading, Mass.: Addison-Wesley, 1997.

[48] Grebogi, C., Ott, E., and Yorke, J. A., "Chaotic attractors in crisis," *Phys. Rev. Lett.*, vol. 48, no. 22, pp. 1507–1510, 1982.

[49] Green, K. and others, "Bifurcation analysis of a spatially extended laser with optical feedback," *SIAM J. Appl. Dyn. Syst.*, vol. 8, no. 1, pp. 222–252, 2009.

[50] Green, K., Krauskopf, B., Marten, F., and Lenstra, D., "Bifurcation analysis of a spatially extended laser with optical feedback," *SIAM J. Appl. Dyn. Syst.*, vol. 8, no. 1, pp. 222–252, 2009.

[51] Gull, S. F., "Developments in maximum-entropy data analysis," in *Maximum Entropy and Bayesian Methods* (Skilling, J., ed.), pp. 53–71, Dordrecht: Kluwer Academic, 1989.

[52] Guo, H., Tang, W., Liu, Y., and Wei, W., "Truly random number generation based on measurement of phase noise of a laser," *Phys. Rev. E*, vol. 81, no. 5, 2010.

[53] Haken, H., "Analogy between higher instabilities in fluids and lasers," *Phys. Lett. A*, vol. A 53, no. 1, pp. 77–78, 1975.

[54] Haken, H., "Analogy between higher instabilities in fluids and lasers," *Physics Letters A*, vol. 53, no. 1, pp. 77 – 78, 1975.

[55] Hanson, K. M., "Introduction to Bayesian image analysis," in *Medical Imaging: Image Processing* (Loew, M. H., ed.), vol. 1898 of *Proc. SPIE*, pp. 716–731, 1993.

[56] Harayama, T., Sunada, S., Yoshimura, K., Davis, P., Tsuzuki, K., and Uchida, A., "Fast nondeterministic random-bit generation using on-chip chaos lasers," *Phys. Rev. A*, vol. 83, p. 031803, Mar 2011.

[57] Harayama, T., Sunada, S., Yoshimura, K., Muramatsu, J., Arai, K.-i., Uchida, A., and Davis, P., "Theory of fast nondeterministic physical random-bit generation with chaotic lasers," *Phys. Rev. E*, vol. 85, no. 4, 2012.

[58] Harayama, T., Sunada, S., Yoshimura, K., Muramatsu, J., Arai, K.-i., Uchida, A., and Davis, P., "Theory of fast nondeterministic physical random-bit generation with chaotic lasers," *Phys. Rev. E*, vol. 85, p. 046215, Apr 2012.

[59] Harayama, T., Sunada, S., Yoshimura, K., Muramatsu, J., Arai, K., Uchida, A., and Davis, P., "Theory of fast nondeterministic physical random-bit generation with chaotic lasers," *Phys. Rev. E*, vol. 85, no. 4, 2012.

[60] Heil, T. and others, "Coexistence of low-frequency fluctuations and stable emission on a single high-gain mode in semiconductor lasers with external optical feedback," *Phys. Rev. A*, vol. 58, no. 4, pp. R2672–R2675, 1998.

[61] Heil, T., Fischer, I., and Elser, W., "Coexistence of low-frequency fluctuations and stable emission on a single high-gain mode in semiconductor lasers with external optical feedback," *Phys. Rev. A*, vol. 58, no. 4, pp. R2672–R2675, 1998.

[62] Heil, T., Fischer, I., and Elser, W., "Stabilization of feedback-induced instabilities in semiconductor lasers," *Journal of Optics B: Quantum and Semiclassical Optics*, vol. 2, no. 3, p. 413, 2000.

[63] Heil, T., Fischer, I., and Elsaesser, W. E., "Dynamics of DFB lasers subject to optical feedback: stability properties of the stable modes," pp. 510–520, 2000.

[64] Heil, T., Fischer, I., Elsssser, W., Mulet, J., and Mirasso, C. R., "Statistical properties of low-frequency fluctuations during single-mode operation in distributed-feedback lasers: experiments and modeling," *Opt. Lett.*, vol. 24, no. 18, pp. 1275–1277, 1999.

[65] Heiligenthal, S., Jüngling, T., D'Huys, O., Arroyo-Almanza, D. A., Soriano, M. C., Fischer, I., Kanter, I., and Kinzel, W., "Strong and weak chaos in networks of semiconductor lasers with time-delayed couplings," *Phys. Rev. E*, vol. 88, p. 012902, Jul 2013.

[66] Henry, C. H. and Kazarinov, R. F., "Instability of semiconductor-lasers due to optical feedback from distant reflectors," *IEEE J. Quantum Electron.*, vol. 22, no. 2, pp. 294–301, 1986.

[67] Hirano, K., Amano, K., Uchida, A., Naito, S., Inoue, M., Yoshimori, S., Yoshimura, K., and Davis, P., "Characteristics of fast physical random bit generation using chaotic semiconductor lasers," *Quantum Electronics, IEEE Journal of*, vol. 45, pp. 1367–1379, Nov 2009.

[68] Hirano, K., Yamazaki, T., Morikatsu, S., Okumura, H., Aida, H., Uchida, A., Yoshimori, S., Yoshimura, K., Harayama, T., and Davis, P., "Fast random bit generation with bandwidth-enhanced chaos in semiconductor lasers," *Opt. Express*, vol. 18, pp. 5512–5524, Mar 2010.

[69] Hohl, A. and Gavrielides, A., "Bifurcation cascade in a semiconductor laser subject to optical feedback," *Phy. Rev. Lett.*, vol. 82, no. 6, pp. 1148–1151, 1999.

[70] Holman, W., Connelly, J., and Dowlatabadi, A., "An integrated analog/digital random noise source," *Circuits and Systems I: Fundamental Theory and Applications, IEEE Transactions on*, vol. 44, pp. 521–528, Jun 1997.

[71] Hong, Y. and Shore, K. A., "Statistical measures of the power dropout ratio in semiconductor lasers subject to optical feedback," *Opt. Lett.*, vol. 30, pp. 3332–3334, Dec 2005.

[72] Honjo, T., Uchida, A., Amano, K., Hirano, K., Someya, H., Okumura, H., Yoshimura, K., Davis, P., and Tokura, Y., "Differential-phase-shift quantum key distribution experiment using fast physical random bit generator with chaotic semiconductor lasers," *Opt. Express*, vol. 17, pp. 9053–9061, May 2009.

[73] Hui, R., Mecozzi, A., D'Ottavi, A., and Spano, P., "Novel measurement technique of alpha factor in dfb semiconductor lasers by injection locking," *Electronics Letters*, vol. 26, pp. 997–998, July 1990.

[74] Huyet, G., Hegarty, S., Giudici, M., de Bruyn, B., and McInerney, J. G., "Statistical properties of the dynamics of semiconductor lasers with optical feedback," *Europhys. Lett.*, vol. 40, no. 6, pp. 619–624, 1997.

[75] Huyet, G., White, J. K., Kent, A. J., Hegarty, S. P., Moloney, J. V., and McInerney, J. G., "Dynamics of a semiconductor laser with optical feedback," *Phys. Rev. A*, vol. 60, pp. 1534–1537, Aug 1999.

[76] Johansson, T. and Jonsson, F., "Theoretical analysis of a correlation attack based on convolutional codes," *IEEE Trans. Informat. Theo.*, vol. 48, no. 8, pp. 2173–2181, 2002.

[77] Kane, D., *Unlocking dynamical diversity : optical feedback effects on semiconductor lasers / Deborah Kane, editor*. Wiley Chichester, 2005.

[78] Kanter, I., Aviad, Y., Reidler, I., Cohen, E., and Rosenbluh, M., "An optical ultrafast random bit generator," *Nature Photon.*, vol. 4, no. 1, pp. 58–61, 2010.

[79] Kazarinov, R. F. and Suris, R. A., "Heterodyne reception of light by an injection laser," *Soviet Journal of Experimental and Theoretical Physics*, vol. 39, p. 522, Sept. 1974.

[80] Kim, B. and others, "Bifurcation-cascade diagrams of an external-cavity semiconductor laser: Experiment and theory," *IEEE J. Quantum Electron.*, vol. 50, pp. 965–972, Dec 2014.

[81] Kim, B., Li, N., Locquet, A., and Citrin, D. S., "Experimental bifurcation-cascade diagram of an external-cavity semiconductor laser," *Opt. Express*, vol. 22, pp. 2348–2357, Feb 2014.

[82] Kim, B., Locquet, A., Li, N., Choi, D., and Citrin, D., "Bifurcation-cascade diagrams of an external-cavity semiconductor laser: Experiment and theory," *IEEE J. Quantum Electron.*, vol. 50, pp. 965–972, Dec 2014.

[83] Kim, B., Locquet, A., Choi, D., and Citrin, D. S., "Experimental route to chaos of an external-cavity semiconductor laser," *Phys. Rev. A*, vol. 91, p. 061802, Jun 2015.

[84] Knuth, D., *The Art of Computer Programming: Volume 3: Sorting and Searching*. Pearson Education, 1998.

[85] Knuth, D. E., *The Art of Computer Programming, Volume 3: (2Nd Ed.) Sorting and Searching*. Redwood City, CA, USA: Addison Wesley Longman Publishing Co., Inc., 1998.

[86] Koga, H. and Han, T., *Information-Spectrum Methods in Information Theory*. Stochastic Modelling and Applied Probability, Springer Berlin Heidelberg, 2002.

[87] Krauskopf, B. and Lenstra, D., *Fundamental Issues of Nonlinear Laser Dynamics: Concepts,Mathematics, Physics,and Applications International Spring School, Texel, The Netherlands 16-19 April 2000*. AIP Conference Proceedings, American Inst. of Physics, 2000.

[88] Kuntsevich, B. F., Mel'nikov, A. A., and Kononenko, V. K., "Nonlinear response of the semiconductor laser with pump current modulation," *Journal of Applied Spectroscopy*, vol. 70, no. 2, pp. 285–291.

[89] Lakshmanan, M. and Senthilkumar, D., *Dynamics of Nonlinear Time-Delay Systems*. Springer Series in Synergetics, Springer, 2011.

[90] Lamport, L., *LaTeX: A Document Preparation System*. Reading, Mass.: Addison-Wesley, 1994.

[91] Lang, R. and Kobayashi, K., "External optical feedback effects on semiconductor injection-laser properties," *IEEE J. Quantum Electron.*, vol. 16, no. 3, pp. 347–355, 1980.

[92] Lang, R. and Kobayashi, K., "External optical feedback effects on semiconductor injection-laser properties," *IEEE J. Quantum Electron.*, vol. 16, no. 3, pp. 347–355, 1980.

[93] Larger, L., Soriano, M. C., Brunner, D., Appeltant, L., Gutierrez, J. M., Pesquera, L., Mirasso, C. R., and Fischer, I., "Photonic information processing beyond turing: an optoelectronic implementation of reservoir computing," *Opt. Express*, vol. 20, pp. 3241–3249, Jan 2012.

[94] Lawandy, N. M., "Instabilities in laser-pumped gas lasers: experimental oscillation line shapes," *J. Opt. Soc. Am. B*, vol. 2, no. 1, pp. 108–111, 1985.

[95] Levine, A., van Tartwijk, G., Lenstra, D., and Erneux, T., "Diode lasers with optical feedback: Stability of the maximum gain mode," *Phys. Rev. A*, vol. 52, pp. R3436–R3439, Nov 1995.

[96] Lűdge, K., *Nonlinear Laser Dynamics: From Quantum Dots to Cryptography*. Annual Reviews of Nonlinear Dynamics and Complexity, Wiley, 2012.

[97] Li, H., Ye, J., and McInerney, J., "Detailed analysis of coherence collapse in semiconductor lasers," *Quantum Electronics, IEEE Journal of*, vol. 29, pp. 2421–2432, Sep 1993.

[98] Li, N. and others, "Statistics of the optical intensity of a chaotic external-cavity dfb laser," *Opt. Lett.*, vol. 39, pp. 5949–5952, Oct 2014.

[99] Li, N., Kim, B., Locquet, A., Choi, D., Pan, W., and Citrin, D. S., "Statistics of the optical intensity of a chaotic external-cavity dfb laser," *Opt. Lett.*, vol. 39, pp. 5949–5952, Oct 2014.

[100] Li, X.-Z. and Chan, S.-C., "Random bit generation using an optically injected semiconductor laser in chaos with oversampling," *Opt. Lett.*, vol. 37, no. 11, pp. 2163–2165, 2012.

[101] Li, X.-Z. and Chan, S.-C., "Random bit generation using an optically injected semiconductor laser in chaos with oversampling," *Opt. Lett.*, vol. 37, pp. 2163–2165, Jun 2012.

[102] Li, X.-Z. and Chan, S.-C., "Heterodyne random bit generation using an optically injected semiconductor laser in chaos," *Quantum Electronics, IEEE Journal of*, vol. 49, pp. 829–838, Oct 2013.

[103] Li, X., Cohen, A. B., Murphy, T. E., and Roy, R., "Scalable parallel physical random number generator based on a superluminescent led," *Opt. Lett.*, vol. 36, no. 6, pp. 1020–1022, 2011.

[104] Lim, Y. L., Bertling, K., Rio, P., Tucker, J. R., and Rakic, A. D., "Displacement and distance measurement using the change in junction voltage across a laser diode due to the self-mixing effect," 2005.

[105] Lin, F.-Y. and Liu, J.-M., "Chaotic lidar," *IEEE J. Sel. Topics Quantum Electron.*, vol. 10, pp. 991–997, Sept 2004.

[106] Liu, H. F. and Ngai, W. F., "Nonlinear dynamics of a directly modulated 1.55-um InGaAsP distributed-feedback semiconductor-laser," *IEEE J. Quantum Electron.*, vol. 29, no. 6, pp. 1668–1675, 1993.

[107] Liu, J. M., Chen, H. F., and Tang, S., "Optical-communication systems based on chaos in semiconductor lasers," *IEEE Transactions on Circuits and Systems I: Fundamental Theory and Applications*, vol. 48, pp. 1475–1483, Dec 2001.

[108] Liu, Y., Davis, P., Takiguchi, Y., Aida, T., Saito, S., and Liu, J.-M., "Injection locking and synchronization of periodic and chaotic signals in semiconductor lasers," *IEEE Journal of Quantum Electronics*, vol. 39, pp. 269–278, Feb 2003.

[109] Locquet, A., *Physical-layer chaos-based secure communications using semiconductor lasers.* as a chapter of the Handbook on Communication and Information Security, Springer, 2009.

[110] Locquet, A., Masoller, C., Megret, P., and Blondel, M., "Comparison of two types of synchronization of external-cavity semiconductor lasers," *Opt. Lett.*, vol. 27, no. 1, pp. 31–33, 2002.

[111] Locquet, A., Rogister, F., Sciamanna, M., Megret, P., and Blondel, M., "Two types of synchronization in unidirectionally coupled chaotic external-cavity semiconductor lasers," *Phys. Rev. E*, vol. 64, no. 4, 2001.

[112] Lorenz, E. N., "Deterministic nonperiodic flow," *J. Atmos. Sci.*, vol. 20, no. 2, pp. 130–141, 1963.

[113] Ma, X., Xu, F., Xu, H., Tan, X., Qi, B., and Lo, H.-K., "Postprocessing for quantum random-number generators: Entropy evaluation and randomness extraction," *Phys. Rev. A*, vol. 87, p. 062327, Jun 2013.

[114] Marsaglia, G., "The diehard test suite","http:// www. csis. hku. hk/diehard.ent-a pseudorandom sequence test program."

[115] Masoller, C. and Abraham, N. B., "Stability and dynamical properties of the coexisting attractors of an external-cavity semiconductor laser," *Phys. Rev. A*, vol. 57, no. 2, pp. 1313–1322, 1998.

[116] Metropolis, N., Rosenbluth, A. W., Rosenbluth, M. N., Teller, A. H., and Teller, E., "Equations of state calculations by fast computing machine," *J. Chem. Phys.*, vol. 21, pp. 1087–1091, 1953.

[117] Midavaine, T., Dangoisse, D., and Glorieux, P., "Observation of chaos in a frequency-modulated CO_2 laser," *Phys. Rev. Lett.*, vol. 55, no. 19, p. 1989, 1985.

[118] Mikami, T., Kanno, K., Aoyama, K., Uchida, A., Ikeguchi, T., Harayama, T., Sunada, S., Arai, K.-i., Yoshimura, K., and Davis, P., "Estimation of entropy rate in a fast physical random-bit generator using a chaotic semiconductor laser with intrinsic noise," *Phys. Rev. E*, vol. 85, p. 016211, Jan 2012.

[119] ming Liu, J., foo Chen, H., and Tang, S., "Synchronized chaotic optical communications at high bit rates," *IEEE Journal of Quantum Electronics*, vol. 38, pp. 1184–1196, Sep 2002.

[120] Mitsuhashi, Y., Morikawa, T., Sakurai, K., Seko, A., and Shimada, J., "Self-coupled optical pickup," *Optics Communications*, vol. 17, no. 1, pp. 95 – 97, 1976.

[121] Mitsuhashi, Y., Shimada, J., and Mitsutsuka, S., "Voltage change across the self-coupled semiconductor laser," *IEEE Journal of Quantum Electronics*, vol. 17, pp. 1216–1225, Jul 1981.

[122] Mittelbach, F., Goossens, M., Braams, J., and Carlisle, D., *The LaTeX Companion*. Reading, Mass.: Addison-Wesley, second ed., 2004.

[123] Mork, J., Mark, J., and Tromborg, B., "Route to chaos and competition between relaxation oscillations for a semiconductor-laser with optical feedback," *Phy. Rev. Lett.*, vol. 65, no. 16, pp. 1999–2002, 1990.

[124] Mork, J., Tromborg, B., and Mark, J., "Chaos in semiconductor lasers with optical feedback: Theory and experiment," *IEEE J. Quantum Electron.*, vol. 28, no. QE-28, pp. 93–108, 1992.

[125] Mukai, T. and Otsuka, K., "New route to optical chaos: Successive-subharmonic-oscillation cascade in a semiconductor laser coupled to an external cavity," *Phys. Rev. Lett.*, vol. 55, no. 17, pp. 1711–1714, 1985.

[126] Murakami, A., "Phase locking and chaos synchronization in injection-locked semiconductor lasers," *IEEE Journal of Quantum Electronics*, vol. 39, pp. 438–447, Mar 2003.

[127] Murphy, T. E. and Roy, R., "Chaotic lasers: The world's fastest dice," *Nat Photon*, vol. 2, pp. 714–715, Dec 2008.

[128] Nelson, D. F. and Boyle, W. S., "A continuously operating ruby optical maser," *Appl. Opt.*, vol. 1, pp. 181–183, Mar 1962.

[129] Nguimdo, R. M., Colet, P., Larger, L., and Pesquera, L., "Digital key for chaos communication performing time delay concealment," *Phys. Rev. Lett.*, vol. 107, p. 034103, Jul 2011.

[130] Nguimdo, R. M., Verschaffelt, G., Danckaert, J., Leijtens, X., Bolk, J., and Van der Sande, G., "Fast random bits generation based on a single chaotic semiconductor ring laser," *Opt. Express*, vol. 20, no. 27, pp. 28603–28613, 2012.

[131] Nishizawa, J. and Ishida, K., "Injection-induced modulation of laser light by the interaction of laser diodes," *IEEE Journal of Quantum Electronics*, vol. 11, pp. 515–519, Jul 1975.

[132] Ohtsubo, J., *Semiconductor Lasers-Stability, Instability and Chaos*. Springer, 2006.

[133] Ohtsubo, J., "Feedback induced instability and chaos in semiconductor lasers and their applications," *Opt. Rev.*, vol. 6, no. 1, pp. 1–15, 1999.

[134] Oliver, N., Cornelles Soriano, M., Sukow, D., and Fischer, I., "Fast random bit generation using a chaotic laser: Approaching the information theoretic limit," *Quantum Electronics, IEEE Journal of*, vol. 49, pp. 910–918, Nov 2013.

[135] Oliver, N., Soriano, M. C., Sukow, D. W., and Fischer, I., "Dynamics of a semiconductor laser with polarization-rotated feedback and its utilization for random bit generation," *Opt. Lett.*, vol. 36, no. 23, pp. 4632–4634, 2011.

[136] Oliver, N., Soriano, M. C., Sukow, D. W., and Fischer, I., "Dynamics of a semiconductor laser with polarization-rotated feedback and its utilization for random bit generation," *Opt. Lett.*, vol. 36, pp. 4632–4634, Dec 2011.

[137] Ott, E., *Chaos in Dynamical Systems*. Cambridge University Press, 2002.

[138] Paoli, T. and Ripper, J., "Frequency stabilization and narrowing of optical pulses from cw gaas injection lasers," *IEEE Journal of Quantum Electronics*, vol. 6, pp. 335–339, Jun 1970.

[139] Paquot, Y., Duport, F., Smerieri, A., Dambre, J., Schrauwen, B., Haelterman, M., and Massar, S., "Optoelectronic reservoir computing," *Sci. Rep.*, vol. 2, pp. 287:1–287:6, 2012.

[140] Paul, J., Masoller, C., Mandel, P., Hong, Y., Spencer, P. S., and Shore, K. A., "Experimental and theoretical study of dynamical hysteresis and scaling laws in the polarization switching of vertical-cavity surface-emitting lasers," *Phys. Rev. A*, vol. 77, p. 043803, Apr 2008.

[141] Pecora, L. M. and Carroll, T. L., "Synchronization in chaotic systems," *Phys. Rev. Lett.*, vol. 64, pp. 821–824, Feb 1990.

[142] Peil and others, "Spectral broadband dynamics of semiconductor lasers with resonant short cavities," *Phys. Rev. A*, vol. 73, p. 023805, Feb 2006.

[143] Peil, M., Fischer, I., and Elsässer, W., "Spectral broadband dynamics of semiconductor lasers with resonant short cavities," *Phys. Rev. A*, vol. 73, p. 023805, Feb 2006.

[144] Perelman, L. C., Paradis, J., and Barrett, E., *Mayfield Handbook of Technical and Scientific Writing*. Mayfield: Mountain View, April 1997. http://mit.imoat.net/handbook/.

[145] Peterman, K., "External optical feedback phenomena in semiconductor lasers," *IEEE J. Sel. Topics Quantum Electron.*, vol. 1, pp. 480–489, Jun 1995.

[146] Phillips, M., Gong, H., Ferguson, A., and Hanna, D., "Optical chaos and hysteresis in a laser-diode pumped nd doped fibre laser," *Opt. Comm.*, vol. 61, no. 3, pp. 215 – 218, 1987.

[147] Pieroux, D. and others, "Interacting pairs of periodic solutions lead to tori in lasers subject to delayed feedback," *Phys. Rev. E*, vol. 63, p. 036211, Feb 2001.

[148] Pieroux, D. and Mandel, P., "Bifurcation diagram of a complex delay-differential equation with cubic nonlinearity," *Physical Review E*, vol. 67, no. 5, p. 056213, 2003.

[149] Pironio, S., Acin, A., Massar, S., de la Giroday, A. B., Matsukevich, D. N., Maunz, P., Olmschenk, S., Hayes, D., Luo, L., Manning, T. A., and Monroe, C., "Random numbers certified by bell's theorem," *Nature*, vol. 464, no. 7291, pp. 1021–1024, 2010.

[150] Pisarchik, A., Barmenkov, Y., and Kir'yanov, A., "Experimental characterization of the bifurcation structure in an erbium-doped fiber laser with pump modulation," *IEEE J. Quantum Electron.*, vol. 39, pp. 1567–1571, Dec 2003.

[151] Poincare, H., *Science et Methodes, Chap IV. Le Hasard.* E.Flammarion, 1908.

[152] Porte, X., Soriano, M. C., and Fischer, I., "Similarity properties in the dynamics of delayed-feedback semiconductor lasers," *Phys. Rev. A*, vol. 89, p. 023822, Feb 2014.

[153] Prasad, A., Lai, Y.-C., Gavrielides, A., and Kovanis, V., "Complicated basins in external-cavity semiconductor lasers," *Phys. Rev. A*, vol. 314, no. 12, pp. 44 – 50, 2003.

[154] Priyadarshi, S., Hong, Y., Pierce, I., and Shore, K., "Experimental investigations of time-delay signature concealment in chaotic external cavity vcsels subject to variable optical polarization angle of feedback," *Selected Topics in Quantum Electronics, IEEE Journal of*, vol. 19, pp. 1700707–1700707, July 2013.

[155] Qi, B., Chi, Y.-M., Lo, H.-K., and Qian, L., "High-speed quantum random number generation by measuring phase noise of a single-mode laser," *Opt. Lett.*, vol. 35, no. 3, pp. 312–314, 2010.

[156] Ray, W., Lam, W.-S., Guzdar, P., and Roy, R., "Observation of chaotic itinerancy in the light and carrier dynamics of a semiconductor laser with optical feedback," *Phys. Rev. E*, vol. 73, p. 026219, Feb 2006.

[157] Reategui, R. J., Kir'yanov, A. V., Pisarchik, A. N., Barmenkov, Y. O., and Il'ichev, N. N., "Experimental study and modeling of coexisting attractors and bifurcations in an erbium-doped fiber laser with diode-pump modulation," *Laser Phys.*, vol. 14, no. 10, pp. 1277–1281, 2004.

[158] Reidler, I., Aviad, Y., Rosenbluh, M., and Kanter, I., "Ultrahigh-speed random number generation based on a chaotic semiconductor laser," *Phy. Rev. Lett.*, vol. 103, no. 2, 2009.

[159] Renyi, A., "On measures of entropy and information," in *Proc. Fourth Berkeley Symp. Math. Stat. and Probability*, vol. 1, pp. 547–561, University of California Press, 1961.

[160] Risch, C. and Voumard, C., "Self-pulsation in output intensity and spectrum of gaas-aigaas cw diode-lasers coupled to a frequency-selective external optical cavity," *J. Appl. Phys.*, vol. 48, no. 5, pp. 2083–2085, 1977.

[161] Ritter, A. and Haug, H., "Theory of laser-diodes with weak optical feedback .1. small-signal analysis and side-mode spectra," *J. Opt. Soc. Am. B-Opt. Phys.*, vol. 10, no. 1, pp. 130–144, 1993.

[162] Ritter, A. and Haug, H., "Theory of the bistable limit cycle behavior of laser diodes induced by weak optical feedback," *IEEE J. Quantum Electron.*, vol. 29, pp. 1064–1070, Apr 1993.

[163] Rontani, D., Locquet, A., Sciamanna, M., and Citrin, D. S., "Loss of time-delay signature in the chaotic output of a semiconductor laser with optical feedback," *Opt. Lett.*, vol. 32, pp. 2960–2962, Oct 2007.

[164] Rontani, D., Sciamanna, M., Locquet, A., and Citrin, D. S., "Multiplexed encryption using chaotic systems with multiple stochastic-delayed feedbacks," *Phys. Rev. E*, vol. 80, no. 6, p. 066209, 2009.

[165] Rontani, D., Locquet, A., Sciamanna, M., Citrin, D. S., and Ortin, S., "Time-delay identification in a chaotic semiconductor laser with optical feedback: A dynamical point of view," *IEEE J. Quantum Electron.*, vol. 45, no. 7, pp. 879–891, 2009.

[166] Rosin, D. P., Rontani, D., and Gauthier, D. J., "Ultrafast physical generation of random numbers using hybrid boolean networks," *Phys. Rev. E*, vol. 87, p. 040902, Apr 2013.

[167] Roy, R. and Thornburg, K. S., "Experimental synchronization of chaotic lasers," *Phy. Rev. Lett.*, vol. 72, no. 13, pp. 2009–2012, 1994.

[168] Roy, R. and Thornburg, K. S., "Experimental synchronization of chaotic lasers," *Phys. Rev. Lett.*, vol. 72, pp. 2009–2012, Mar 1994.

[169] Ruelle, D. and Takens, F., "On the nature of turbulence," *Commun. Math. Phys.*, vol. 20, no. 3, pp. 167–192, 1971.

[170] Ruiz-Oliveras, F. R. and Pisarchik, A. N., "Synchronization of semiconductor lasers with coexisting attractors," *Phys. Rev. E*, vol. 79, no. 1, p. 016202, 2009.

[171] Rukhin, A., Soto, J., Nechvatal, J., Smid, M., Barker, E., Leigh, S., and Levenson, M., "A statistical test suite for random and pseudorandom number generators for cryptographic applications," tech. rep., 2001. Nat. Inst. Standards and Technology, Special Publication 800-22.

[172] Rukhin, A., Soto, J., Nechvatal, J., Barker, E., Leigh, S., Levenson, M., Banks, D., Heckert, A., Dray, J., Vo, S., Rukhin, A., Soto, J., Smid, M., Leigh, S., Vangel, M., Heckert, A., Dray, J., and Iii, L. E. B., "A statistical test suite for random and pseudorandom number generators for cryptographic applications," 2001.

[173] Ruprecht, P. and Brandenberger, J., "Enhancing diode laser tuning with a short external cavity," *Optics Communications*, vol. 93, no. 1, pp. 82 – 86, 1992.

[174] Sacher, J., Baums, D., Panknin, P., Elsässer, W., and Göbel, E. O., "Intensity instabilities of semiconductor lasers under current modulation, external light injection, and delayed feedback," *Phys. Rev. A*, vol. 45, pp. 1893–1905, Feb 1992.

[175] Sacher, J., Elsässer, W., and Göbel, E. O., "Intermittency in the coherence collapse of a semiconductor laser with external feedback," *Phys. Rev. Lett.*, vol. 63, pp. 2224–2227, Nov 1989.

[176] Sahai, A. A., Kim, B., Choi, D., Locquet, A., and Citrin, D. S., "Mapping the nonlinear dynamics of a laser diode via its terminal voltage," *Opt. Lett.*, vol. 39, pp. 5630–5633, Oct 2014.

[177] Sciamanna, M., Masoller, C., Rogister, F., Mégret, P., Abraham, N. B., and Blondel, M., "Fast pulsing dynamics of a vertical-cavity surface-emitting laser operating in the low-frequency fluctuation regime," *Phys. Rev. A*, vol. 68, p. 015805, Jul 2003.

[178] Seko, A., Mitsuhashi, Y., Morikawa, T., Shimada, J., and Sakurai, K., "Selfquenching in semiconductor lasers and its applications in optical memory readout," *Applied Physics Letters*, vol. 27, no. 3, 1975.

[179] Shannon, C. E., "A mathematical theory of communication," *SIGMOBILE Mob. Comput. Commun. Rev.*, vol. 5, pp. 3–55, Jan. 2001.

[180] Simpson, T. B., Liu, J. M., Gavrielides, A., Kovanis, V., and Alsing, P. M., "Perioddoubling route to chaos in a semiconductor laser subject to optical injection," *Applied Physics Letters*, vol. 64, no. 26, 1994.

[181] Simpson, T., "Mapping the nonlinear dynamics of a distributed feedback semiconductor laser subject to external optical injection," *Opt. Commun.*, vol. 215, no. 13, pp. 135 – 151, 2003.

[182] Sivaprakasam, S. and Shore, K. A., "Demonstration of optical synchronization of chaotic external-cavity laser diodes," *Opt. Lett.*, vol. 24, no. 7, pp. 466–468, 1999.

[183] Soriano, M. C., Ortn, S., Brunner, D., Larger, L., Mirasso, C. R., Fischer, I., and Pesquera, L., "Optoelectronic reservoir computing: tackling noise-induced performance degradation," *Opt. Express*, vol. 21, no. 1, pp. 12–20, 2013.

[184] Soriano, M. C., García-Ojalvo, J., Mirasso, C. R., and Fischer, I., "Complex photonics: Dynamics and applications of delay-coupled semiconductors lasers," *Rev. Mod. Phys.*, vol. 85, no. 1, pp. 421–470, 2013.

[185] Stavroulakis, P. and Stamp, M., *Handbook of Information and Communication Security*. Handbook of Information and Communication Security, Springer Berlin Heidelberg, 2010.

[186] Stojanovski, T., Pihl, J., and Kocarev, L., "Chaos-based random number generators - part ii: Practical realization," *IEEE Trans. Circ. Syst. I*, vol. 48, no. 3, pp. 382–385, 2001.

[187] Stojanovski, T., Pihl, J., and Kocarev, L., "Chaos-based random number generators. part ii: practical realization," *Circuits and Systems I: Fundamental Theory and Applications, IEEE Transactions on*, vol. 48, pp. 382–385, Mar 2001.

[188] Strogatz, S., *Nonlinear Dynamics and Chaos: With Applications to Physics, Biology, Chemistry, and Engineering*. Studies in Nonlinearity, Westview Press, 2014.

[189] Strogatz, S. H., *Nonlinear Dynamics And Chaos: With Applications To Physics, Biology, Chemistry, And Engineering (Studies in Nonlinearity)*. Studies in nonlinearity, Westview Press, 1 ed., Jan. 2001.

[190] Sugawara, T., Tachikawa, M., Tsukamoto, T., and Shimizu, T., "Observation of synchronization in laser chaos," *Phy. Rev. Lett.*, vol. 72, no. 22, pp. 3502–3505, 1994.

[191] Sugawara, T., Tachikawa, M., Tsukamoto, T., and Shimizu, T., "Observation of synchronization in laser chaos," *Phys. Rev. Lett.*, vol. 72, pp. 3502–3505, May 1994.

[192] Sukow, D. W., Heil, T., Fischer, I., Gavrielides, A., Hohl-AbiChedid, A., and Elsasser, W., "Picosecond intensity statistics of semiconductor lasers operating in the low-frequency fluctuation regime," *Phys. Rev. A*, vol. 60, no. 1, pp. 667–673, 1999.

[193] Syvridis, D., Argyris, A., and Bogris, A., "Chaos-based communications at high bit rates using commercial fibre-optic links," vol. 6353, pp. 63531K–63531K–11, 2006.

[194] Tien-Yien Li, J. A. Y., "Period three implies chaos," *The American Mathematical Monthly*, vol. 82, no. 10, pp. 985–992, 1975.

[195] Tkach, R. and Chraplyvy, A., "Regimes of feedback effects in 1.5- μm distributed feedback lasers," *Journal of Lightwave Technology*, vol. 4, pp. 1655–1661, Nov 1986.

[196] Toomey, J. P. and Kane, D. M., "Mapping the dynamic complexity of a semiconductor laser with optical feedback using permutation entropy," *Optics Express*, vol. 22, p. 1713, Jan. 2014.

[197] Torcini, A., Barland, S., Giacomelli, G., and Marin, F., "Low-frequency fluctuations in vertical cavity lasers: Experiments versus lang-kobayashi dynamics," *Phys. Rev. A*, vol. 74, p. 063801, Dec 2006.

[198] Tromborg, B. and Mork, J., "Stability analysis and the route to chaos for laser diodes with optical feedback," *IEEE Photon. Technol. Lett.*, vol. 2, pp. 549–552, Aug 1990.

[199] Tromborg, B., Osmundsen, J., and Olesen, H., "Stability analysis for a semiconductor laser in an external cavity," *IEEE Journal of Quantum Electronics*, vol. 20, pp. 1023–1032, Sep 1984.

[200] Uchida, A., *Optical Communication with Chaotic Lasers: Applications of Nonlinear Dynamics and Synchronization*. Optical Communication with Chaotic Lasers: Applications of Nonlinear Dynamics and Synchronization, Wiley, 2012.

[201] Uchida, A., Amano, K., Inoue, M., Hirano, K., Naito, S., Someya, H., Oowada, I., Kurashige, T., Shiki, M., Yoshimori, S., Yoshimura, K., and Davis, P., "Fast physical random bit generation with chaotic semiconductor lasers," *Nature Photon.*, vol. 2, no. 12, pp. 728–732, 2008.

[202] Vadhan, S. P., *Pseudorandomness*, vol. 7. Now publishers, 2012.

[203] Valling, S., Krauskopf, B., Fordell, T., and Lindberg, A. M., "Experimental bifurcation diagram of a solid state laser with optical injection," *Opt. Comm.*, vol. 271, no. 2, pp. 532–542, 2007.

[204] van Tartwijk, G. H. M. and Agrawal, G. P., "Laser instabilities: a modern perspective," *Prog. Quant. Electron.*, vol. 22, no. 2, pp. 43–122, 1998.

[205] van Tartwijk, G. H. M. and Lenstra, D., "Semiconductor lasers with optical injection and feedback," *Quantum and Semiclassical Optics: Journal of the European Optical Society Part B*, vol. 7, no. 2, p. 87, 1995.

[206] VanWiggeren, G. D. and Roy, R., "Communication with chaotic lasers," *Science*, vol. 279, no. 5354, pp. 1198–1200, 1998.

[207] Walkeri, J., "Ent-a pseudorandom sequence test program","http://www.fourmilab.ch/random."

[208] Wang, A., Li, P., Zhang, J., Zhang, J., Li, L., and Wang, Y., "4.5 gbps high-speed real-time physical random bit generator," *Opt. Express*, vol. 21, pp. 20452–20462, Aug 2013.

[209] Wayne, M. A. and Kwiat, P. G., "Low-bias high-speed quantum random number generator via shaped optical pulses," *Opt. Express*, vol. 18, pp. 9351–9357, Apr 2010.

[210] Weiss, C. O., Godone, A., and Olafsson, A., "Routes to chaotic emission in a cw he-ne laser," *Phys. Rev. A*, vol. 28, pp. 892–895, Aug 1983.

[211] Weiss, C. O. and Vilaseca, R., "Dynamics of lasers," *NASA STI/Recon Technical Report A*, vol. 92, Nov. 1991.

[212] Wieczorek and others, "Bifurcations and chaos in a semiconductor laser with coherent or noisy optical injection," *Opt. Commun.*, vol. 282, no. 12, pp. 2367–2379, 2009.

[213] Wieczorek, S., Krauskopf, B., and Lenstra, D., "A unifying view of bifurcations in a semiconductor laser subject to optical injection," *Optics Comm.*, vol. 172, no. 1-6, pp. 279–295, 1999.

[214] Wieczorek, S., Krauskopf, B., Simpson, T., and Lenstra, D., "The dynamical complexity of optically injected semiconductor lasers," *Phys. Rep.*, vol. 416, no. 1-2, pp. 1–128, 2005.

[215] Wieczorek, S., Krauskopf, B., and Lenstra, D., "A unifying view of bifurcations in a semiconductor laser subject to optical injection," *Optics Communications*, vol. 172, no. 16, pp. 279 – 295, 1999.

[216] Williams, C. R. S., Salevan, J. C., Li, X., Roy, R., and Murphy, T. E., "Fast physical random number generator using amplified spontaneous emission," *Opt. Lett.*, vol. 18, no. 23, pp. 23584–23597, 2010.

[217] Wu, J. G., Tang, X., Wu, Z. M., Xia, G. Q., and Feng, G. Y., "Parallel generation of 10 gbits/s physical random number streams using chaotic semiconductor lasers," *Laser Physics*, vol. 22, no. 10, pp. 1476–1480, 2012.

[218] Xia, G.-Q., Chan, S.-C., and Liu, J.-M., "Multistability in a semiconductor laser with optoelectronic feedback," *Opt. Express*, vol. 15, pp. 572–576, Jan 2007.

[219] Yamazaki, T. and Uchida, A., "Performance of random number generators using noise-based superluminescent diode and chaos-based semiconductor lasers," *Selected Topics in Quantum Electronics, IEEE Journal of*, vol. 19, pp. 0600309–0600309, July 2013.

[220] Ye, J., Li, H., and McInerney, J., "Period-doubling route to chaos in a semiconductor laser with weak optical feedback," *Phys. Rev. A*, vol. 47, no. 3, pp. 2249–2252, 1993.

[221] Zhang, J., Wang, Y., Liu, M., Xue, L., Li, P., Wang, A., and Zhang, M., "A robust random number generator based on differential comparison of chaotic laser signals," *Opt. Express*, vol. 20, pp. 7496–7506, Mar 2012.

[222] Zhang, W. L., Pan, W., Luo, B., Zou, X. H., Wang, M. Y., and Zhou, Z., "Chaos synchronization communication using extremely unsymmetrical bidirectional injections," *Opt. Lett.*, vol. 33, no. 3, pp. 237–239, 2008.

VITA

Byungchil Kim received the B.S. and M.S. degrees in electrical and computer engineering from the Georgia Institute of Technology, Atlanta, GA, USA, in 2006 and 2008, respectively, where he is currently pursuing the Ph.D. degree. His research interests include nonlinear dynamics of semiconductor lasers,time-delay systems, chaos synchronization, and cryptography.